الجمهورية الجزائرية الديمقراطية الشعبية
République Algérienne Démocratique et Populaire
وزارة التعليم العالي و البحث العلمي
Ministère de l'Enseignement Supérieur et de la Recherche Scientifique

Université Mohamed Khider – Biskra
Faculté des Sciences exactes et science
de le nature et de la vie
Department : science de la matière
Ref : …….

جامعة محمد خيضر بسكرة
كلية العلوم الدقيقة و علوم الطبيعة و الحياة
قسم : علوم المادة
المرجع : .....

Thèse présentée en vue de l'obtention
du diplôme de

Doctorat en sciences en : Physique

Option : Semi-Conducteurs

Optimisation des conditions opératoires des couches minces de SnO_2 élaborées par ultra son

Présenté par :

Mr. Achour RAHAL

Soutenue publiquement le 03/07/2017

Devant le jury composé de :

M : Nadir ATTAF	**Professeur à l'Université de Constantine**	**Président**
M : Saad RAHMANE	**Professeur à l'Université de Biskra**	**Examinateur**
M : Med Salah AIDA	**Professeur à l'Université de Constantine**	**Examinateur**
M : Abdallah ATTAF	**Professeur à l'Université de Biskra**	**Examinateur**
M : Boubaker BEN HAOUA	**Professeur à l'Université El oued**	**Rapporteur**

Acknowledgements

Firstly *many thanks to* ***ALLAH*** *for his grace and help, who let me finishing my thesis research.*

Secondly*, I would like to express my sincere gratitude to my advisor Prof.* ***Boubaker BEN HAOUA*** *for the continuous support of my thesis study and research, for his patience, motivation, enthusiasm, and immense knowledge. His guidance helped me in all the time of research and writing of this thesis. I could not have imagined having a better advisor and mentor for my Doctoral study. I attribute the level of my Doctoral degree to his unlimited encouragement and efforts. Also without him, this thesis would not have been completed or written.*

I *address my thanks to Prof* ***Nadir ATTAF,*** *Prof* ***Saad RAHMANE****, Prof* ***Med Salah AIDA*** *and Prof* ***Abdallah ATTAF*** *for their acceptance to judge this modest work.*

Last but not the least*; I would like to thank my family: my parents, for giving birth to meet the first place and supporting me spiritually throughout my life. I cannot forget my brothers and all my friends for their help and advising.*

Achour RAHAL

Contents

Contents

CHAPTER III

Effect of tin precursor concentration

CHAPTER IV

Effect of tin solvent

CHAPTER V

Effect of doping elements

CHAPTER VI

Summary and conclusion

GENERAL INTRODUCTION

Introduction

A combination of transparency and conduction can be achieved in two classes of material. The first group is formed by extremely thin (~10 nm) metal films, especially Ag, Au or Cu. The luminous transmittance can go up to 50%, and even higher when the metal is sandwiched between anti-reflecting layers [1]. The conductivity is strongly thickness dependant, and therefore quite low for these very thin films. The second class of materials consists of wide band gap semiconductors. As early as 1907, the coexistence of electrical conductivity and optical transmittance was first observed in cadmium oxide [2] which firstly was reported by Badeker. However, the technological advances in Transparent conducting oxides (TCOs) emerged only after 1940, as the potential applications in industry and research became evident. In 1956 Thelen et al. [3] found transparency and conduction in indium oxide, which was later used in applications for heated windows. Years of extensive research finally led to Sn-doped In_2O_3 (known as indium tin oxide or ITO) with excellent electrical and optical properties [4]. However, indium is an expensive substance and the abundance of indium is low suggesting alternatives.

Limitations of TCOs become more critical as passive and active devices based on these materials get more sophisticated. For example, as displays become larger and writing speeds get faster, it becomes increasingly important to decrease resistivity while the transparency is maintained [5]. Simply increasing the thickness is not acceptable since the optical absorption will increase. A deep understanding of the fundamental aspects of transparent semiconductors is therefore required in order to improve either the properties of existing materials or design a new type of TCOs. These insights are of great scientific importance whether the realization of

high-performance TCOs on substrates is possible.

At present, Indium Tin Oxide (ITO) is commonly used as transparent electrodes, especially in large-area applications such as displays letting it become the primary end user of the world's indium production as seen from figure 1 which displays its quickly disappearance. The supply of indium has become unreliable during the last 20 years [6], whereas the display market is still expanding. Indium prices are therefore subjected to major instabilities. Alternative materials are welcome to manufacturers of flat panel displays, and much research is conducted on suitable candidates.

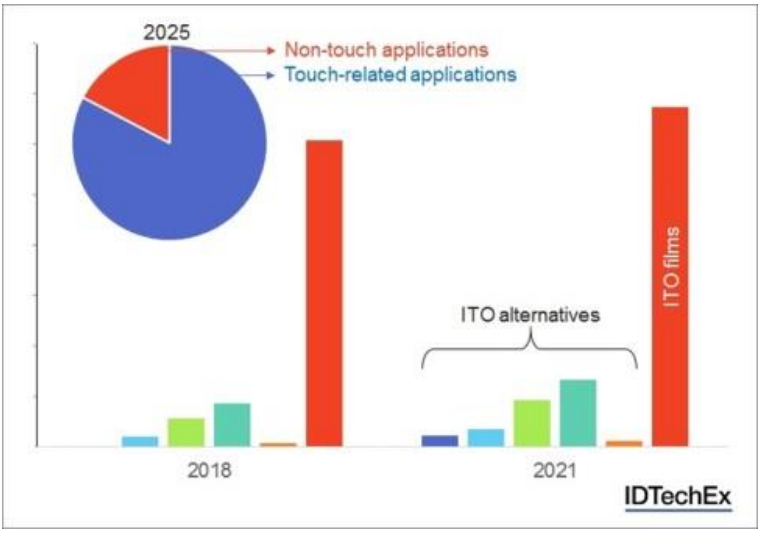

Fig. The market for ITO and ITO alternatives in 2018 and 2021(http://www.idtechex.com/).

One of the ITO alternatives is Tin oxide (SnO_2) as promoter n-type TCOs. SnO_2 is a non-stoichiometric semiconductor with a wide bandgap ($E_g \geq 3.1$ *eV*) at room temperature with tetragonal rutile structure [7]. SnO_2 thin films are characterized by their low cost, low resistivity, high

transmittance in the visible wavelength region, and high chemical and thermal stabilities compared to other TCOs [8]. SnO_2 films are widely used in optoelectronic applications, heat mirror coatings, photocatalysis, organic light emitting diodes, gas sensors, solar energy collectors and so on [9-14].There are several methods for preparing SnO_2 films as it will be described in state and of TCOs **Chapter**. Various parameters such as annealing temperature, deposition rate, oxygen partial pressure and substrate temperature have a significant influence on characteristics of SnO_2 films. Among these parameters, substrate temperature, precursor concentration, nature of the solvent, and doping have a major role in decreasing the intrinsic stress, improving homogeneity and crystallinity, increasing the mobility of charge carriers and figure of merit of the films to get better qualities and to become an alternative to ITO.

The aim of the present thesis is the investigation of the influence of the deposition parameters on the properties of SnO_2 thin films prepared by ultrasonic spray pyrolysis in order to optimize these parameters to produce a suitable collector layer with low cost solar cells which is the main goal of this study and gas sensor for sensing organic vapor and different gases. A systematic study of the influence of various parameters related to this ultrasonically technique on the elaborated SnO_2 thin films properties such as structural, optical, electrical and figure of merit will be carried in the present work.

The thesis is organized as following:

Firstly **In Chapter I,** we will present a literature survey on SnO_2 thin films, an insight upon its different properties and applications will be outlined, secondly in the three next chapters which are the goals of this thesis; Results and discussion on the ultrasonically deposited tin oxide (SnO_2) thin films with different substrate temperatures will be represented in **Chapter II,** Results and discussion on the ultrasonically deposited tin oxide (UD-SnO_2) thin films with effect of tin precursor concentration, on physical properties will be exhibited in **Chapter III**; in **Chapter IV,** we will represent the results and discussion on the UD-SnO_2 thin films with effect of solvent (water/methanol) on its physical properties also. In **Chapter V:** We present the brief summary of obtained results, concluding remarks and suggestions for future works.
Finally, the **general conclusion** about this work will be given.

References

[1] C.G. Granqvist, A. Hultåker, Transparent and conducting ITO films: new developments and applications, Thin solid films, 411 (2002) 1-5.
[2] K. Badeker, Electrical conductivity and thermo-electromotive force of some metallic compounds, Ann. Phys, 22 (1907) 749.
[3] A. Thelen, H. König, Elektrische Leitfähigkeit und Struktur aufgestäubter Indiumoxydschichten, Naturwissenschaften, 43 (1956) 297-298.
[4] R. Groth, E. Kauer, Thermal insulation of sodium lamps, Philips Technical Review, 26 (1965) 105-&.
[5] D.S. Ginley, C. Bright, Transparent conducting oxides, Mrs Bulletin, 25 (2000) 15-18.
[6] B. O'Neill, Indium: Supply, demand & flat panel displays, Minor Metals, (2004) 21-22.
[7] G.J. McCarthy, J.M. Welton, X-ray diffraction data for SnO 2. An illustration of the new powder data evaluation methods, Powder Diffraction, 4 (1989) 156-159.
[8] A. Benhaoua, A. Rahal, B. Benhaoua, M. Jlassi, Effect of fluorine doping on the structural, optical and electrical properties of SnO 2 thin films prepared by spray ultrasonic, Superlattices and Microstructures, 70 (2014) 61-69.
[9] I. Kim, J. Ko, D. Kim, K. Lee, T. Lee, J.-H. Jeong, B. Cheong, Y.-J. Baik, W. Kim, Scattering mechanism of transparent conducting tin oxide films prepared by magnetron sputtering, Thin Solid Films, 515 (2006) 2475-2480.
[10] Y.-M. Lu, C.-P. Hu, The colored and bleached properties of tungsten oxide electrochromic films with different substrate conductivities, Journal of Alloys and Compounds, 449 (2008) 389-392.
[11] S.S. Srinivasan, J. Wade, E.K. Stefanakos, Y. Goswami, Synergistic effects of sulfation and co-doping on the visible light photocatalysis of TiO 2, Journal of Alloys and Compounds, 424 (2006) 322-326.
[12] B. Thangaraju, Structural and electrical studies on highly conducting spray deposited fluorine and antimony doped SnO 2 thin films from SnCl 2 precursor, Thin solid films, 402 (2002) 71-78.
[13] D. Vaufrey, M.B. Khalifa, M. Besland, C. Sandu, M. Blanchin, V. Teodorescu, J. Roger, J. Tardy, Reactive ion etching of sol–gel-processed SnO 2 transparent conducting oxide as a new material for organic light emitting diodes, Synthetic Metals, 127 (2002) 207-211.
[14] M.-R. Yang, S.-Y. Chu, R.-C. Chang, Synthesis and study of the SnO

2 nanowires growth, Sensors and Actuators B: Chemical, 122 (2007) 269-273.

STATE OF THE TCOs ART

I.I Transparent conducting oxides (TCOs)

Transparent conducting oxides (TCOs) are materials having the property of simultaneously conducting electricity and exhibiting transparency in the visible region of the electromagnetic spectrum. The materials are often a compound of oxygen and one or two metallic elements and the material properties are highly dependent on used elements. The properties are also affected by the quality of the material and the deposition method. High-quality TCO films having a thickness between (30-420nm) deposited by pulsed laser deposition and magnetron sputtering have shown transparency as high as ~90% and a resistivity in the $10^{-5}\Omega$ cm range [1, 2].

TCOs were first reported by Badeker in 1907. He discovered that a thin film of cadmium could be made transparent by oxidizing it. Fortunately, the film was still conducting electricity. Since then, several other materials have been shown to exhibit this unique combination of properties. Some of the most frequently applied TCOs today are an antimony-doped tin oxide (ATO), tin doped indium oxide (ITO), aluminum doped zinc oxide (AZO), fluorine-doped tin oxide (FTO) and niobium doped titanium oxide [3].

Over the last decade, new transparent and conducting materials for flexible substrate application have been studied intensively. Fortunately, research on materials like nanowires of pure metals, plasmonic graphene, and highly doped conjugated organic polymers has shown that they exhibit sufficient optical transparency and electrical conductivity as transparent conducting materials [4-6].

In our daily lives, TCO materials are used in numerous devices. Their applications are mostly found in display technology, organic light-emitting-diodes (OLEDs), thin-film solar photovoltaics and “smart

windows". Both in existing as well as new applications the implementation of a polymer support instead of the commonly used rigid glass has become significant in the field of research, for example in the realization of flexible displays. As polymer materials with functional or protective coatings are combined, the flexibility, light-weight, and cost-effectiveness of the substrate offer many new advantages for device engineering. With regard to processing, however, the manufacturing temperature of TCO materials on polymers is limited, which negatively influences their performance [7].

As cited above, in general, TCOs are utilized for a lot of applications. Though, the applications are dominated by only a handful of TCOs: FTO, ITO and a variety of different doped ZnO.

The most common TCO applied in the industry today is FTO. This material is used in the production of windows having a low radiative heat loss, called "energy efficient windows" or low emissivity windows called too "low-e windows". Such windows are able to maintain the heat indoor during the winter months and reflect or absorb the infrared light from outside during the summer months. This way, both heating and cooling costs will decrease [3, 5].

The second largest application area for TCOs is flat panel displays. This is a continuously growing market and ITO is the main TCO applied. Though, recently amorphous indium doped zinc oxide has partly replaced ITO due to better patterning properties and thermal stability [3].

The third largest industry application for TCOs is front electrodes in photovoltaics. ITO is the most utilized TCO for this purpose. However, indium is an expensive substance and the abundance of indium is low. This has raised zinc oxide as an alternative TCO in photovoltaics area [3].

Other important application areas of TCOs are for instance gas sensors,

oxide based thin film transistors, and electrochromic devices, e.g. windows with adjustable transparency, and automatically dimming of rear-view mirrors for automobiles[8-10]. It is obvious that applications of TCOs show that such materials play an important role in the development of "green" technologies: Energy efficient windows and light-emitting diodes (LED) for indoor lighting [11] have a significant impact on lowering energy consumption, while photovoltaics are contributing to a more sustainable and clean power generation [3, 12].

I.2. Methods and Elaboration

There are several methods for preparing SnO_2 films: The screen printing technique [13], chemical vapor deposition [14], reactive evaporation [15], DC and RF sputtering [16] and pulsed laser ablation [17], thermal evaporation [18], electron beam evaporation [19], metal–organic deposition [20], sol–gel deposition [21]and spray pyrolysis [22]. Among these methods, thermal evaporation has the advantages of producing high purity crystalline products and durable films in a single step. Various parameters such as annealing temperature, deposition rate, oxygen partial pressure and substrate temperature have a significant influence on characteristics of SnO_2 films. Among these parameters, substrate temperature has a major role in decreasing the intrinsic stress, increasing the mobility of charge carriers, and improving homogeneity and crystallinity of films to get better quality films.

I.3 Basic physics

As previously stated, the unique combination of transmitting and conducting properties of TCOs makes the materials suitable for several

applications. However, the two properties are not independent. A change of which one of them will affect the other.

The nature of the transmitting property is associated with the wide band gap exhibited by the TCO. In order to be transparent in the visible range, the TCO material generally has a band gap larger than 3 eV, which implies an absorption onset at approximately 400 nm. At the long wavelength side of the visible spectrum (near infrared), the transmission is limited by the electron plasma oscillation [23]. Both limits are influenced by changes in the electron concentration:

- One effect of increased electron concentration (n_e) is a shift of the Fermi level to higher energies, called the Burstein-Moss shift [24, 25]. When the Fermi level shifts and overlaps the conduction band, the lowest states in the conduction band are blocked. This requires incident photons of higher energy in order to be absorbed, and hence the onset of the absorption is shifted toward higher energies [3, 14, 26, 27]; generally, this phenomenon occurs after doping.
- The second effect of increasing the electron concentration is a shift of the plasma frequency towards higher frequencies, as seen on Eq. I.6; where ω_p is the plasma frequency and n_e is the number of electrons [28]. This introduces absorption and hence, a reduction in transparency at longer wavelengths. The illustrated example, in Fig. I. 1, shows optical reflection, transmission and absorption spectra, for a typical SnO_2 TCO on the glass, which, collectively, shows the key spectral features of a TCO material. First, the material is quite transparent, 80%, in the visible portion of the spectrum, 400-700 nm. Across this spectral region where the sample is transparent, oscillations due to thin film interference effects can be seen in both the transmission and reflection spectra. From which,

generally film thickness is deduced. The short wavelength cut-off in the transmission at 300 nm is due to the fundamental band gap excitation from the valence band to the conduction band as depicted in the right panel of Fig. I.1. The gradual long wavelength decrease in the transmission starting at 1000 nm and its corresponding increase in the reflection starting at 1500 nm are due to collective oscillations of conduction band electrons which are known as plasma oscillations for short wavelength. There, Substantial absorption can also proceed which is due to these plasma oscillations as is the case for this particular sample with the maximum absorption, occurring, at the characteristic plasma wavelength, λ_p, as shown in the same figure. As the number of electrons in the conduction band, n_e, is increased, such as by substitution doping, the plasma wavelength shifts to shorter wavelengths [3].

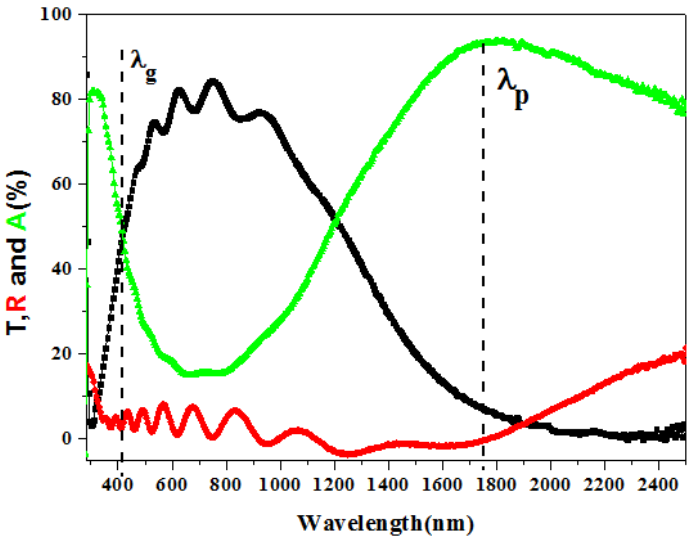

Figure I.1: Spectral dependence of TCO (F-doped SnO_2): λ_{gap} and λ_p are the wavelengths at which the band gap absorption and free electron plasma absorption takes place [29].

I.4.Optical properties

An important feature of TCOs is the existence of a transmission window covering most part of the visible spectrum. In literature, the optical transmission is defined as the ratio between incoming light intensity and transmitted intensity averaged over all values in between 400-700nm. A typical spectral dependence of TOSs is schematically shown in figure I. 1. The transmission window is defined by two regions where no light is transmitted due to two different phenomena. At low wavelengths ($\lambda<\lambda_{gap}$) the absorption due to the fundamental band gap dominates. The photon energy in this near-and deep-UV part of the spectrum is high enough ~~to~~ equal the band gap energy (3-4 eV). This energy is absorbed and as consequence to this band to band electron transitions happens, and no light is transmitted because of this quantum phenomenon. For longer wavelengths, in the (near) infrared (IR) part of the spectrum, no light is transmitted due to the plasma edge ($\lambda>\lambda p$). Here the light is electronically reflected as it was best described by the classical Drude free-electron theory [30].

In the free electron model, the electrons may be thought as plasma whose density is set into motion by the electric field component of the electromagnetic field. The plasma oscillates at a natural frequency ω_p, which is so called the resonance or plasma frequency. This wavelength λ_p corresponds to the plasma frequency is ranged in 1-4 μm for TCOs [12]. The interaction of free electrons with the electromagnetic field influences the relative permittivity, ε, of the material, which is expressed as a complex number in the following equation:

$$\varepsilon = (n - ik)^2 \qquad \textbf{(I. 1)}$$

where the real part is the refractive index (***n***) and the imaginary one is extinction coefficient (***k***) respectively. These parameters determine the reflectance and absorptance of the material. Close to the plasma frequency the properties of the material change drastically. In the infrared (IR) part of the spectrum, below this critical value ($\omega<\omega_p$, or $\lambda>\lambda_p$) the imaginary part of "the electron velocity V_F" is large, and the penetrating wave drops off exponentially [31]. The real part is negative, and the material has near-unity reflectance. For ($\omega>\omega_p$ or $\lambda< \lambda_p$), the imaginary part tends to zero, and absorption is small. The refractive index is positive and almost constant with frequency according to the equation:

$$n = \sqrt{\varepsilon_\infty}\sqrt{\left(1 - \left(\frac{\omega_p}{\omega}\right)^2\right)} \approx \sqrt{\varepsilon_\infty} \qquad \textbf{(I. 2)}$$

Here ε is the high-frequency permittivity. The TCO behaves like a dielectric and is transparent in the region for ($\omega>\omega_p$) [32]. In this transparent regime, the film is weakly absorbing ($k^2<<n^2$) and the transmission can be expressed as [33]:

$$T = (1 - R)\exp(-\alpha d) \qquad \textbf{(I. 3)}$$

R is the zero degrees incidence reflectance, ***d*** is the film thickness and α is the absorption coefficient and depends on the wavelength according to the following expression:

$$\alpha = \frac{4\pi k}{\lambda} \qquad \text{(I.4)}$$

Close to $\boldsymbol{\lambda_{gap}}$ the reflectance is zero and the absorption coefficient, as a function of wavelength, can be obtained easily from the transmission curve. The following relation is commonly applied for directly allowed transitions:

$$\boldsymbol{\alpha \propto \sqrt{h\nu - E_g}} \qquad \text{(I.5)}$$

where *hv* is the photon energy and $\boldsymbol{E_g}$ is the band gap. The latter is calculated from the Tauc plot giving α^2 versus the photon energy $\boldsymbol{h\nu}$ [34]. By extrapolating $\boldsymbol{\alpha^2}$ to the *x*-axis intersection (it means $\boldsymbol{\alpha}$=0) in formula I.5, it implies that the photon energy equals the bandgap energy ($\boldsymbol{h\nu \approx E_g}$). This method is usually to extract band gap energies from transmission data.

I.5.Correlation between optical and electrical properties

The optical parameters of TCOs are affected by the electrical properties of the material. The earlier mentioned plasma resonance frequency is not a fixed value but varies with the electron concentration. The plasma frequency in relation to the carrier concentration is expressed by:

$$\boldsymbol{\omega_p^2 = \frac{e^2 n_e}{\varepsilon_0 \varepsilon_\infty m^*}} \qquad \text{(I.6)}$$

here $\boldsymbol{\omega_p}$ is the plasma frequency, $\boldsymbol{\varepsilon}$ is f the relative permittivity, $\boldsymbol{\varepsilon_\infty}$ is the permittivity limit of the material, $\boldsymbol{n_e}$, $\boldsymbol{e}$ and $\mathbf{m}^*$ are the carriers concentration, the electron charge and the reduced effective mass of the electron carriers respectively.

At this frequency, the dielectric-like visible transmittance equals the

metallic-like IR reflectance (T=R). Thus the IR reflectivity of the material can be tuned, which is important for heat reflecting or low emissive window applications. For example, the plasma wavelength of ITO films can be tuned from 1.5 µm to 4 µm due to the carrier concentration by changing the composition and deposition parameters [35, 36].

The refractive index of commonly TCO materials varies in between 1.7 and 2.1 [37]. Moreover, a large spread of the similar material is frequently reported. The main reason is that also the refractive index is dependent on the carrier concentration according to:

$$\boldsymbol{\varepsilon = n^2 = \varepsilon_\infty - \left(\frac{e^2 n_e}{4\pi c^2 \varepsilon_0 m^*}\right)\lambda^2} \qquad \text{(I.7)}$$

Here ω is the frequency of incoming light. Changing the refractive index is useful for waveguide applications. For instance, in ITO this value can be tuned between 1.70 and 2.05 [38, 39].

For heavily doped oxide semiconductors a gradual shift of the band gap towards higher energy as the electron density increases is generally observed [40]. This well-known effect is attributed to the Burstein-Moss shift (BM shift) [24]. In heavily doped semiconductors, the lowest states in the conduction band are blocked. Hence transition can only take place to energies above E_F, enlarging the effective optical gap. The energy gap between the top of the valence band and lowest empty state in the conduction band (both assumed parabolic) can be given by:

$$\boldsymbol{E_g = E_{g0} + \Delta E_g^{B-M}} \qquad \text{(I.8)}$$

In this formula, E_{g0} is the intrinsic band gap and the BM shift is given by the following expression:

$$\Delta E_g^{B-M} = \frac{\hbar^2}{2m_{cv}^*}(3\pi^2 n_e)^{2/3} \qquad \text{(I.9)}$$

Here m_{cv}^* is the reduced effective mass of the electron carriers given by:

$$\frac{1}{m_{cv}^*} = \frac{1}{m_c^*} + \frac{1}{m_v^*} \qquad \text{(I.10)}$$

Where m_c^* and m_v^* are effective mass of the carriers in the conduction and valence band respectively.

I.6. General properties

Preparation method, for growing high-quality TCO films, is of great importance. The physical properties of TCO thin films are strongly dependant on the structure, morphology and composition of the thin films, and the nature of the incorporated impurities. These factors are influenced by the deposition parameters of the different growth techniques. For TCO thin film preparation, a wide variety of growth techniques has been reported and examined extensively.

Effective TCOs should possess both high electrical conductivity and low absorption of visible light. Thus the ratio between the transmittance (T) and sheet resistance (R_s) of transparent conducting films is named a figure of merit (FOM) for rating these materials. Later Haacke defined a more suitable measure, as for some applications, optical absorption is too low at maximum FOM [41]. This new parameter ϕ_{TC} representing the figure of merit is defined as:

$$\phi_{TC} = {T^{10}}/{R_s} \qquad \textbf{(I.11)}$$

Besides the electrical and optical properties, other criteria influence the choice of material and deposition method. For material processing the etching properties, production cost or toxicity are important. In view of applications the plasma frequency, mechanical hardness; thermal or chemical stability and minimum deposition temperature are essential. An overview of these criteria tailored to a different application is reported by Gordon [12].

I.7.Structural Properties

SnO_2 belongs to the space-group symmetry $P_{42/mnm}$ and with lattice constants, $a = b = 4.7382$, $c = 3.1871$ [42]. The Sn and O atoms have 6-3 coordination, that is, Sn atoms are six-fold coordinated and O atoms are three-fold coordinated, as depicted in Fig. I. 2. SnO_2 is usually regarded as an oxygen-deficient *n-type* semiconductor. This means that SnO_2 prefers to give up oxygen and can accommodate electrons more easily than holes in its lattice [43]. Thus, oxygen vacancies are always the source of electron carriers for an undoped material. SnO_2 is a prototype material for the development of transparent conducting oxides. Its wide direct band gap characteristics (~3.6-3.8 eV), high transparency in the visible region, high mechanical hardness, and environmental compatibility are the interesting features that are essential and plausible properties for electrode materials [44, 45], gas sensors [46-49], solar cell fabrication [50-52], transparent and protective coatings [53-55], and other device applications.

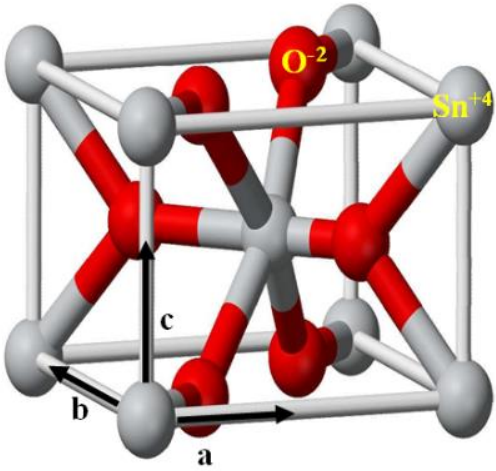

Figure I. 2: Rutile structure of SnO_2: gray and red circles are tin and oxygen atoms, respectively (https://en.wikipedia.org/wiki/Tin_dioxide) .

In gas sensors applications, when the SnO_2 surface is exposed to air, oxygen absorbs onto the surface as O^{2-} ads or O^- ads. These adsorbed molecules form an electron depletion layer just below the SnO_2 surface and consequently make the SnO_2 highly resistive [56, 57]. When reducing gases (e.g. H_2 and CO) are introduced as gas ambient, the adsorbed oxygen species are removed through the oxidation of reducing gases and the electrons that are being captured in the process are restored in the conduction band. This results, in decreasing the resistance and/or resistivity of the oxide material, can be recorded and measured easily as the response of gas detection [58]. Moreover, photochemically deposited SnO_2 thin films as hydrogen gas sensors are found to be highly sensitive at room temperature [59, 60]. Introducing impurities such as Cu, Fe, Co, Al, Zn and Ni on the undoped SnO_2 can enhance the electrical properties of the material [61-66] and promote change or modify the surface morphology and decrease the grain size [67].

Completely stoichiometric undoped tin oxide would be an insulator, but a reasonable degree of conductivity can be achieved by stoichiometric deviation or by doping. Undoped tin oxide films often show some degree of conductivity because of unintentional doping with Cl^- or due to non-stoichiometry, mostly caused by oxygen vacancies in the lattice. These vacancies contain electrons from the removed oxygen atom, which can be excited to the conduction band. If too many oxygen vacancies are created, the structure can change into SnO with excess oxygen, which often has a negative influence on the conductivity. Another possibility for increasing the conductivity of tin oxide is the incorporation of suitable ions in the lattice. Substituting Sb^{5+}, Sb^{3+}, In^{3+}, P^{5+}, Sm^{3+}or $As^{3+}$for Sn^{4+}, or substituting F^-, Cl^- for O^{2-}, results in a donor level in the energy [68-73]
band gap causing a higher conductivity. The charge carriers generated by non-stoichiometry and doping are scattered by various mechanisms, like ionized impurity scattering, neutral impurity scattering, grain boundary scattering, and scattering at other defects and dislocations. Thus, the conductivity is dependent on the composition and the morphology of the layer, which in turn is dependent on deposition parameters like substrate temperature, film thickness, gas flow rate, precursor composition, and post-deposition annealing [58].

At the end of this chapter, an overview on *n*-type and *p*-type TCOs is given in Table I.1. in these tables are selected on the best performance of the TCO, but are merely a selection of the vast amount of literature on these materials. It illustrates the diversity of materials and corresponding properties deposited by different deposition methods.

Table I.1: *Reported properties of transparent conducting oxides*

TCO	References
Sb-doped SnO_2 by spray pyrolysis	[74]
Cl-doped SnO_2 by spray pyrolysis	[75]
F-doped SnO_2 by spray pyrolysis	[76]
Sn-doped In_2O_3 by spray pyrolysis	[77]
Sn-doped In_2O_3 by sputtering	[78]
Sb-doped SnO_2 by CVD	[79]
Cd_2SnO_4 by sputtering	[80]
Cd_2SnO_4 by spray pyrolysis	[81]
F-doped SnO_2 by CVD	[82]
TiN by CVD	[83]
Al-doped ZnO by spray pyrolysis	[84]
Al-doped ZnO by sputtering	[85]
In doped ZnO by sputtering	[86]
B-doped ZnO by CVD	[87]
Ga-doped ZnO by sputtering	[88]
Al-doped ZnO by CVD	[89]
Ga-doped ZnO by CVD	[90]
Zn_2SnO_4 by sputtering	[91]
Cd_2SnO_4 by pulsed laser deposition	[92]

References

[1] S. Ray, R. Banerjee, N. Basu, A. Batabyal, A.K. Barua, Properties of tin doped indium oxide thin films prepared by magnetron sputtering, Journal of Applied Physics, 54 (1983) 3497-3501.
[2] A. Suzuki, T. Matsushita, T. Aoki, Y. Yoneyama, M. Okuda, Pulsed laser deposition of transparent conducting indium tin oxide films in magnetic field perpendicular to plume, Japanese Journal of Applied Physics, 40 (2001) L401.
[3] H. Hosono, D.C. Paine, D. Ginley, Handbook of transparent conductors, Springer Science & Business Media, 2010.
[4] C.-H. Liu, X. Yu, Silver nanowire-based transparent, flexible, and conductive thin film, Nanoscale research letters, 6 (2011) 75.
[5] A. Pron, P. Rannou, Processible conjugated polymers: from organic semiconductors to organic metals and superconductors, Progress in polymer science, 27 (2002) 135-190.
[6] G. Xu, J. Liu, Q. Wang, R. Hui, Z. Chen, V.A. Maroni, J. Wu, Plasmonic graphene transparent conductors, Advanced Materials, 24 (2012).
[7] B. O'Neill, Indium: Supply, demand & flat panel displays, Minor Metals, (2004) 21-22.
[8] J. Livage, D. Ganguli, Sol–gel electrochromic coatings and devices: a review, Solar Energy Materials and Solar Cells, 68 (2001) 365-381.
[9] T. Miyata, T. Hikosaka, T. Minami, High sensitivity chlorine gas sensors using multicomponent transparent conducting oxide thin films, Sensors and Actuators B: chemical, 69 (2000) 16-21.
[10] K. Nomura, H. Ohta, A. Takagi, T. Kamiya, M. Hirano, H. Hosono, Room-temperature fabrication of transparent flexible thin-film transistors using amorphous oxide semiconductors, Nature, 432 (2004) 488-492.
[11] Y.-H. Tak, K.-B. Kim, H.-G. Park, K.-H. Lee, J.-R. Lee, Criteria for ITO (indium–tin-oxide) thin film as the bottom electrode of an organic light emitting diode, Thin Solid Films, 411 (2002) 12-16.
[12] R.G. Gordon, Criteria for choosing transparent conductors, MRS bulletin, 25 (2000) 52-57.
[13] S. Peng, F. Cheng, J. Liang, Z. Tao, J. Chen, Facile solution-controlled growth of CuInS 2 thin films on FTO and TiO 2/FTO glass substrates for photovoltaic application, Journal of Alloys and Compounds, 481 (2009) 786-791.
[14] E. Fortunato, D. Ginley, H. Hosono, D.C. Paine, Transparent conducting oxides for photovoltaics, MRS bulletin, 32 (2007) 242-247.

[15] J. Berry, D. Ginley, P.E. Burrows, Organic light emitting diodes using a Ga: ZnO anode, Applied Physics Letters, 92 (2008) 170.
[16] K. Omura, P. Veluchamy, M. Tsuji, T. Nishio, M. Murozono, A Pyrosol Technique to Deposit Highly Transparent, Low-Resistance SnO2: F Thin Films from Dimethyltin Dichloride, Journal of The Electrochemical Society, 146 (1999) 2113-2116.
[17] A. Moholkar, S. Pawar, K. Rajpure, C. Bhosale, J. Kim, Effect of fluorine doping on highly transparent conductive spray deposited nanocrystalline tin oxide thin films, Applied Surface Science, 255 (2009) 9358-9364.
[18] A. Banerjee, R. Maity, P. Ghosh, K. Chattopadhyay, Thermoelectric properties and electrical characteristics of sputter-deposited p-CuAlO 2 thin films, Thin Solid Films, 474 (2005) 261-266.
[19] N. Shaalan, T. Yamazaki, T. Kikuta, Influence of morphology and structure geometry on NO 2 gas-sensing characteristics of SnO 2 nanostructures synthesized via a thermal evaporation method, Sensors and Actuators B: Chemical, 153 (2011) 11-16.
[20] A.F. Khan, M. Mehmood, M. Aslam, M. Ashraf, Characteristics of electron beam evaporated nanocrystalline SnO 2 thin films annealed in air, Applied Surface Science, 256 (2010) 2252-2258.
[21] T. Tsuchiya, K. Daoudi, I. Yamaguchi, T. Manabe, T. Kumagai, S. Mizuta, Preparation of tin oxide films on various substrates by excimer laser metal organic deposition, Applied surface science, 247 (2005) 145-150.
[22] W. Hamd, Y. Wu, A. Boulle, E. Thune, R. Guinebretière, Microstructural study of SnO 2 thin layers deposited on sapphire by sol–gel dip-coating, Thin Solid Films, 518 (2009) 1-5.
[23] J. Perkins, J. Del Cueto, J. Alleman, C. Warmsingh, B. Keyes, L. Gedvilas, P. Parilla, B. To, D. Readey, D. Ginley, Combinatorial studies of Zn-Al-O and Zn-Sn-O transparent conducting oxide thin films, Thin solid films, 411 (2002) 152-160.
[24] E. Burstein, Anomalous optical absorption limit in InSb, Physical Review, 93 (1954) 632.
[25] T. Moss, The interpretation of the properties of indium antimonide, Proceedings of the Physical Society. Section B, 67 (1954) 775.
[26] I. Hamberg, C. Granqvist, K.-F. Berggren, B.E. Sernelius, L. Engström, Band-gap widening in heavily Sn-doped In 2 O 3, physical Review B, 30 (1984) 3240.
[27] P. King, T.D. Veal, Conductivity in transparent oxide semiconductors, Journal of Physics: Condensed Matter, 23 (2011) 334214.

[28] T.J. Coutts, D.L. Young, T.A. Gessert, Modeling, characterization, and properties of transparent conducting oxides, in: Handbook of Transparent Conductors, Springer, 2011, pp. 51-110.
[29] A. Rahal, S. Benramache, B. Benhaoua, Preparation of n-type semiconductor SnO2 thin films, Journal of Semiconductors, 34 (2013) 083002.
[30] P. Drude, Zur elektronentheorie der metalle, Annalen der Physik, 306 (1900) 566-613.
[31] E. Hecht, Optics, 4th, International edition, Addison-Wesley, San Francisco, 3 (2002).
[32] T.J. Coutts, D.L. Young, X. Li, Characterization of transparent conducting oxides, Mrs Bulletin, 25 (2000) 58-65.
[33] J. Manifacier, M. De Murcia, J. Fillard, E. Vicario, Optical and electrical properties of SnO 2 thin films in relation to their stoichiometric deviation and their crystalline structure, Thin Solid Films, 41 (1977) 127-135.
[34] J. Tauc, R. Grigorovici, A. Vancu, Optical properties and electronic structure of amorphous germanium, physica status solidi (b), 15 (1966) 627-637.
[35] P.K. Biswas, A. De, N. Pramanik, P. Chakraborty, K. Ortner, V. Hock, S. Korder, Effects of tin on IR reflectivity, thermal emissivity, Hall mobility and plasma wavelength of sol–gel indium tin oxide films on glass, Materials letters, 57 (2003) 2326-2332.
[36] H. Kim, J. Horwitz, A. Pique, C. Gilmore, D. Chrisey, Electrical and optical properties of indium tin oxide thin films grown by pulsed laser deposition, Applied Physics A: Materials Science & Processing, 69 (1999) S447-S450.
[37] H. Hartnagel, Semiconducting transparent thin films, CRC Press, 1995.
[38] R. Chen, D. Robinson, Electro-optic and all-optical phase modulator on an indium tin oxide single-mode waveguide, Applied physics letters, 60 (1992) 1541-1543.
[39] F. Simonis, M. Van Der Leij, C. Hoogendoorn, Physics of doped tin dioxide films for spectral-selective surfaces, Solar Energy Materials, 1 (1979) 221-231.
[40] I. Hamberg, C.G. Granqvist, Evaporated Sn-doped In2O3 films: Basic optical properties and applications to energy-efficient windows, Journal of Applied Physics, 60 (1986) R123-R160.
[41] G. Haacke, New figure of merit for transparent conductors, Journal of Applied Physics, 47 (1976) 4086-4089.

[42] G.J. McCarthy, J.M. Welton, X-ray diffraction data for SnO 2. An illustration of the new powder data evaluation methods, Powder Diffraction, 4 (1989) 156-159.
[43] P.J. Van der Put, The inorganic chemistry of materials: How to make things out of elements, Springer Science & Business Media, 2013.
[44] K.-H. Houng, Electrochemical Properties of CVD Oxide (SnO_2 and TiO_2) Covered Electrodes, 中央研究院化學研究所集刊, (1982) 19-23.
[45] J. Kane, M. Ling, Electroluminescent device and a method of making same, in, Google Patents, 1988.
[46] E. Comini, G. Faglia, G. Sberveglieri, Z. Pan, Z.L. Wang, Stable and highly sensitive gas sensors based on semiconducting oxide nanobelts, Applied Physics Letters, 81 (2002) 1869-1871.
[47] C. Wang, L. Yin, L. Zhang, D. Xiang, R. Gao, Metal oxide gas sensors: sensitivity and influencing factors, Sensors, 10 (2010) 2088-2106.
[48] N. Yamazoe, New approaches for improving semiconductor gas sensors, Sensors and Actuators B: Chemical, 5 (1991) 7-19.
[49] N. Yamazoe, G. Sakai, K. Shimanoe, Oxide semiconductor gas sensors, Catalysis Surveys from Asia, 7 (2003) 63-75.
[50] R. Jose, V. Thavasi, S. Ramakrishna, Metal oxides for dye-sensitized solar cells, Journal of the American Ceramic Society, 92 (2009) 289-301.
[51] J. You, C.C. Chen, L. Dou, S. Murase, H.S. Duan, S.A. Hawks, T. Xu, H.J. Son, L. Yu, G. Li, Metal oxide nanoparticles as an electron-transport layer in high-performance and stable inverted polymer solar cells, Advanced Materials, 24 (2012) 5267-5272.
[52] B.D. Yuhas, P. Yang, Nanowire-based all-oxide solar cells, Journal of the American Chemical Society, 131 (2009) 3756-3761.
[53] C.M. Egert, Protective coatings for sensitive materials, in, Google Patents, 1997.
[54] F.H. Gillery, Sputtered films of metal alloy oxides and method of preparation thereof, in, Google Patents, 1986.
[55] J. Gray, B. Luan, Protective coatings on magnesium and its alloys—a critical review, Journal of alloys and compounds, 336 (2002) 88-113.
[56] J.W. Gardner, H.V. Shurmer, P. Corcoran, Integrated tin oxide odour sensors, Sensors and Actuators B: Chemical, 4 (1991) 117-121.
[57] S. Mishra, C. Ghanshyam, N. Ram, S. Singh, R. Bajpai, R. Bedi, Alcohol sensing of tin oxide thin film prepared by sol-gel process, Bulletin of Materials Science, 25 (2002) 231-234.
[58] A.M.B. van Mol, Chemical vapour deposition of tin oxide thin films, (2003).
[59] H. Huang, Y. Lee, O. Tan, W. Zhou, N. Peng, Q. Zhang, High

sensitivity SnO2 single-nanorod sensors for the detection of H2 gas at low temperature, Nanotechnology, 20 (2009) 115501.
[60] B. Wang, L. Zhu, Y. Yang, N. Xu, G. Yang, Fabrication of a SnO2 nanowire gas sensor and sensor performance for hydrogen, The Journal of Physical Chemistry C, 112 (2008) 6643-6647.
[61] V. Bilovol, C. Herme, S. Jacobo, A. Cabrera, Study of magnetic behaviour of Fe-doped SnO 2 powders prepared by chemical method, Materials Chemistry and Physics, 135 (2012) 334-339.
[62] X. Kou, C. Wang, M. Ding, C. Feng, X. Li, J. Ma, H. Zhang, Y. Sun, G. Lu, Synthesis of Co-doped SnO 2 nanofibers and their enhanced gas-sensing properties, Sensors and Actuators B: Chemical, 236 (2016) 425-432.
[63] Z. Lin, N. Li, Z. Chen, P. Fu, The effect of Ni doping concentration on the gas sensing properties of Ni doped SnO 2, Sensors and Actuators B: Chemical, 239 (2017) 501-510.
[64] C. Wang, W. Zeng, L. Luo, P. Zhang, Z. Wang, Gas-sensing properties and mechanisms of Cu-doped SnO 2 spheres towards H 2 S, Ceramics International, 42 (2016) 10006-10013.
[65] C. Wei, G. Zhang, Y. Bai, D. Yan, C. Yu, N. Wan, W. Zhang, Al-doped SnO 2 hollow sphere as a novel anode material for lithium ion battery, Solid State Ionics, 272 (2015) 133-137.
[66] B. Xu, X.-G. Ren, G.-R. Gu, L.-L. Lan, B.-J. Wu, Structural and optical properties of Zn-doped SnO 2 films prepared by DC and RF magnetron co-sputtering, Superlattices and Microstructures, 89 (2016) 34-42.
[67] G. Korotcenkov, V. Brinzari, I. Boris, (Cu, Fe, Co, or Ni)-doped tin dioxide films deposited by spray pyrolysis: doping influence on film morphology, Journal of materials science, 43 (2008) 2761-2770.
[68] M.A. Abdulsattar, S.S. Batros, A.J. Addie, Indium doped SnO 2 nanostructures preparation and properties supported by DFT study, Superlattices and Microstructures, 100 (2016) 342-349.
[69] B.M. Faustino, P. Foot, R. Kresinski, Synthesis and photoluminescent properties of Sm 3+-doped SnO 2 nanoparticles, Ceramics International, 42 (2016) 18474-18478.
[70] R.R. Kumar, K.N. Rao, K. Rajanna, A. Phani, Novel co-evaporation approach for the growth of Sb doped SnO 2 nanowires, Materials Letters, 106 (2013) 164-167.
[71] N. Manjula, A. Balu, Double doping (Mn+ Cl) effects on the structural, morphological, photoluminescence, optoelectronic properties and antibacterial activity of CdO thin films, Optik-International Journal for

Light and Electron Optics, 130 (2017) 464-472.
[72] Q.-P. Tran, J.-S. Fang, T.-S. Chin, Properties of fluorine-doped SnO 2 thin films by a green sol–gel method, Materials Science in Semiconductor Processing, 40 (2015) 664-669.
[73] S. Vishwakarma, J. Upadhyay, H. Prasad, Physical properties of arsenic-doped tin oxide thin films, Thin Solid Films, 176 (1989) 99-110.
[74] S.-Y. Lee, B.-O. Park, Structural, electrical and optical characteristics of SnO 2: Sb thin films by ultrasonic spray pyrolysis, Thin solid films, 510 (2006) 154-158.
[75] M. Oshima, K. Yoshino, Structural and Electronic Structure of SnO2 by the First-Principle Study, in: Materials Science Forum, Trans Tech Publ, 2012, pp. 265-268.
[76] S. Aukkaravittayapun, N. Wongtida, T. Kasecwatin, S. Charojrochkul, K. Unnanon, P. Chindaudom, Large scale F-doped SnO 2 coating on glass by spray pyrolysis, Thin Solid Films, 496 (2006) 117-120.
[77] S. Rozati, T. Ganj, Transparent conductive Sn-doped indium oxide thin films deposited by spray pyrolysis technique, Renewable Energy, 29 (2004) 1671-1676.
[78] K. Noda, H. Sato, H. Itaya, M. Yamada, Characterization of Sn-doped In2O3 film on roll-to-roll flexible plastic substrate prepared by DC magnetron sputtering, Japanese journal of applied physics, 42 (2003) 217.
[79] K.-S. Kim, S.-Y. Yoon, W.-J. Lee, K.H. Kim, Surface morphologies and electrical properties of antimony-doped tin oxide films deposited by plasma-enhanced chemical vapor deposition, Surface and Coatings technology, 138 (2001) 229-236.
[80] M. El-Nahass, A. Atta, M.A. El-Raheem, A. Hassanien, Structural and optical properties of DC Sputtered Cd 2 SnO 4 nanocrystalline films, Journal of Alloys and Compounds, 585 (2014) 1-6.
[81] R. Kumaravel, K. Ramamurthi, Structural, optical and electrical properties of In-doped Cd 2 SnO 4 thin films by spray pyrolysis method, Journal of Alloys and Compounds, 509 (2011) 4390-4393.
[82] Z. Remes, M. Vanecek, H. Yates, P. Evans, D. Sheel, Optical properties of SnO2: F films deposited by atmospheric pressure CVD, Thin Solid Films, 517 (2009) 6287-6289.
[83] M. Avinun, N. Barel, W. Kaplan, M. Eizenberg, M. Naik, T. Guo, L. Chen, R. Mosely, K. Littau, S. Zhou, Nucleation and growth of CVD Al on different types of TiN, Thin Solid Films, 320 (1998) 67-72.
[84] E. Bacaksiz, S. Aksu, S. Yılmaz, M. Parlak, M. Altunbaş, Structural, optical and electrical properties of Al-doped ZnO microrods prepared by spray pyrolysis, Thin Solid Films, 518 (2010) 4076-4080.

[85] W. Yang, Z. Liu, D.-L. Peng, F. Zhang, H. Huang, Y. Xie, Z. Wu, Room-temperature deposition of transparent conducting Al-doped ZnO films by RF magnetron sputtering method, Applied Surface Science, 255 (2009) 5669-5673.
[86] T. Minami, T. Yamamoto, T. Miyata, Highly transparent and conductive rare earth-doped ZnO thin films prepared by magnetron sputtering, Thin Solid Films, 366 (2000) 63-68.
[87] Q. Yu, J. Li, H. Li, Q. Wang, S. Cheng, L. Li, Fabrication, structure, and photocatalytic activities of boron-doped ZnO nanorods hydrothermally grown on CVD diamond film, Chemical Physics Letters, 539 (2012) 74-78.
[88] Q.-B. Ma, Z.-Z. Ye, H.-P. He, J.-R. Wang, L.-P. Zhu, B.-H. Zhao, Substrate temperature dependence of the properties of Ga-doped ZnO films deposited by DC reactive magnetron sputtering, Vacuum, 82 (2007) 9-14.
[89] D. Kim, I. Yun, H. Kim, Fabrication of rough Al doped ZnO films deposited by low pressure chemical vapor deposition for high efficiency thin film solar cells, Current Applied Physics, 10 (2010) S459-S462.
[90] J. Zhong, S. Muthukumar, Y. Chen, Y. Lu, H. Ng, W. Jiang, E. Garfunkel, Ga-doped ZnO single-crystal nanotips grown on fused silica by metalorganic chemical vapor deposition, Applied Physics Letters, 83 (2003) 3401-3403.
[91] K. Satoh, Y. Kakehi, A. Okamoto, S. Murakami, F. Uratani, T. Yotsuya, Influence of oxygen flow ratio on properties of Zn2SnO4 thin films deposited by RF magnetron sputtering, Japanese journal of applied physics, 44 (2004) L34.
[92] E. Leja, T. Stapiński, K. Marszałek, Electrical and optical properties of conducting n-type Cd2SnO4 thin films, Thin Solid Films, 125 (1985) 119-122.

Effect of substrate temperatures

II.1 Introduction

Tin oxide (SnO_2) is a non-stoichiometric semiconductor with a wide bandgap ($E_g \geq 3.1$ eV) at room temperature with tetragonal structure[1]. SnO_2 films have unique characteristics such as low cost, low resistivity, high transmittance in the visible wavelength region, and high chemical and thermal stabilities compared to other transparent conductive oxides (TCOs) [2]. SnO_2 films are widely used in optoelectronic applications, heat mirror coatings, photocatalysis, organic light emitting diodes, gas sensors, solar energy collectors and so on [3-8]. There are several methods for preparing SnO_2 films: The screen printing technique[9], chemical vapor deposition[10], reactive evaporation [11] , dc and rf sputtering[12] and pulsed laser ablation[13] , thermal evaporation [14], electron beam evaporation [15], metal–organic deposition[16], sol–gel deposition[17]and spray pyrolysis[18]. Among these methods, thermal evaporation has the advantages of producing high purity crystalline products and durable films in a single step. Various parameters such as annealing temperature, deposition rate, oxygen partial pressure and substrate temperature have a significant influence on characteristics of SnO_2 films. Among these parameters, substrate temperature has a major role in decreasing the intrinsic stress, increasing the mobility of charge carriers, and improving homogeneity and crystallinity of films to get better quality films. To the best of our knowledge, not much attention has been paid to the study of the substrate temperature effect on characteristics of undoped SnO_2 thin films deposited by spray ultrasonic.

In this work, the structural, optical and electrical properties of SnO_2 thin films deposited on glass substrates at various deposition temperatures by spray ultrasonic have been investigated using X-ray diffraction (XRD),

UV–visible spectrophotometer and a conventional four-point probe technique.

II.2Experimental details

SnO_2 films were ultrasonically deposited on a glass substrate heated between 400–500 °C. As a precursor for tin, used in this work, was a 99.99% pure stannous chloride ($SnCl_2$ $2H_2O$) dissolved in double distilled water and methanol (volume ratio1:1) with adding few drops of (HCl). The precursor concentration was (0.1 M). The later was stirred at room temperature (rt) for half an hour to yield a clear and transparent solution. The blend so obtained was used as a stock solution for spray ultrasonic. An R217102 microscopic glass slide in a size of (75 x 25 x 1.1 mm^3) was used as substrates. Those substrates were cleaned with alcohol in an ultrasonic bath and distilled water then blow-dried with dry nitrogen gas. The substrate temperature was varied between 400–500 °C and steeped by 20 °C[19]. To read and control the substrate temperature a Chromel–Alumel and K type thermocouple were used. The time deposition was maintained 3 min for each experiment. After deposition, the films were allowed to cool down naturally to room temperature.

II.3 Film Characterizations

The structural properties of the film were investigated using X-ray Diffractometer (XPERT-PRO X-ray Diffractometer system under 30 kV, 30 mA conditions) equipped with X'Pert High Score under Cu K_α (k = 1.5406 Å) radiation in the scanning range of (2θ) between 20-90°. The grain size of the films was estimated using X'Pert High Score. The optical

transmission spectra were obtained using a UV-visible spectrophotometer (Shimadzu, Model 1800) and measured in the range of 300-900 nm; whereas the different optical parameters such as the bandgap, Urbach energy, electron plasma frequency and film thickness were determined using data and fitting of the transmission spectrum. The resistivity of thin films was characterized using four point probe method on 1x1 cm^2 sample sheet. All measurements were carried out at room temperature (rt).

II.4Results and discussion

II.4.1 X-ray diffraction studies

The XRD patterns of SnO_2 thin films deposited at various substrate temperatures are shown in (Fig. II.1). As it can be seen the diffraction peaks were observed at 2θ = 26.65°, 33.939°, 38.035°, 51.771°, 54.7124°, 61.886°, 65.898° and 78.597° which are related to the following plans (110), (101), (200), (211), (220), (310), (301) and (321) respectively. The obtained XRD spectra matched well with the space group P42mnm[1] according to JCPDS (No. 41-1445) of the tetragonal, rutile SnO_2structure and indicated the polycrystalline nature of the thin films; the tin dioxides thin films deposited at temperature down to 420 °C were partially crystalline in nature [20] and they contain (101) SnO peak according to JCPDS (No. 06-395) this peak is signalized by a start (*) in Fig. II.1. It is worth noting that the crystallinity was increased as the substrate temperature increases (peak intensities) from 420 °C to 500 °C, indicating the formation of more crystallites with well-defined orientation along (110) plane and some other less prominent peaks such as (200) and (211) planes which were also present in the XRD

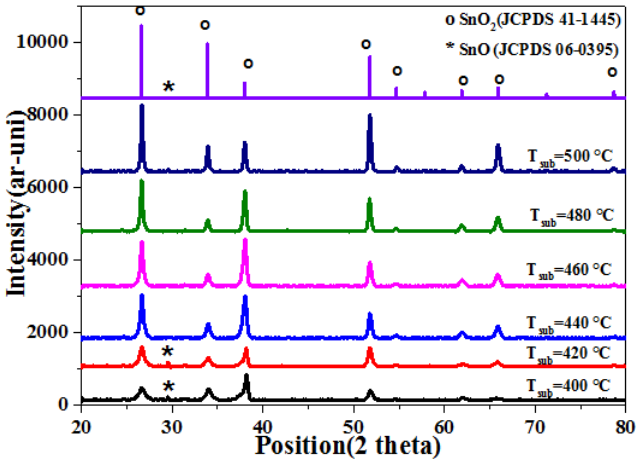

Fig. II.1. XDR patterns of undoped SnO_2 thin films with different substrate temperatures.

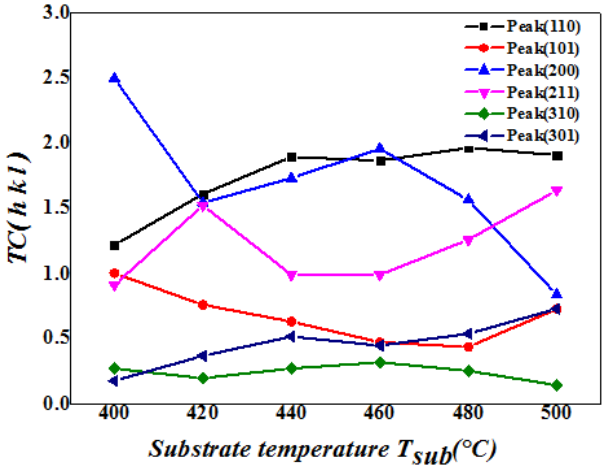

Fig. II.2. Variation of *TC*(*hkl*) with different substrate temperatures in SnO_2thin films.

patterns (Fig. II.1). The increase in crystallinity with substrate temperature is may be due to the optimum rate of supply of thermal energy for recrystallization with substrate temperature as reported by Nikale et al.[21].

The texture coefficient *TC(hkl)*represents the texture of the particular plane, deviation of which from unity implies the preferred growth. The different texture coefficient *TC(hkl)*have been calculated from the X-ray data using the well-known formula [22]:

$$\boldsymbol{TC(hkl)} = \frac{\boldsymbol{I(hkl)/I_0(hkl)}}{\boldsymbol{N^{-1}\sum_n^N I(hkl)/I_0(hkl)}} \qquad \text{(II.1)}$$

where *I(hkl)*is the measured relative intensity of a plane *(hkl), I_0(hkl)* is the standard intensity of the plane *(hkl)* taken from the JCPDS data, N is the reflection number and n is the number of diffraction peaks. *TC(hkl)* values of all the films for (110), (101), (200), (211), (310) and (301) with increasing substrate temperature are shown in (Fig. II.2). The peaks were less than unity confirming the polycrystalline nature of the films. However, the films deposited up to 480 °C presented a possible oriented growth along the (110) plane direction and with other less oriented growth along the (211) plane as seen in Fig. II.2. It is worth noting that preparation of the (110) surface in vacuum alone always results in an oxygen deficient surface [23], the (110) surface exhibits the lowest energy surface followed by the (211), and (200) surfaces.

The lattice constant ‘a’ and ‘c’, for the tetragonal phase structure is determined by the relation[24]:

$$2d_{hkl}\sin(\theta) = n\lambda \quad \text{and} \quad \frac{1}{d_{hkl}^2} = \frac{h^2+k^2}{a^2} + \frac{l^2}{c^2} \qquad \text{(II.2)}$$

where ‘d’ is the interplaner distance and (hkl) are Miller indices, respectively. The lattice constants a and c are calculated and given in Table II.1. The lattice constant a and c first increase to reach a maximum value at around 480 °C and then decrease. It was observed that lattice constants a and c calculated for 480 °C match well with the standard JCPDS data card [1]. The variation in lattice constant (Δa and Δc) for the spray-deposited thin film over the bulk clearly suggests that the film grains are strained, which may be due to the nature and concentration of the native imperfections changing (oxygen vacancies, vacancy clusters, and local lattice disorders) [25].

The average nanoparticles crystallite size of SnO_2, with a varying substrate temperature, was determined from XRD broadening using the Williamson–Hall formula [26]:

$$\frac{\beta cos\theta}{\lambda} = \frac{0.9}{D} + \varepsilon\frac{sin\theta}{\lambda} \qquad \text{(II.3)}$$

Table II.1: Crystallite size D, dislocation density d, strain ε, and lattice parameters a and c of undoped SnO_2 thin films with different substrate temperatures.

T_{sub} (°C)	D nm	δx10^{15} (lines/m^2)	ε x10^{-3}	Lattice constants (Å)			
				a	Δa	c	Δc
400	6.52	23.51	-27	4.722	-0.015	3.173	-0.013
420	8.23	14.75	-18	4.725	-0.012	3.179	-0.007
440	13.27	5.67	-7	4.724	-0.013	3.179	-0.007
460	15.52	4.15	-4	4.727	-0.010	3.180	-0.006
480	20.27	2.43	-2	4.731	-0.006	3.184	-0.002
500	29.80	1.12	-1	4.724	-0.013	3.183	-0.003

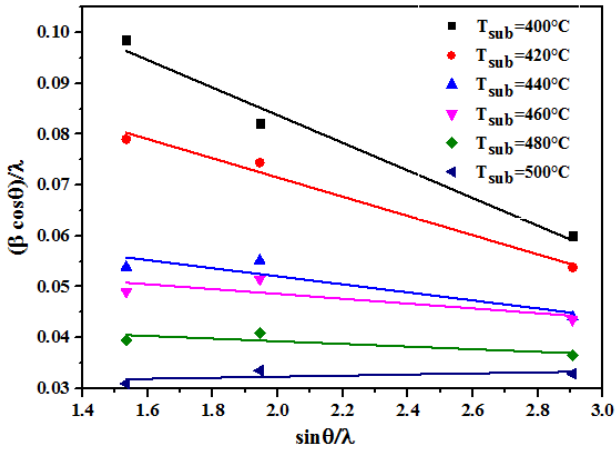

Fig. II.3. Williamson–Hall plots of undoped SnO_2thin films with different substrate temperatures.

where λ is the wavelength of X-ray radiation, β is the full width at half maximum of the peak at diffraction angle θ [27] and the average crystallite sizes were found to be in the range of 6.52–29.80 nm and increases with increasing substrates temperature. The increase may due to non-uniform stress or strain during the grain growth or to the existence of local structural disorder in the material. In fact, the growth mechanism involving

dislocation is a matter of importance. Dislocations are imperfect in a crystal associated with the miss-registry of the lattice in one part of the crystal with respect to another part. Unlike, vacancies and interstitials atoms, dislocations are not equilibrium imperfections i.e., thermodynamic considerations are insufficient to account for their existence in the observed dislocation densities [28]. In our case, dislocation density (d) was determined using the relation [29] as given below:

$$\boldsymbol{\delta = \frac{1}{D^2}} \qquad \text{(II.4)}$$

The calculated dislocation density (δ) was given in Table II.1. It was observed that d decreases with increasing substrate temperatures from 400 °C to 500 °C and having accordance with the lattice constant a, c and microstrain tendency, as seen in Table II.1.

The effective lattice strain, of the present synthesized SnO_2 nanoparticles, was calculated by using Williamson–Hall equation [26]:

$$\boldsymbol{\frac{\beta cos\theta}{\lambda} = \frac{0.9}{D} + \varepsilon \frac{sin\theta}{\lambda}} \qquad \text{(II.5)}$$

where β is the full-width at the half maximum (FWHM) of the diffraction peak, θ is the Bragg angle, λ is the wavelength of X-ray used, D is the average crystallite size and ε is the effective lattice strain.

The effective lattice strain calculated by using the above equation was plotted in (Fig. II.3). The slope of the straight line of (β cos θ / λ) vs. (sin θ / λ) represents the effective strain. The average crystallite size, lattice

parameters and strain values obtained from the XRD pattern and Williamson–Hall plots are given in Table II.1. The negative value of strain implies a compressive strain in lattice [26, 30].

II.4.2 Optical transmission and optical band gap

Fig. II.4 shows the variation of transmittance with respect to the wavelength of SnO_2 thin films deposited at various substrate temperatures. The average transmission in the visible region has been found to be ranging from 43.8% to 66% depending upon the substrate temperature. An increase in transmission is observed with increase in temperature. At lower temperatures, i.e. at 400 °C, relatively lower transmission is well remarked which is due to the formation of milky films and that is because of incomplete decomposition of the sprayed droplets. The relatively higher transmittance of about 75% at more than 800 nm for films prepared at 480 °C has been observed. A drastic decrease in transparency is located between 300–360 nm revealing the region of the absorption edge in the layers due to the transition between the valence band and the conduction band (optical band gap: Eg); in this region, the transmission decreases because of the onset fundamental absorption. The band gap (Eg) values of pure SnO_2 were deduced from the transmittance data according to Tauc's relation [31] giving $(\alpha h\nu)^2$ versus incident photon energy, $(h\nu)$, plots. The graphs are represented in (Fig. II.5). The band gap energy values, as shown in Table II.2, were found to be ranged in 4.03–4.133 eV for SnO_2 thin films with increasing the substrate temperature from 400 to 500 °C. These results are in good agreement with that obtained ones from bulk SnO_2 [32, 33]. More investigations will be taken below using Urbach energy.

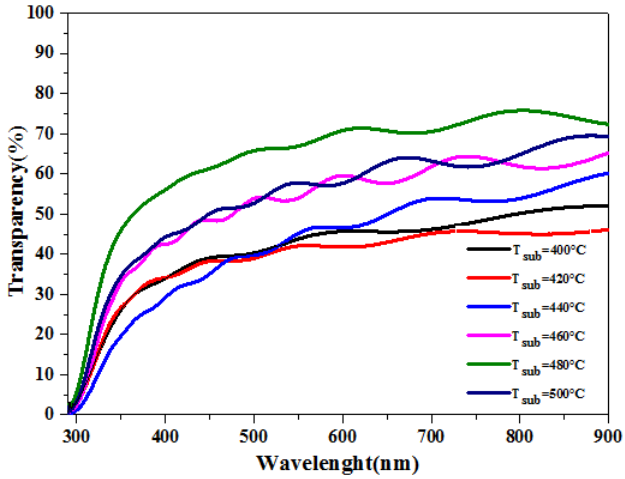

Fig. II.4. Spectral transmittance plots of undoped SnO_2 thin films with different substrate temperatures.

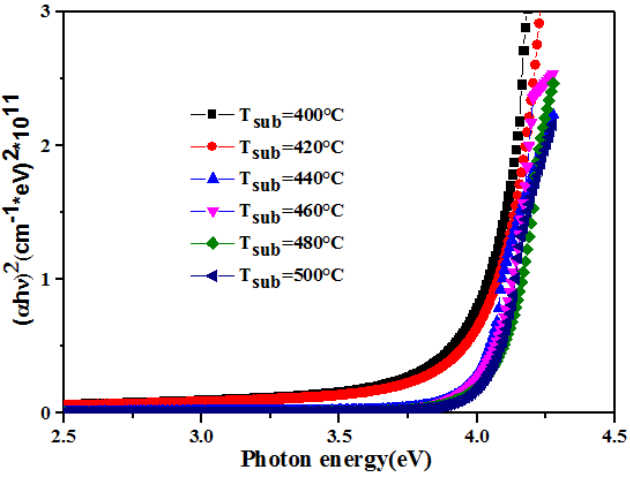

Fig. II.5. Band-gap (E_g) estimation from Tauc's relation of undoped SnO_2thin films with different substrate temperatures.

Table II.2: Optical gap (E_g), Urbach energy (E_u), refractive index(n), Permittivity (ε_L), number of free electrons N, and Plasma frequency ω_p with different substrate temperatures.

T_{sub} (°C)	Thickness (nm)	E_g (eV)	E_u (meV)	n	ε_L	$n_e x10^{+19}$ cm^{-3}	ω_p Hz
400	446	4.0303	328.45	1.937	3.643	5.259	4.09
420	600	4.1328	290.61	1.823	3.228	4.489	3.78
440	716	4.0120	189.37	1.963	3.745	5.460	4.17
460	788	4.1327	192.66	1.903	3.521	5.011	3.99
480	696	4.1328	203.68	1.755	2.994	4.221	3.66
500	707	4.0716	182.01	1.905	3.526	5.025	4.00

At lower values of the absorption coefficient a (i.e. near the band edge), the extent of the exponential tail of the absorption edge is characterized by the Urbach energy ($\boldsymbol{E_u}$) indicating the width of band tails of the localized states within the optical band gap and is given by [34]:

$$\boldsymbol{\alpha = \alpha_0 exp\left(\frac{h\nu}{E_u}\right)} \qquad \text{(II.6)}$$

where α_0 and E_u are respectively a constant and width of the band tail of localized states at the optical band gap. E_u is also known as band tail width and is due to the disorder in the thin film material. The variation of bond length and bond angle from their standard value in the crystalline material is called disorder[35]. The Urbach energy of prepared SnO_2 thin films

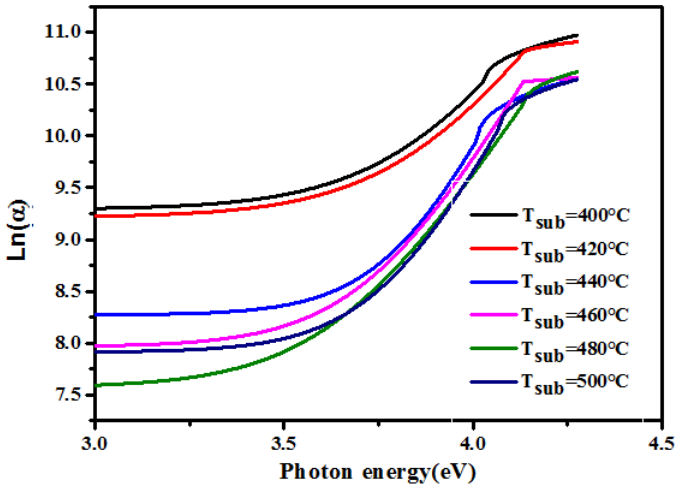

Fig. II.6. Urbach energy (E_u) estimation of undoped SnO_2thin films with different substrate temperatures.

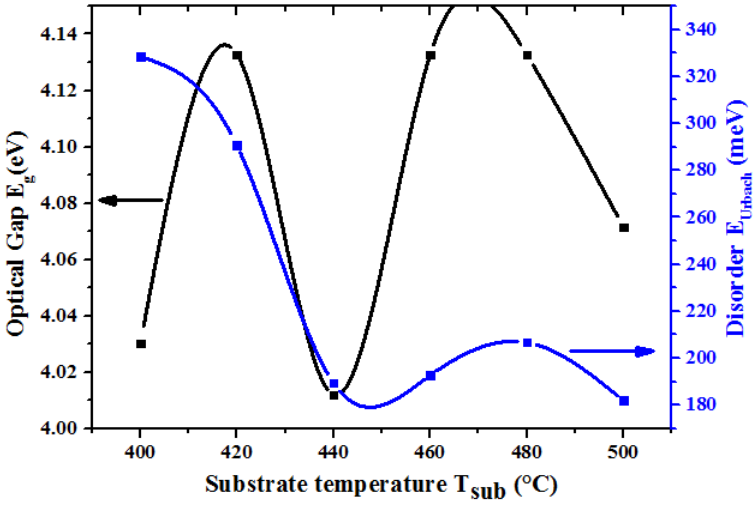

Fig. II.7. Variation of Band-gap (E_g) and Urbach energy (E_u) for undoped SnO_2thin films as functions substrate temperatures.

depends on the structural defects, dislocations density and some defects of the vacancy and interstitial states in the films [36]. It can be determined from the reciprocal gradient of the linear portion of ln(α) versus (hν) plots. Fig. II.6 shows the Urbach energy plot of SnO_2 thin films with substrate temperature. From Table II.2 one can that Eu decreases from 328 to 182 meV. This decrease in Urbach energy with increasing substrate temperature is due to the disappearance of localized states[37]and highlighting the correlation of E_u with a decrement in energy band gap (see Fig. II.7). It also correlates with the improvement in crystallinity of films observed from XRD results.

Lattice dielectric constant ($\boldsymbol{\varepsilon_L=n^2}$) can be evaluated from the mathematical equation which is associated with the refractive index (***n***) and wavelength ($\boldsymbol{\lambda}$) and it is given by the following equation[38]:

$$\boldsymbol{\varepsilon = n^2 = \varepsilon_L - \left(\frac{e^2 n_e}{4\pi^2 c^2 \varepsilon_0 m^*}\right)\lambda^2} \qquad \text{(II.7)}$$

where $\boldsymbol{\varepsilon_L}$ is the lattice dielectric constant, ***e*** is the electronic charge, ***c*** is the velocity of light, $\boldsymbol{n_e}$ the free carrier concentration, ***m**** the effective mass of the charge carriers and $\boldsymbol{\varepsilon_0}$ is free space dielectric constant ($8.854\text{x}10^{-12}$ F/m) [39, 40]. The nature of the dispersion of $\varepsilon_L = n^2$ as a function of wavelength (λ^2) for different substrate temperatures is shown in (Fig. 8). The values extracted from the intercept and slope gives the amount of $\boldsymbol{\varepsilon_L}$ and $\boldsymbol{n_e}$ respectively and they are shown in Table II.2. With increasing substrate temperature it was found that both ε_L and $\boldsymbol{n_e}$ exhibit a little fluctuation, as shown in the insert of Fig. II.8. $\boldsymbol{n_e}$ fluctuated around 5.10^{+19} cm^{-3}, which may be due to the interaction between the free carrier and low

lattice phonon. It is worth noting that n_e estimated from the above law leads to predict that, in SnO_2 material, the effective density of conduction band states is about 5.10^{+19} cm^{-3} as a minimum limit.

Plasma frequency (ω_p) is the characteristic frequency at which the material response changes from metallic to dielectric behavior. It is given by the relation:

$$\omega_p^2 = \frac{e^2 n_e}{\varepsilon_0 m^*} \qquad \text{(II.8)}$$

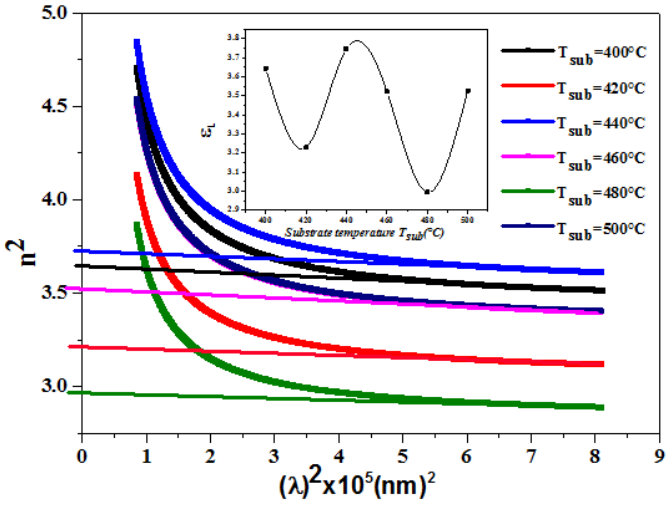

Fig. II.8. Plots of n^2 versus (λ^2) of undoped SnO_2 thin films for different substrate temperatures. Insert represent the variation of the lattice dielectric constant ε_L as functions substrate temperatures.

The plasma resonance frequency (ω_p) of all electrons involved in the optical transitions was calculated using the above relation and the values are reported in Table II.2. Plasma frequency (ω_p), which was estimated from the above law was about 4.10^{14} Hz of the elaborated SnO_2 thin films.

II.4.3 Electrical conductivity

Fig. II.9 shows the plot of films resistivity (ρ) and crystallite size D as a function of substrate temperature. As can be seen from 420 °C slight increase in resistivity then decreases to reach $9.19x10^{-3}\Omega.cm$, for the sample deposited at 480 °C, which is comparable to the reported one[40] and increases again (see Table II.3). Initially, with an increase in temperature up to 480 °C, the thickness increases (see Table II.2) leading to decreases in resistivity. Furthermore, 480 °C the resistivity increases again even thought the thickness remains constant which means that the resistivity and the thin films thickness are not inverted whereas the crystallite size D increases from 6 to 29.8 nm with increasing temperature in the considered average.

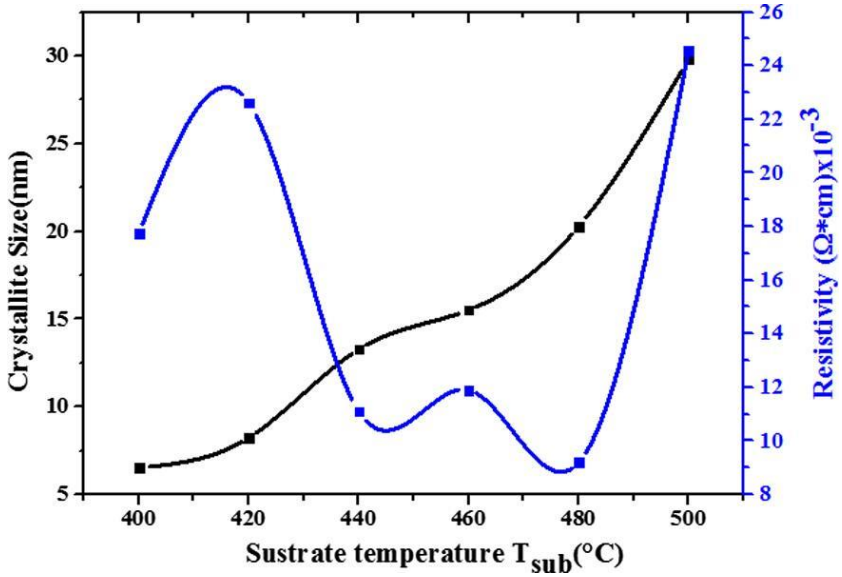

Fig. II.9. Plots of resistivity and crystallite size of undoped SnO_2thin films with different substrate temperatures.

Table II.3: Sheet resistance (R_{sh}) and Resistivity (**ρ**) with different substrate temperatures.

Substrate temp (°C)	Sheet resistance $R_{sh}(\Omega)$	Resistivity ρ (Ω*cm)10^{-3}
400	397.76	17.75
420	376.72	22.62
440	154.96	11.10
460	150.96	11.89
480	132.05	9.19
500	347.31	24.55

Under the optics of crystallite size D of the films at the average temperature lower than 420 °C; hence D (6–8 nm) is not higher than the mean free path l of the electron in SnO_2 materials (l = 4 nm) as given by Prins et al.[41] one can consider that the porters diffusion is limited by grain size leading to the high resistivity of the films. Whereas the films prepared at 440–480 °C had low R_{sh} leading to low resistivity owing to their considerable crystallite size (D = 13.27–20.27 nm) which is higher than the mean free path l of the electron in SnO_2 materials, the porters diffusion is not limited by grain size yielding to low resistivity. Beyond 480°C it was mentioned that the growth of the films has (110) surface as preferred one leading to out-diffused oxygen. This out-diffusion of oxygen (oxygen vacancies) leads to an increase in surface defect concentration[42] (i.e. a decrease in surface conductivity); as consequence an increase in resistivity (sheet resistance) was expected which was observed in the case of the sample elaborated at 500 °C even thought the increase in grain size (D = 29.8 nm) .

II.5.Conclusions

In this work, we have reported the preparation and characterization of the SnO_2 thin films ultrasonically sprayed onto heated microscopic glass substrates. The thin films were deposited on glass at large scale of temperature ranged in 400–500 °C and stepped by 20 °C. The effect of substrate temperature on structural, electrical and optical properties was studied using X-ray diffraction (XRD), UV–visible spectrophotometer and a conventional four-point probe technique. XRD showed that all the films were polycrystalline with major reflex along (110) plane and minimum

surface energy, manifested with amelioration of grain size from 6.51 to 29.80 nm upon increasing substrate temperature. Lattice constant ‘a’, ‘c’, microstrains and dislocation densities were affected by the substrate temperature. The transmittance of about 75% at more than 800 nm for films prepared at 480 °C has been observed. With increasing the substrate temperature the direct band gap energy was averaged in 4.03–4.133 eV. Plasma frequency ($\boldsymbol{\omega_p}$) of the elaborated thin films revealing the change from metallic to dielectric response was estimated to be 4.10^{14} Hz whereas the optically deduced number of free electrons $\boldsymbol{n_e}$ leads to predict that, in SnO_2 material, the effective density of conduction band states was round 5.10^{+19} cm^{-3}. Among all the samples the film that deposited at 480 °C exhibited the lowest resistivity of about $9.19x10^{-3}\Omega.cm$.

References

[1] G.J. McCarthy, J.M. Welton, X-ray diffraction data for SnO 2. An illustration of the new powder data evaluation methods, Powder Diffraction, 4 (1989) 156-159.
[2] A. Benhaoua, A. Rahal, B. Benhaoua, M. Jlassi, Effect of fluorine doping on the structural, optical and electrical properties of SnO 2 thin films prepared by spray ultrasonic, Superlattices and Microstructures, 70 (2014) 61-69.
[3] I. Kim, J. Ko, D. Kim, K. Lee, T. Lee, J.-H. Jeong, B. Cheong, Y.-J. Baik, W. Kim, Scattering mechanism of transparent conducting tin oxide films prepared by magnetron sputtering, Thin Solid Films, 515 (2006) 2475-2480.
[4] Y.-M. Lu, C.-P. Hu, The colored and bleached properties of tungsten oxide electrochromic films with different substrate conductivities, Journal of Alloys and Compounds, 449 (2008) 389-392.
[5] S.S. Srinivasan, J. Wade, E.K. Stefanakos, Y. Goswami, Synergistic effects of sulfation and co-doping on the visible light photocatalysis of TiO 2, Journal of Alloys and Compounds, 424 (2006) 322-326.
[6] B. Thangaraju, Structural and electrical studies on highly conducting spray deposited fluorine and antimony doped SnO 2 thin films from SnCl 2 precursor, Thin solid films, 402 (2002) 71-78.
[7] D. Vaufrey, M.B. Khalifa, M. Besland, C. Sandu, M. Blanchin, V. Teodorescu, J. Roger, J. Tardy, Reactive ion etching of sol–gel-processed SnO 2 transparent conducting oxide as a new material for organic light emitting diodes, Synthetic Metals, 127 (2002) 207-211.
[8] M.-R. Yang, S.-Y. Chu, R.-C. Chang, Synthesis and study of the SnO 2 nanowires growth, Sensors and Actuators B: Chemical, 122 (2007) 269-273.
[9] S. Peng, F. Cheng, J. Liang, Z. Tao, J. Chen, Facile solution-controlled growth of CuInS 2 thin films on FTO and TiO 2/FTO glass substrates for photovoltaic application, Journal of Alloys and Compounds, 481 (2009) 786-791.
[10] E. Fortunato, D. Ginley, H. Hosono, D.C. Paine, Transparent conducting oxides for photovoltaics, MRS bulletin, 32 (2007) 242-247.
[11] J. Berry, D. Ginley, P.E. Burrows, Organic light emitting diodes using a Ga: ZnO anode, Applied Physics Letters, 92 (2008) 170.
[12] K. Omura, P. Veluchamy, M. Tsuji, T. Nishio, M. Murozono, A Pyrosol Technique to Deposit Highly Transparent, Low-Resistance SnO2:

F Thin Films from Dimethyltin Dichloride, Journal of The Electrochemical Society, 146 (1999) 2113-2116.
[13] A. Moholkar, S. Pawar, K. Rajpure, C. Bhosale, J. Kim, Effect of fluorine doping on highly transparent conductive spray deposited nanocrystalline tin oxide thin films, Applied Surface Science, 255 (2009) 9358-9364.
[14] A. Banerjee, K. Chattopadhyay, Recent developments in the emerging field of crystalline p-type transparent conducting oxide thin films, Progress in Crystal Growth and Characterization of Materials, 50 (2005) 52-105.
[15] N. Shaalan, T. Yamazaki, T. Kikuta, Influence of morphology and structure geometry on NO 2 gas-sensing characteristics of SnO 2 nanostructures synthesized via a thermal evaporation method, Sensors and Actuators B: Chemical, 153 (2011) 11-16.
[16] A.F. Khan, M. Mehmood, M. Aslam, M. Ashraf, Characteristics of electron beam evaporated nanocrystalline SnO 2 thin films annealed in air, Applied Surface Science, 256 (2010) 2252-2258.
[17] T. Tsuchiya, K. Daoudi, I. Yamaguchi, T. Manabe, T. Kumagai, S. Mizuta, Preparation of tin oxide films on various substrates by excimer laser metal organic deposition, Applied surface science, 247 (2005) 145-150.
[18] W. Hamd, Y. Wu, A. Boulle, E. Thune, R. Guinebretière, Microstructural study of SnO 2 thin layers deposited on sapphire by sol–gel dip-coating, Thin Solid Films, 518 (2009) 1-5.
[19] R. Kasar, N. Deshpande, Y. Gudage, J. Vyas, R. Sharma, Studies and correlation among the structural, optical and electrical parameters of spray-deposited tin oxide (SnO 2) thin films with different substrate temperatures, Physica B: Condensed Matter, 403 (2008) 3724-3729.
[20] J. Melsheimer, D. Ziegler, Band gap energy and Urbach tail studies of amorphous, partially crystalline and polycrystalline tin dioxide, Thin Solid Films, 129 (1985) 35-47.
[21] V. Nikale, N. Gaikwad, K. Rajpure, C. Bhosale, Structural and optical properties of spray-deposited CdIn 2 Se 4 thin films, Materials chemistry and physics, 78 (2003) 363-366.
[22] P. Paufler, CS Barrett, TB Massalski. Structure of Metals. Pergamon Press Oxford, New York, Toronto, Sydney, Paris Frankfurt/M 1980 654 Seiten, 113 Abbildungen, 19 Tabellen und über 1400 Literaturhinweise. Preis US $20.–, Crystal Research and Technology, 16 (1981) 982-982.
[23] M. Batzill, U. Diebold, The surface and materials science of tin oxide, Progress in surface science, 79 (2005) 47-154.

[24] C. Marcel, N. Naghavi, G. Couturier, J. Salardenne, J. Tarascon, Scattering mechanisms and electronic behavior in transparent conducting Zn x In 2 O x+ 3 indium–zinc oxide thin films, Journal of applied physics, 91 (2002) 4291-4297.
[25] C. Agashe, M. Takwale, B. Marathe, V. Bhide, Correlation between the structural and electrical transport properties of SnO 2 films, Journal of Materials Science, 24 (1989) 2628-2636.
[26] G. Williamson, W. Hall, X-ray line broadening from filed aluminium and wolfram, Acta metallurgica, 1 (1953) 22-31.
[27] B.D. Cullity, Answers to Problems: Elements of X-ray Diffraction, Addison-Wesley Publishing Company, 1978.
[28] D.P. Joseph, P. Renugambal, M. Saravanan, S.P. Raja, C. Venkateswaran, Effect of Li doping on the structural, optical and electrical properties of spray deposited SnO 2 thin films, Thin Solid Films, 517 (2009) 6129-6136.
[29] G. Williamson, R. Smallman, III. Dislocation densities in some annealed and cold-worked metals from measurements on the X-ray debye-scherrer spectrum, Philosophical Magazine, 1 (1956) 34-46.
[30] L.J. Kennedy, P. Magesan, J.J. Vijaya, M. Umapathy, U. Aruldoss, Biominerals doped nanocrystalline nickel oxide as efficient humidity sensor: A green approach, Materials Science and Engineering: B, 190 (2014) 13-20.
[31] J. Tauc, Amorphous and Liquid Semiconductors, Plenum, London, (1974).
[32] K. Chopra, S. Major, D. Pandya, Transparent conductors—A status review, Thin solid films, 102 (1983) 1-46.
[33] W. Spence, The UV absorption edge of tin oxide thin films, Journal of Applied Physics, 38 (1967) 3767-3770.
[34] F. Urbach, The long-wavelength edge of photographic sensitivity and of the electronic absorption of solids, Physical Review, 92 (1953) 1324.
[35] C. Lokhande, K. Gadave, Chemical deposition of MnS thin films from thiosulphate bath, Turk. J. Phys, 18 (1994) 83-87.
[36] F. Al-Shaikley, Electrical and optical properties dependence on annealing temperature for CdS thin films, Indian J. Appl. Res, 3 (2013) 544-548.
[37] S.J. Ikhmayies, R.N. Ahmad-Bitar, An investigation of the bandgap and Urbach tail of spray-deposited SnO2: F thin films, Physica Scripta, 84 (2011) 055801.
[38] M. El-Den, M. El-Nahass, Optical properties of AsSe 1.5− x Te x glassy system, Optics & Laser Technology, 35 (2003) 335-340.

[39] T.S. Moss, G.J. Burrell, B. Ellis, Semiconductor opto-electronics, Butterworth-Heinemann, 2013.
[40] M. Bender, J. Trube, J. Stollenwerk, Deposition of transparent and conducting indium-tin-oxide films by the rf-superimposed DC sputtering technology, Thin Solid Films, 354 (1999) 100-105.
[41] M. Prins, K.-O. Grosse-Holz, J. Cillessen, L. Feiner, Grain-boundary-limited transport in semiconducting SnO 2 thin films: Model and experiments, Journal of applied physics, 83 (1998) 888-893.
[42] J. Erickson, S. Semancik, Surface conductivity changes in SnO2 (110): Effects of oxygen, Surface science, 187 (1987) L658-L668.

Effect of tin precursor concentration

III.1. Introduction

Tin oxide (SnO_2) is a semiconductor with a wide bandgap (Eg ≥3.1 eV) at room temperature with tetragonal structure[1]. SnO_2 is widely used in optoelectronic applications, heat mirror coatings. In thin films structure, tin oxide has unique characteristics such as high transmittance in visible wavelength region low resistivity, low cost, and high chemical and thermal stabilities compared to other transparent conductive oxides (TCOs). It also employed in photocatalysis, gas sensors, organic light emitting diodes and solar energy collectors [2-7]. There are several methods for preparing SnO_2thin films [8-17]. Among these methods, ultrasonically deposition has the advantages of producing high purity crystalline products and durable films in a single step. Various parameters such as substrate temperature deposition [18]and partial pressure or positive presence of oxygen have a significant influence on characteristics of SnO_2 films [19]. For instance, free carrier concentrations as high as $3x10^{20}cm^{-3}$ are obtained by vacancy doping which was done by properly adjusting oxygen partial pressure, tin partial pressure, and subsequent annealing conditions. Among these parameters, precursor concentration has a major role in improving films homogeneity and crystallinity. To the best of our knowledge, little attention has been paid to the effect of tin concentration, in the precursor, on SnO_2 thin films characteristics, deposited by spray ultrasonic. Hence kinetic reactions between oxygen and tin occurred at high temperature [20], and leads to SnO_2, the arrival of such elements on the substrate has its effect namely when its concentration was varied. Effect of tin amount concentration, in the precursor solution, on physical properties of SnO_2 thin films is few reported. At my best acknowledgment Muruganantham et al.[21] studies the use of high concentration.

The aim of this work is to investigate the effect of tin amount concentration in precursor solution on the structural, optical and electrical properties of SnO_2 thin films deposited, by spray ultrasonic, on maintained 480°C heated glass substrates. X-ray diffraction (XRD), UV-visible spectrophotometer and conventional four-point probe techniques are used to study the effect of tin concentration, in the starting solution, on SnO_2thin films properties.

III.2. Experimental details

III.2.1 Preparation of solution and SnO_2 thin films

To elaborate undoped SnO_2 thin films, solutions at different molarities concentration were prepared by dissolving pure stannous chloride ($SnCl_2$ $2H_2O$) in a mixture of double distilled water and methanol (volume ratio1:1) with adding few drops of (HCl). Tin concentration of the precursor solution is varied as (0.05, 0.075, 0.1, 0.125, 0.15 and 0.2 M) in solutions and named in the following C_1, C_2, C_3, C_4, C_5 and C_6 respectively. SnO_2 thin films were deposited on 480 °C heated glass substrate [18] by chemical spray ultrasonic technique. The solutions were stirred at room temperature (*rt*) for half an hour to yield a clear and transparency mother precursor. The blend so obtained was used as a stock solution for spray ultrasonic. An R217102 microscopic glass slide was used as substrates. The substrates were cleaned with alcohol in an ultrasonic bath and distilled water. The temperature of the substrates was monitored using a temperature controller with chromel-alumel and K type thermocouple. The time deposition was 3 min for each experiment. After

deposition, the films were allowed to cool down naturally to room temperature.

III.2.2 thin films characterizations

The microstructure of the SnO_2 films was examined by X-ray diffraction measurements (XPERT-PROX-ray Diffractometer system with a 30 kV, 30 mA, Cu K_α radiation with a wavelength of 1.5406Å as operating conditions). The grain size of the films was estimated using X'Pert HighScore. The optical transmission spectra of $SnO_2$and band gap were obtained using a UV-visible spectrophotometer (Shimadzu, Model 1800). On 1x1 cm^2 sample sheet, four-point probe and Hall Effect was done to evaluate electrical sheet resistance carrier concentration and mobility of obtained thin films. All measurements were carried out at room temperature (*rt*).

III.3. Results and discussion

III.3.1 X-ray diffraction studies

The XRD patterns of SnO_2 thin films deposited with a various tin concentration in precursor solution are shown in (Fig.III.1). As it can be seen diffraction peaks were observed at around 2θ = 26.631°, 33.939°, 38.041°, 51.741°, 54.550°,61.791°, 65.931° and 78.600° which are related to the following plans (*110*), (*101*), (*200*), (*211*), (*220*), (*310*), (*301*) and (*321*) matching well with the space group P42mnm according to JCPDS (No. 41-1445) of the tetragonal, rutile SnO_2; whereas the other peaks observed at 2θ =29.53°and 2θ =31.82° are associated to (*101*) and (*111*)

planes of SnO and cubic crystal system of SnO_2 according to JCPDS (No. 06-0395) and (No. 50-1429) [22, 23] respectively. The obtained XRD spectra are an evident indication of the polycrystalline nature of all elaborated thin films. It is worth noting that apparition of SnO_2 cubic phase is more attended in the case of samples elaborated with concentration C_4 than others. This has happened, of course, with complete absence growth along (*110*) of rutile SnO_2as in Fig.III.1. Based on the unit volume and its compacity (5.63% for SnO_2 and 6.95% for SnO) Apparition of SnO phase is more provoked with higher concentrations (C_5 and C_6). Emerged peaks (*200*)/(*111*) with overlap intensities are remarked in the case of concentrations (C_2, C_4, and C_6) with complete absence growth along (*110*) of rutile SnO_2 even thought growth along this direction needs minimum energy. This may be explained by the arrival of more Sn entities than oxygen ones on the substrate during the tin oxide formation which leads to SnO matter instead of SnO_2.

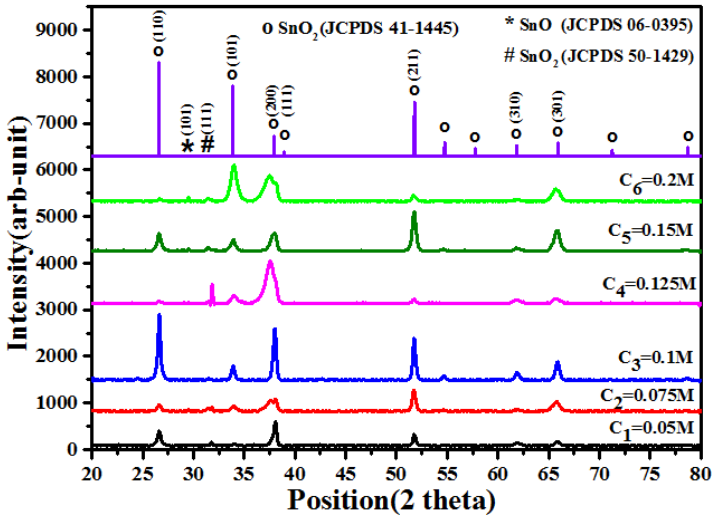

Fig. III.1.XDR patterns of undoped SnO_2 thin films with different tin precursor concentration in solution.

For more details, about the preferred growth, different texture coefficient *TC(hkl)* have been calculated from the X-ray data. The texture coefficient *TC(hkl)* represents the texture of the particular plane, deviation of which from unity implies the preferred growth. *TC(hkl)* coefficients have been evaluated using the well-known formula[24]:

$$\boldsymbol{TC(hkl)} = \frac{\boldsymbol{I(hkl)/I_0(hkl)}}{\boldsymbol{N^{-1}\sum_n^N I(hkl)/I_0(hkl)}} \qquad \text{(III.1)}$$

where *I(hkl)* is the measured relative intensity of a plane *(hkl)*, I_o*(hkl)* is the standard intensity of the plane *(hkl)* taken from the JCPDS data, *n* is the reflection number and *N* is the number of diffraction peaks.*TC(hkl)* values of all thin films for (*110*), (*101*), (*200*), (*211*), (*310*) and (*301*) with varying concentration of tin in precursor are shown in (Fig.III.2). Peaks intensities were less than unity confirming the polycrystalline nature of the films. However, the films deposited using C_4 presented a preferred oriented growth along (*200*) plane direction. It is worth noting that a dominance in *TC*(*hkl*) are remarked: *TC*(*211*) with two concentrations C_2 and C_5, *TC*(*200*) with two concentrations C_1 and C_4 whereas *TC*(*110*) is dominant only for C_3 as previously carried out [18] and finally *TC*(*101*) for C_6 as seen in Fig.III.2.

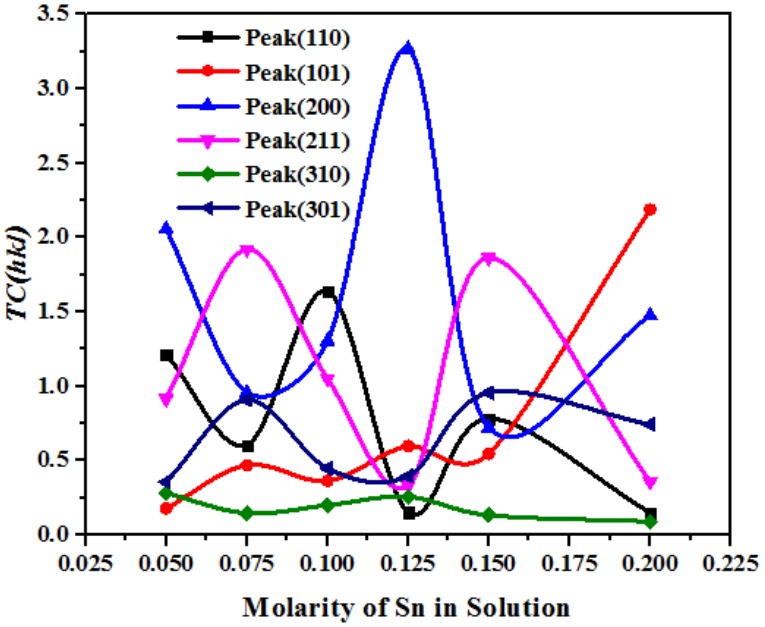

Fig.III.2. Variation of TC(*hkl*) of SnO_2 thin films with different tin precursor concentration in solution.

The lattice constant ‘a’ and ‘c’, for the tetragonal phase structure is determined by the relation [25]:

$$2d_{hkl}\,sin(\theta) = n\lambda \quad \text{and} \quad \frac{1}{d_{hkl}^2} = \frac{h^2+k^2}{a^2} + \frac{l^2}{c^2} \qquad \text{(III.2)}$$

where ‘d’ is the interplaner distance and (*hkl*) are Miller indices, respectively. The lattice constants ‘a’ and ‘c’ are calculated and given in Table III.1 and plotted in (Fig.III.3).

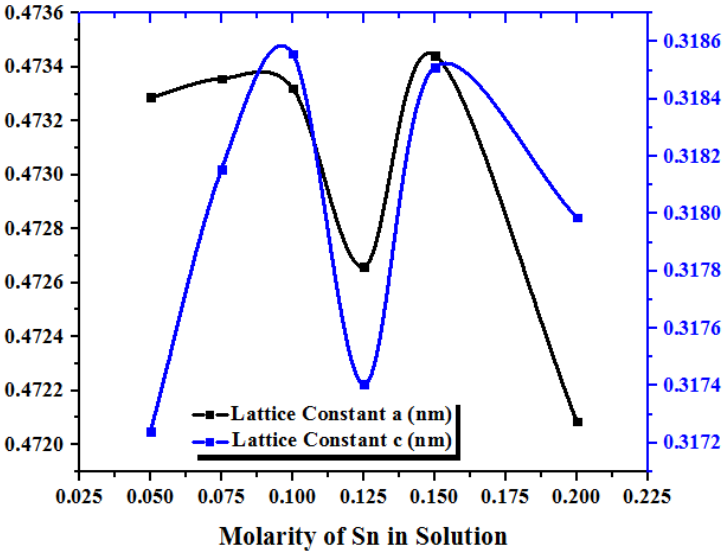

Fig. 3. Variation of lattice parameters of SnO_2 thin films with different tin precursor concentration in solution.

As can be seen a periodic expansion of the lattice parameters reaching its maximum with concentration C_3 and C_5 which means dilatation of the unit cell of SnO_2 matrix. The sample prepared with $C_4$and C_6 exhibits contraction of the unit cell of SnO_2 matrix. This behavior is related to the kinetic formation of SnO_2 product and to crystallite size as it will be seen in the bellowing paragraph.

The average crystallite size (D) of SnO_2 nanoparticles with varying concentrations of tin, in the precursor (C_1, C_2, C_3, C_4, C_5, and C_6), were calculated from XRD data using the Scherer formula[26]:

$$\boldsymbol{D = \frac{0{,}9\lambda}{\beta cos(\theta)}} \qquad \text{(III.3)}$$

where λ is the wavelength of X-ray radiation, β is the full width at half maximum (*FWHM*) of the peak at diffraction angle θ [27] and the average crystallite sizes are calculated and given in Table III.1 and (Fig.III.4). Crystallite size (*D*), in general, decreases gradually as the concentration of tin in solution increases.

Table III.1: unit cell parameters of SnO_2 thin films

Sample	hkl	2θ (°)	Lattice Parameters (nm)	Mean grain size (nm)	Average grain size (nm)
	110	26.626		21.253	
	101	34.008	a = 0.47329	26.742	
C_1=0.050	211	51.783	b = 0.47329	28.795	22.92252
	310	61.945	c = 0.31724	17.872	
	301	65.874		19.951	
	110	26.622		22.039	
	101	33.937	a = 0.47336	17.105	
C_2=0.075	211	51.727	b = 0.47336	24.802	20.08988
	310	61.871	c = 0.31815	22.395	
	301	65.750		14.109	
	110	26.624		27.649	
	101	33.908	a = 0.47332	26.951	
C_3=0.100	211	51.756	b = 0.47332	29.933	26.45637
	310	61.921	c = 0.31855	24.065	
	301	65.874		23.684	
	110	26.662		17.124	
	101	34.010	a = 0.47266	11.789	
C_4=0.125	211	51.745	b = 0.47266	29.472	17.03655
	310	61.893	c = 0.31740	12.905	
	301	65.773		13.892	
	110	26.617		19.195	
	101	33.908	a = 0.47344	17.009	
C_5=0.150	211	51.750	b = 0.47344	23.153	18.93124
	310	61.865	c = 0.31851	19.411	
	301	65.824		15.888	
	110	26.695		22.685	
	101	33.979	a = 0.47208	13.067	
C_6=0.200	211	51.731	b = 0.47208	27.748	17.61595
	310	61.910	c = 0.31798	11.343	
	301	65.748		13.237	

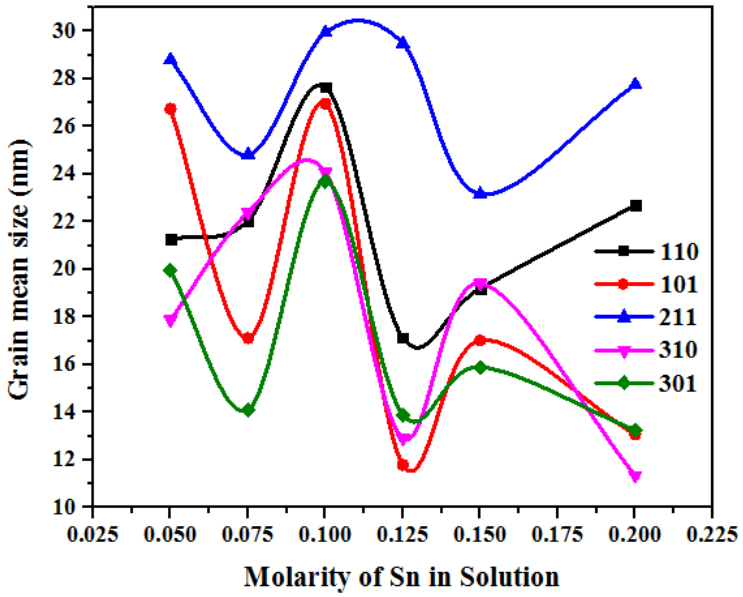

Fig.III.4. Variation of crystallite size of SnO_2 thin films with different tin precursor concentration in the solution.

III.3.2 Optical transmission and optical band gap

In order to have ideas and comparing the transparency of SnO_2 thin films with various concentration of tin in solution, optical spectra of the samples were measured in the UV-visible region (200-900 nm). The optical transparency $T(\lambda)$ of all elaborated SnO_2thin films are shown in Fig.III.5.

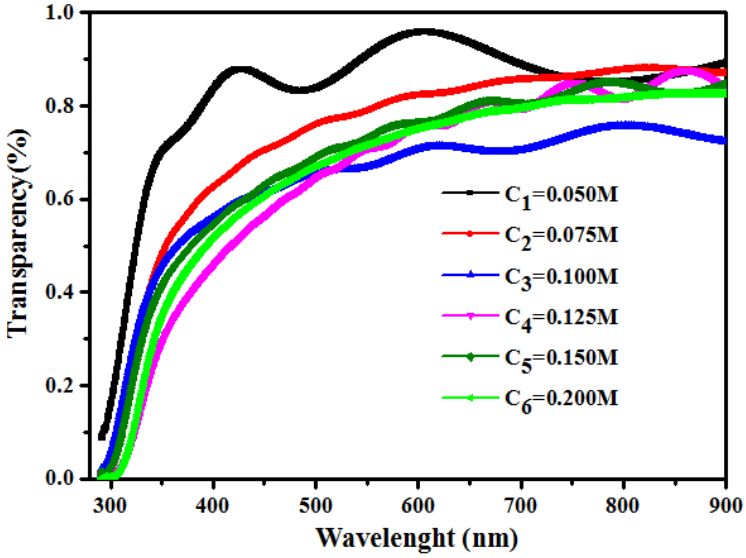

Fig.III.5. Spectral transmittance plots of undoped SnO_2 thin films with different tin precursor concentration.

The average transmission at a wavelength of 550 has been found to be ranged in 67-91.3%.As can be seen from Fig.III.5, that T(λ), in general, decreases gradually as the concentration of tin in solution increases, which may be attributed to the decrease in the grain size. Roman et al. [28] observed similar grain size dependent optical transmittance results for the sprayed SnO_2 films. It is also observed that the optical absorption edge exhibit slight red shift when the concentration of tin in solution increases, indicating a gradual decrease in the optical band gap (E_g) [28]. To evaluate those observations the band gap of undoped SnO_2 is carried out from the transmittance data according to Tauc relation [29]with little modification, to avoid thickness films measurements, as follow: $(hv\ ln(1/T))^2$ versus incident photon energy (hv) is used instead of $(\alpha hv)^2$and plots of which were obtained. The graphs and their extrapolating $(hv\ ln(1/T))^2$ to hv axes

are represented in (Fig.III.6). The band gap energy values of all SnO_2 thin films samples are ranged in 3.65-3.97eV revealing a decrease with increasing the concentration of tin in solution from C_1 to C_6. E_g values are summarized in Table III.2 and shown as features in Fig III.7. These results are in good agreement with those obtained for normal bulk SnO_2 [30, 31]. More investigations will be taken below using Urbach energy.

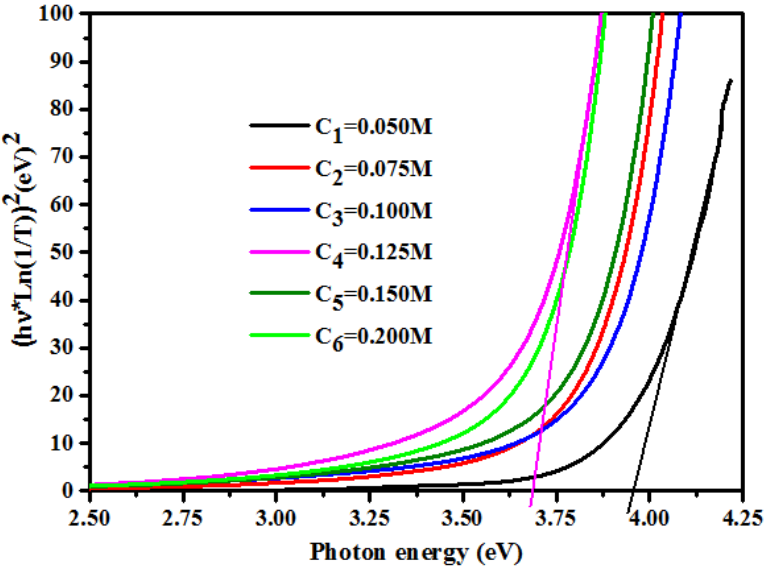

Fig.III.6. Band-gap (***Eg***) estimation from Tauc's relation of undoped SnO2 thin films with different tin precursor concentration.

At lower values of the absorption coefficient a (*i.e.* near the band edge), the extent of the exponential tail of the absorption edge is characterized by the Urbach energy (E_u) indicating the width of band tails of the localized states within the optical band gap and is given by [32]:

$$\alpha = \alpha_0 exp\left(\frac{h\nu}{E_u}\right) \qquad \text{(III.4)}$$

where α_0 and E_u are respectively a constant and width of the band tail of localized states at the optical band gap. E_u is also known as band tail width and is due to the disorder in the thin film material. The variation of bond length and bond angle from their standard value in the crystalline material is called disorder [33]. The Urbach energy of prepared SnO_2 thin films depends on the structural defects, dislocations density and some defects of the vacancy and interstitial states in the films [34]. It can be determined from the reciprocal gradient of the linear portion of $ln(\alpha)$ versus ($h\nu$) plots. Urbach energy values of SnO_2 thin films with different tin precursor concentration are shown and summarized in Fig III.7 and Table III.2 respectively. It is obviously seen that E_u fluctuates between 522 and 682 meV in the considered range of tin concentration in the solution and in respect to their inverted pheromone.

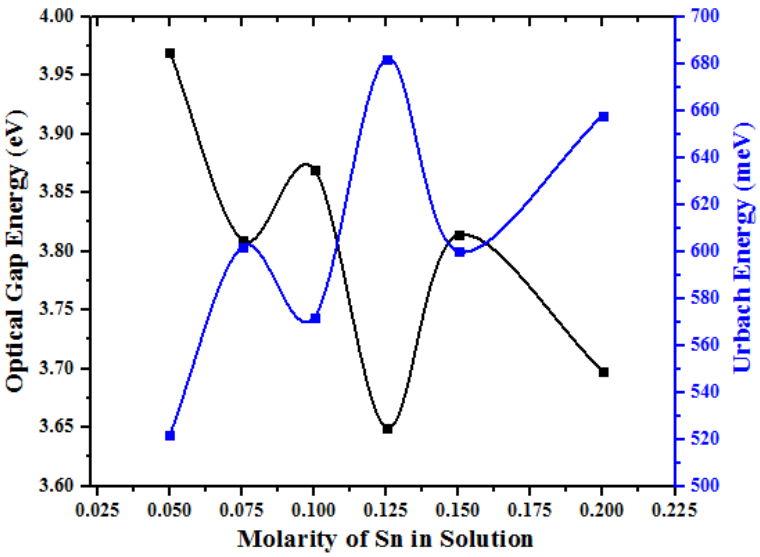

Fig. III.7. Variation of Band-gap (E_g) and Urbach energy (E_u) for undoped SnO_2 thin films different tin precursor concentration.

Table III.2: Optical properties of SnO_2 thin films

Concentration (M)	Urbach energy E_u(meV)	Optical gap E_g (eV)
C_1=0.050	522	3.970
C_2=0.075	602	3.810
C_3=0.100	572	3.870
C_4=0.125	682	3.650
C_5=0.150	600	3.814
C_6=0.200	658	3.698

III.3.3 Electrical properties

For all undoped SnO_2 thin films, the four-point probe is preferred for measurement of sheet resistance (R_{sh}); in the linear four-point probe technique, the current (I) is applied between the outer two probes and the potential difference (V) is taken across the inner two others. Since negligible contact and spreading resistance are associated with the voltage probes, one can obtain a fairly accurate estimation of R_{sh} using the following relation given by Smits [35]:

$$\boldsymbol{R_{sh} = 4.532\left(\frac{V}{I}\right)} \qquad \text{(III.5)}$$

In the above-illustrated configuration, a correction factor of 4.532 was applied to the sample (1×1 cm^2) with equally 1mm spaced probes and the film thickness necessarily being less than the spacing between the probes.
Fig. III.8 exhibits resistance sheet (R_{sh}) plot versus concentration of tin in solution. As can be seen, a part the sample prepared with C_1, R_{sh} reveals

slight variation with concentrations, it increases from 156 Ω/cm^2 for C_2 to reach 372 Ω/cm^2 for C_4 then decreases to 142 Ω/cm^2 as the minimum value.

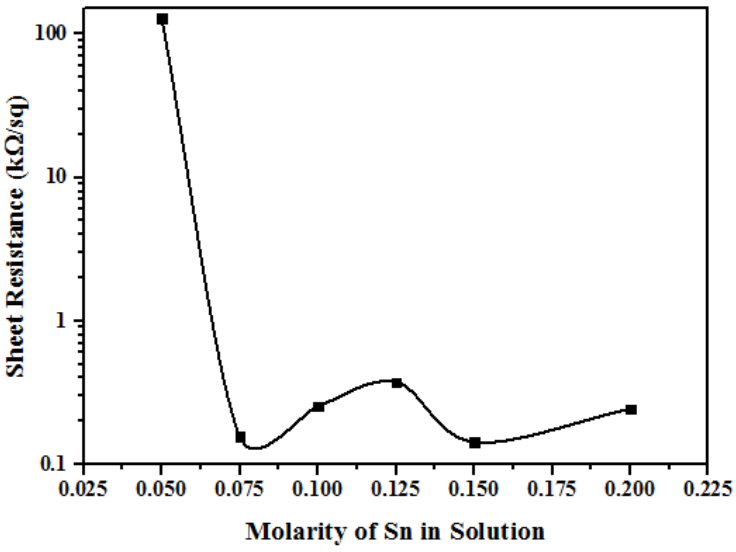

Fig.III.8. Variation of sheet resistance (R_{sh}) of SnO_2 thin films with different tin precursor concentration.

Such results are agreed with those obtained in the literature [36, 37]. R_{sh} in the case of the sample prepared with C_1 which is higher than others may find its origin in the insulating proper character of material since his $\boldsymbol{E_g}$ value is more than 3.97eV. Also one can observe easily from Fig. III.9 that the free carrier concentration ($\boldsymbol{n_e}$) in the case of C_1 having a minimum value ($\boldsymbol{n_e}$ = 4.17. 10^{14}cm^{-3}) and it starts to increase with concentration until C_4 where its value reaches 2.56.10^{19}cm^{-3} as maximum value; This behavior may be due to the presence of high amount of oxygen vacancies as donors [38] caused by the execs of Sn causing oxygen vacancies in the SnO_2

lattice (oxygen atmosphere become unable to ensure stoichiometric structure of SnO_2 with the provided Sn from precursor) [20]. As seen from Fig. 9, at the

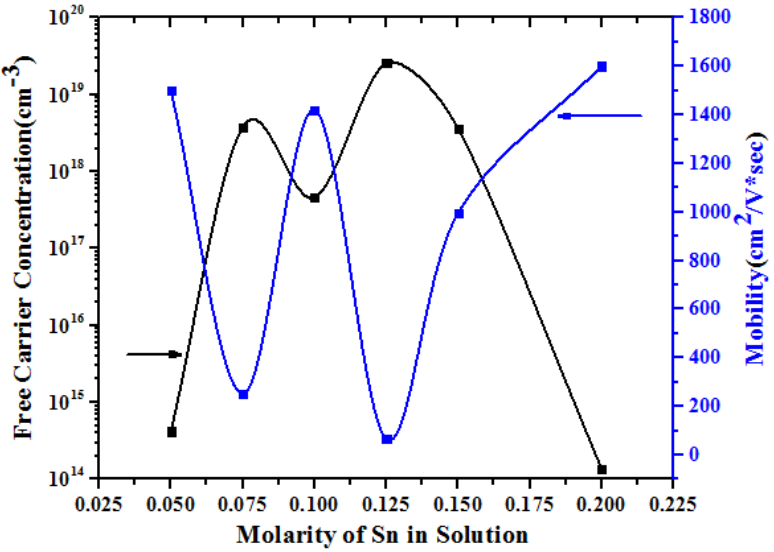

Fig. III.9. Variation of Mobility and carrier concentration of undoped SnO_2 thin films with different tin precursor concentration.

the condition of samples prepared with C_5 and C_6 a drastic decrease in the free carrier concentration (n_e = 1.37. $10^{14}cm^{-3}$ for C_6 =0.2M in the solution) which may be originated from acceptor character of Sn interstitial (Sn_{in}) in the lattice [38]. Sn_{in} may even occupy oxygen vacancies reducing the free carrier concentration. For all concentration the mobility is directly inverted to the free carrier concentration as it was shown in the same figure, the values of mobility are more than those found in the literature. Others parameters such as carrier concentration, conductivity, and mobility are recapitulated in Table III.3. As results and from point of view looking for high free carrier concentration of undoped SnO_2, preparing with 0.15M of $SnCl_2$ will be the preferred concentration in the precursor for this technique.

Table III.3: Electrical properties of SnO_2 thin films

Sample	R_{sh} (kΩ/sq)	σ $(\Omega cm)^{-}$	μ (cm^2/vs)	n_e (cm^{-3})
C1	130	0.1	1500	$4.17x10^{14}$
C2	0.156	150	250	$3.76x10^{18}$
C3	0.253	105	1420	$4.62x10^{17}$
C4	0.372	270	65.6	$2.56x10^{19}$
C5	0.142	583	995	$3.65x10^{18}$
C6	0.242	35	1600	$1.37x10^{14}$

III.4. Conclusions

In this chapter, we have reported the effect of varying concentration of tin in precursor solution on physical properties of SnO_2 thin films deposited on 480°C heated glass substrates using spray ultrasonic technique. Structural characterizations of undoped SnO_2 thin films via XRD have shown a polycrystalline structure with a clear characteristic peak of SnO_2 cassiterite under tetragonal rutile, cubic phases, and SnO phase. A dominance in *TC*(*hkl*) with concentrations are remarked: *TC*(*211*)in the case of C_2 and C_5, and *TC*(*200*) with two concentrationsC_3 and C_4. Crystallite size (*D*), in general, decreases gradually from 26 to 17nm as the concentration of tin in solution increases from 0.125 (C_4) to 0.2M (C_6).

The average transmission $T(\lambda)$ at a wavelength of 550 is ranged in 67-91.3%, and it decreases gradually with increasing tin concentration in solution. The optical absorption edge exhibits slight red shift when the

concentration of tin in solution increases, indicating a gradual decrease in the optical band gap (E_g) from 3.970 to 3.698 eV.

For all concentration, the mobility is directly inverted to the free carrier concentration ($\boldsymbol{n_e}$) and has values greater than ones in literature. The two feeble free carrier concentration ($\boldsymbol{n_e}$) in the case of C_1 and C_6 having its origin from the insulator character of the matter in the first case and may be originated from acceptor character of Sn interstitial in the second one. But in the case of concentration (C_4=0.125M), maximum free carrier concentration ($2.56.10^{19}cm^{-3}$) was provided which may be due to the presence of high amount of oxygen vacancies. For high free carrier concentration of undoped SnO_2, elaborating with 0.15M of $SnCl_2$ will be the preferred concentration in the precursor for this technique.

References

[1] G.J. McCarthy, J.M. Welton, X-ray diffraction data for SnO 2. An illustration of the new powder data evaluation methods, Powder Diffraction, 4 (1989) 156-159.

[2] I. Kim, J. Ko, D. Kim, K. Lee, T. Lee, J.-H. Jeong, B. Cheong, Y.-J. Baik, W. Kim, Scattering mechanism of transparent conducting tin oxide films prepared by magnetron sputtering, Thin Solid Films, 515 (2006) 2475-2480.

[3] Y.-M. Lu, C.-P. Hu, The colored and bleached properties of tungsten oxide electrochromic films with different substrate conductivities, Journal of Alloys and Compounds, 449 (2008) 389-392.

[4] S. Peng, F. Cheng, J. Liang, Z. Tao, J. Chen, Facile solution-controlled growth of CuInS 2 thin films on FTO and TiO 2/FTO glass substrates for photovoltaic application, Journal of Alloys and Compounds, 481 (2009) 786-791.

[5] S.S. Srinivasan, J. Wade, E.K. Stefanakos, Y. Goswami, Synergistic effects of sulfation and co-doping on the visible light photocatalysis of TiO 2, Journal of Alloys and Compounds, 424 (2006) 322-326.

[6] D. Vaufrey, M.B. Khalifa, M. Besland, C. Sandu, M. Blanchin, V. Teodorescu, J. Roger, J. Tardy, Reactive ion etching of sol–gel-processed SnO 2 transparent conducting oxide as a new material for organic light emitting diodes, Synthetic Metals, 127 (2002) 207-211.

[7] M.-R. Yang, S.-Y. Chu, R.-C. Chang, Synthesis and study of the SnO 2 nanowires growth, Sensors and Actuators B: Chemical, 122 (2007) 269-273.

[8] A. Banerjee, K. Chattopadhyay, Recent developments in the emerging field of crystalline p-type transparent conducting oxide thin films, Progress

in Crystal Growth and Characterization of Materials, 50 (2005) 52-105.

[9] J. Berry, D. Ginley, P.E. Burrows, Organic light emitting diodes using a Ga: ZnO anode, Applied Physics Letters, 92 (2008) 170.

[10] B. Du Ahn, S.H. Oh, D.U. Hong, D.H. Shin, A. Moujoud, H.J. Kim, Transparent Ga-doped zinc oxide-based window heaters fabricated by pulsed laser deposition, Journal of Crystal Growth, 310 (2008) 3303-3307.

[11] E. Fortunato, D. Ginley, H. Hosono, D.C. Paine, Transparent conducting oxides for photovoltaics, MRS bulletin, 32 (2007) 242-247.

[12] W. Hamd, Y. Wu, A. Boulle, E. Thune, R. Guinebretière, Microstructural study of SnO 2 thin layers deposited on sapphire by sol–gel dip-coating, Thin Solid Films, 518 (2009) 1-5.

[13] D.P. Joseph, P. Renugambal, M. Saravanan, S.P. Raja, C. Venkateswaran, Effect of Li doping on the structural, optical and electrical properties of spray deposited SnO 2 thin films, Thin Solid Films, 517 (2009) 6129-6136.

[14] A.F. Khan, M. Mehmood, M. Aslam, M. Ashraf, Characteristics of electron beam evaporated nanocrystalline SnO 2 thin films annealed in air, Applied Surface Science, 256 (2010) 2252-2258.

[15] K. Omura, P. Veluchamy, M. Tsuji, T. Nishio, M. Murozono, A Pyrosol Technique to Deposit Highly Transparent, Low-Resistance SnO2: F Thin Films from Dimethyltin Dichloride, Journal of The Electrochemical Society, 146 (1999) 2113-2116.

[16] N. Shaalan, T. Yamazaki, T. Kikuta, Influence of morphology and structure geometry on NO 2 gas-sensing characteristics of SnO 2 nanostructures synthesized via a thermal evaporation method, Sensors and Actuators B: Chemical, 153 (2011) 11-16.

[17] T. Tsuchiya, K. Daoudi, I. Yamaguchi, T. Manabe, T. Kumagai, S.

Mizuta, Preparation of tin oxide films on various substrates by excimer laser metal organic deposition, Applied surface science, 247 (2005) 145-150.

[18] A. Rahal, A. Benhaoua, M. Jlassi, B. Benhaoua, Structural, optical and electrical properties studies of ultrasonically deposited tin oxide (SnO 2) thin films with different substrate temperatures, Superlattices and Microstructures, 86 (2015) 403-411.

[19] J. Szuber, G. Czempik, R. Larciprete, B. Adamowicz, The comparative XPS and PYS studies of SnO 2 thin films prepared by L-CVD technique and exposed to oxygen and hydrogen, Sensors and Actuators B: Chemical, 70 (2000) 177-181.

[20] Ç. Kılıç, A. Zunger, Origins of coexistence of conductivity and transparency in SnO 2, Physical Review Letters, 88 (2002) 095501.

[21] G. Muruganantham, K. Ravichandran, K. Saravanakumar, A. Ravichandran, B. Sakthivel, Effect of solvent volume on the physical properties of undoped and fluorine doped tin oxide films deposited using a low-cost spray technique, Superlattices and Microstructures, 50 (2011) 722-733.

[22] J. Haines, J. Léger, O. Schulte, Pa3 modified fluorite-type structures in metal dioxides at high pressure, Science, 271 (1996) 629.

[23] R.M. Organ, J. Mandarino, Romarchite and hydroromarchite. Two new stannous minerals, The Canadian Mineralogist, 10 (1971) 916.

[24] P. Paufler, CS Barrett, TB Massalski. Structure of Metals. Pergamon Press Oxford, New York, Toronto, Sydney, Paris Frankfurt/M 1980 654 Seiten, 113 Abbildungen, 19 Tabellen und über 1400 Literaturhinweise. Preis US $20.–, Crystal Research and Technology, 16 (1981) 982-982.

[25] C. Marcel, N. Naghavi, G. Couturier, J. Salardenne, J. Tarascon,

Scattering mechanisms and electronic behavior in transparent conducting Zn x In 2 O x+ 3 indium–zinc oxide thin films, Journal of applied physics, 91 (2002) 4291-4297.

[26] P. Scherrer, Bestimmung der inneren Struktur und der Größe von Kolloidteilchen mittels Röntgenstrahlen, in: Kolloidchemie Ein Lehrbuch, Springer, 1912, pp. 387-409.

[27] B.D. Cullity, Answers to Problems: Elements of X-ray Diffraction, Addison-Wesley Publishing Company, 1978.

[28] L. Roman, R. Valaski, C.D. Canestraro, E. Magalhaes, C. Persson, R. Ahuja, E. Da Silva, I. Pepe, A.F. Da Silva, Optical band-edge absorption of oxide compound SnO 2, Applied Surface Science, 252 (2006) 5361-5364.

[29] J. Tauc, R. Grigorovici, A. Vancu, Optical properties and electronic structure of amorphous germanium, physica status solidi (b), 15 (1966) 627-637.

[30] K. Chopra, S. Major, D. Pandya, Transparent conductors—A status review, Thin solid films, 102 (1983) 1-46.

[31] W. Spence, The UV absorption edge of tin oxide thin films, Journal of Applied Physics, 38 (1967) 3767-3770.

[32] F. Urbach, The long-wavelength edge of photographic sensitivity and of the electronic absorption of solids, Physical Review, 92 (1953) 1324.

[33] C. Lokhande, K. Gadave, Chemical deposition of MnS thin films from thiosulphate bath, Turk. J. Phys, 18 (1994) 83-87.

[34] F. Al-Shaikley, Electrical and optical properties dependence on annealing temperature for CdS thin films, Indian J. Appl. Res, 3 (2013) 544-548.

[35] F. Smits, Measurement of sheet resistivities with the four-point probe,

Bell Labs Technical Journal, 37 (1958) 711-718.

[36] N. Memarian, S.M. Rozati, Toward Finding a Commercial Method for Deposition of Nanostructured SnO2 Thin Films, Acta Physica Polonica-Series A General Physics, 122 (2012) 202.

[37] A. Rahal, A. Benhaoua, C. Bouzidi, B. Benhaoua, B. Gasmi, Effect of antimony doping on the structural, optical and electrical properties of SnO 2 thin films prepared by spray ultrasonic, Superlattices and Microstructures, 76 (2014) 105-114.

[38] C. Agashe, J. Hüpkes, G. Schöpe, M. Berginski, Physical properties of highly oriented spray-deposited fluorine-doped tin dioxide films as transparent conductor, Solar Energy Materials and Solar Cells, 93 (2009) 1256-1262.

Effect of solvent

IV.1. Introduction

The simultaneous occurrence of high optical transparency in the visible region and high electrical conductivity is not possible in an intrinsic stoichiometric material. The only way to obtain good transparent conductors is to create electron degeneracy in a wide band gap oxide (greater than 3eV) by controllably introducing non-stoichiometry and/or appropriate dopants [1]. SnO_2 has a tetragonal structure, similar to the rutile structure with the wide energy gap of $\boldsymbol{E}_g$ =3.67eV, and behaves as an n-type semiconductor [2, 3]. These conditions are very conveniently obtained in SnO_2 thin films, prepared by a number of deposition techniques. Numerous techniques for depositing X-doped tin oxide (XTO) have been employed [4-12]. Among those techniques, ultrasonically spray pyrolysis is well suited for the preparation of undoped tin oxide thin films because of its simple and inexpensive experimental arrangement [13]. Organic solvents like methanol and ethanol are typically used in this technique to elaborate transparent conducting oxides (TCO). Further, it has been observed that the optical transmission of SnO_2 films could be increased by the addition of few drops of hydrochloric acid to the spray solution [14].

In order to check whether the growth mechanism through the solvent (water/ methanol) composition can be controlled or not, undoped tin oxide (SnO_2) thin films are deposited using different solvent (water/methanol) ratios in the present investigation which constitutes the subject of this chapter. The concentration of [$SnCl_2$] is kept fixed and by changing the volumetric proportions of water to methanol in the spraying solution, the

solvent ratio is changed. Dependence of thin films properties on solvent composition will be the aim of this fourth chapter.

IV.2. Experimental details

IV.2.1 Preparation of solution and SnO_2 thin films

Undoped SnO_2 thin films were ultrasonically deposited using a starting amount of 0.15M tin chloride ($SnCl_2 \cdot 2H_2O$), dissolved in mixtures of water and methanol having a volume of 25ml. The water content to methanol was varied in seven different volumetric proportions as 0:25, 5:20, 10:15, 12.5:12.5, 15:10, 20:5 and 25:0 and the deposits obtained are designated respectively as 0W25M, 5W20M, 10W15M, 12.5W12.5M, 15W10M, 20W5M, and 25W0M for a total solution volume of 25 ml of water-methanol. The heated of the glass substrate on which SnO_2 thin films were deposited is maintained constant at 480 °C [15]. For each experiment, the solution was stirred at room temperature (rt) for half an hour to yield a clear and transparency mother precursor. The blend so obtained was used as a stock solution for spray ultrasonic. As used for the all work, An R217102 microscopic glass slides serve as substrates. The later were cleaned with alcohol in an ultrasonic bath and distilled water. The temperature of the substrates was monitored using a temperature controller with chromel-alumel and K type thermocouple. The time deposition was 3 min for each experiment. After deposition, the films were allowed to cool down naturally to room temperature.

IV.2.2 thin films characterizations

The microstructure of the SnO_2 films was examined by X-ray diffraction measurements (XPERT-PRO X-ray Diffractometer system with a 30 kV, 30 mA, Cu K_α radiation with a wavelength of 1.5406Å as operating conditions). The grain size of the films was estimated using X'Pert High Score. The optical transmission spectra of SnO_2 and band gap were obtained using a UV-visible spectrophotometer (Shimadzu, Model 1800). As usually used in this work, an 1x1 cm^2 samples of the films on which sheet four-point probe and Hall Effect were done to evaluate electrical sheet resistance, carrier concentration, and mobility. All measurements were carried out at room temperature (*rt*).

IV.3. Results and discussion

IV.3.1 X-ray diffraction studies

The XRD patterns of SnO_2 thin films deposited with various solvent (water/methanol) ratios in the starting solution are shown in (Fig.IV.1). As can be seen, diffraction peaks were observed at around 2θ = 26.73°, 34.07°, 38.01°, 51.83°, 54.81°, 61.94°and 65.89° which are related to the following plans (*110*), (*101*), (*200*), (*211*), (*220*), (*310*)and (*301*) matching well with the space group P42mnm according to JCPDS (No. 41-1445) of the tetragonal, rutile SnO_2; whereas the other peaks observed at 2θ =29.53° are associated with (*101*) planes of SnO according to JCPDS (No. 06-0395) [16]. The obtained XRD spectra are an evident indication of the polycrystalline nature of all elaborated thin films. Exclusively it was remarked that beyond 15W10M as a solvent ratio (water/methanol) in the

starting solution, the appearance of diffraction peaks according to JCPDS (No. 41-1445) of the tetragonal SnO_2; with complete growth along (*110*) of rutile SnO_2 which needs minimum energy.

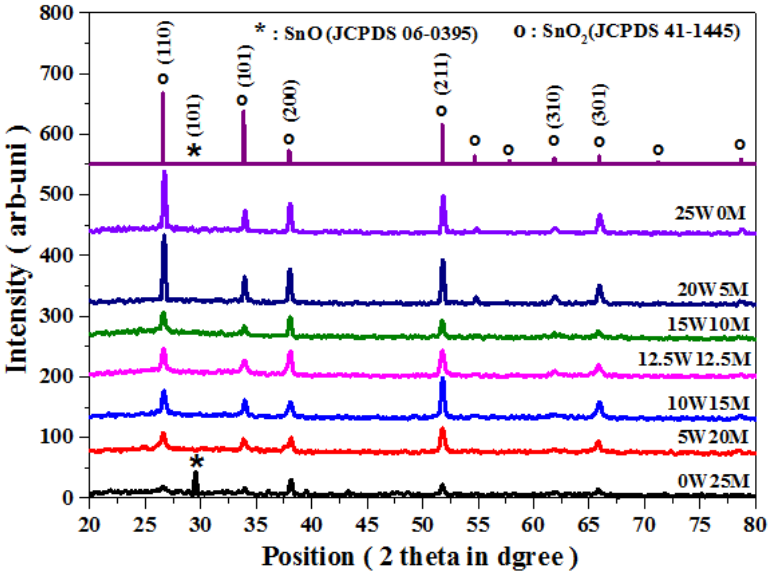

Fig. IV.1.XDR patterns of undoped SnO_2thin films with various solvent (water/methanol) ratios in the starting solution.

For more details, about the preferred growth, different texture coefficient *TC(hkl)* have been calculated from the X-ray data. The texture coefficient *TC(hkl)* represents the texture of the particular plane, deviation of which from unity implies the preferred growth. *TC(hkl)* coefficients have been evaluated using the well-known formula [17]:

$$\boldsymbol{TC(hkl)} = \frac{\boldsymbol{I(hkl)/I_0(hkl)}}{\boldsymbol{N^{-1}\sum_n^N I(hkl)/I_0(hkl)}} \qquad \text{(IV.1)}$$

where *I(hkl)* is the measured relative intensity of a plane *(hkl)*, $I_o(hkl)$ is the standard intensity of the plane *(hkl)* taken from the JCPDS data, *N* is the reflection number and *n* is the number of diffraction peaks. $TC(hkl))$ values of all thin films for (*110*), (*101*), (*200*), (*211*), (*310*) and (*301*) with varying solvent ratios (water/methanol) in the starting solution are shown in Fig.IV.2. Peaks intensities were less than unity confirming the polycrystalline nature of the films. However, the films deposited using presented a preferred oriented growth along (*110*) plane direction. It is worth noting that a dominance in *TC*(*hkl*) is remarked: *TC*(*200*) with two ratios *0W25M* and *15W20M*, whereas *TC*(*211*) is dominant only for *10W15M* and finely *TC*(*110*) for *0W25M* as seen in Fig.IV.2.

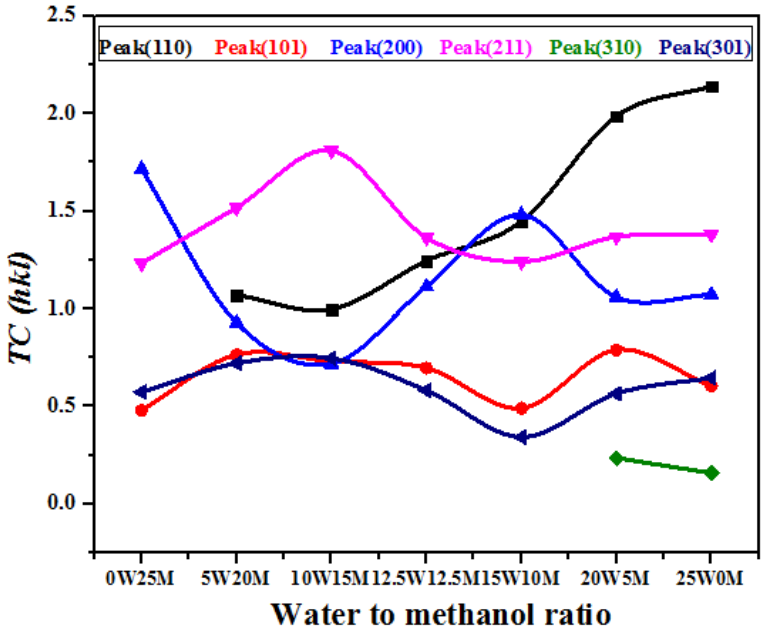

Fig. IV.2. Variation of TC (hkl) in SnO_2 thin films with various solvent (water/methanol) ratios in the starting solution.

The lattice constants ‘a’ and ‘c’, for the tetragonal phase structure is determined by the following relation [18]:

$$2d_{hkl}\,sin(\theta) = n\lambda \text{and } \frac{1}{d_{hkl}^2} = \frac{h^2+k^2}{a^2} + \frac{l^2}{c^2} \text{(IV.2)}$$

where ‘d’ is the interplaner distance and (*hkl*) are Miller indices, respectively. The calculated lattice constants ‘a’ and ‘c’ are plotted in Fig.IV.3.

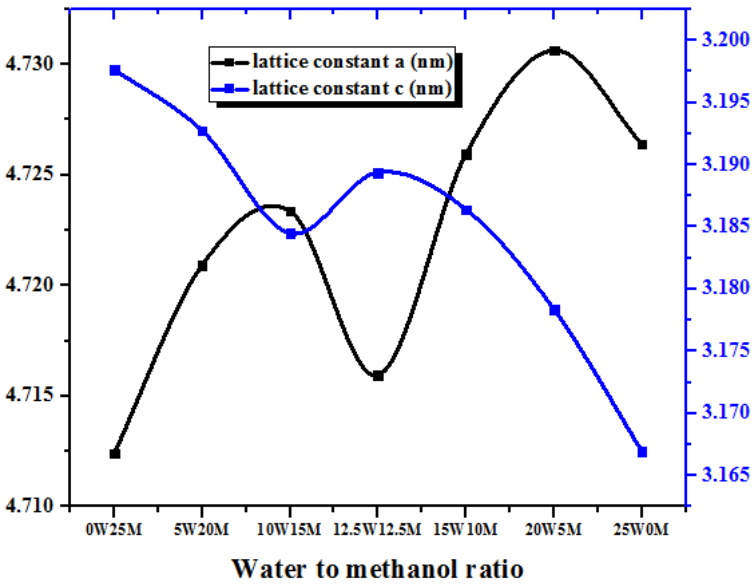

Fig. IV.3. Variation of lattice parameters in SnO_2 thin films with various solvent (water/methanol) ratios in the starting solution.

As can be seen a periodic expansion of the lattice parameters reaching its maximum with solution ratios of *10W15M* and *15W10M* which means dilatation of the unit cell of SnO_2 matrix. Whereas samples prepared with

12.5W12.5M and *20W5M* exhibit contraction of the unit cell of SnO_2 matrix. This behavior may be related to the kinetic formation of SnO_2 product under different conditions of the methanol presence with water which leads to crystallite size variation as it will be seen in the following paragraph.

The average crystallite size (*D*) of SnO_2 nanoparticles of the films, upon the starting solution with all the different ratios (water/methanol), were calculated from XRD data using the Scherer formula [19]:

$$\boldsymbol{D = \frac{0{,}9\lambda}{\beta cos(\theta)}} \qquad \text{(IV.3)}$$

where λ is the wavelength of X-ray radiation, β is the full width at half maximum (*FWHM*) of the peak at diffraction angle θ [20] and the calculated averages of crystallite sizes are plotted in Fig.IV.4. Crystallite size (*D*), in general, decreases gradually as the ratios (water/methanol) in respect of increasing water amount in the starting solution.

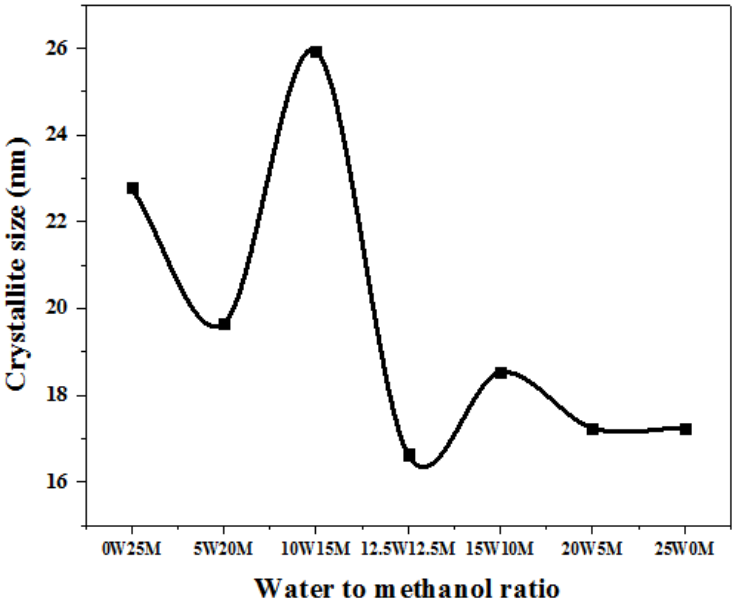

Fig. IV.4. Variation of crystallite size in SnO_2 thin films with various solvent (water/methanol) ratios in the starting solution.

IV.3.2 Optical transmission and optical band gap

Fig.IV.5 shows the optical transmittance spectrum, in the considered wavelength range, of the undoped SnO_2 thin film deposited using starting solutions ratios in the range (*0W25M, 5W20M, 10W15M, 12.5W12.5M, 15W20M, 20W5M,* and *25W0M*).

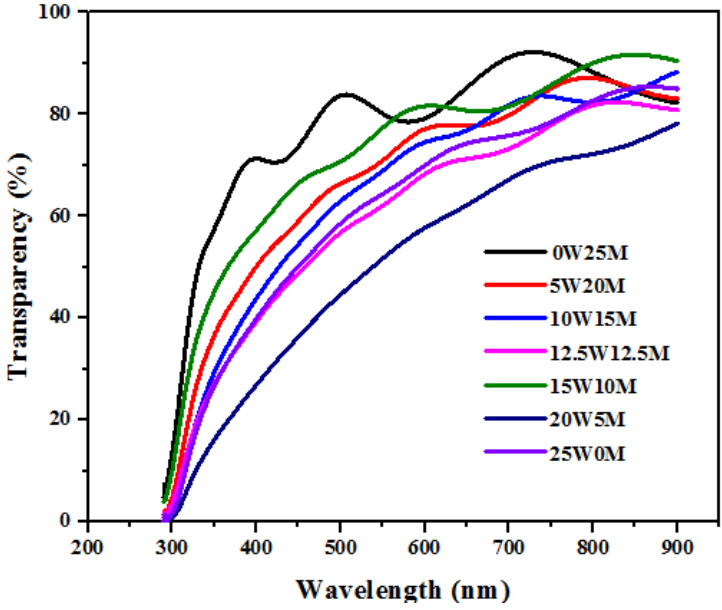

Fig.IV.5. Spectral transmittance plots of undoped SnO_2 thin films with various solvent (water/methanol) ratios in the starting solution.

.

All undoped SnO_2 thin films were transparent in the visible range; transmittance values are lied between 51.64 and 80.12% at the middle of the visible range (550 nm). To evaluate those observations the band gap E_g of undoped SnO_2 is carried out from the transmittance data according to Tauc relation [21] with little modification, to avoid thickness films measurements, as follow: $(ln(1/T)hv)^2$ versus incident photon energy (hv) is used instead of $(\alpha hv)^2$and plots of which were obtained. The graphs and their extrapolating $(ln(1/T)\ hv)^2$ to hv axes are represented in Fig.IV.6. As can be seen, sample deposited from the starting solution with the highest E_g value, around 3.9 eV, in respect of zero water content (*0W25M*), it starts in decrease until the water content of 2*0W5M* and then increases.

The slight red shift when an amount of water increases in the starting solution do not be explained in the optic of Roth trend hence there is no doping provided in the undoped SnO_2 product. These results are in good agreement with those obtained for normal bulk SnO_2 [2, 22]. More investigations will be taken below using Urbach energy.

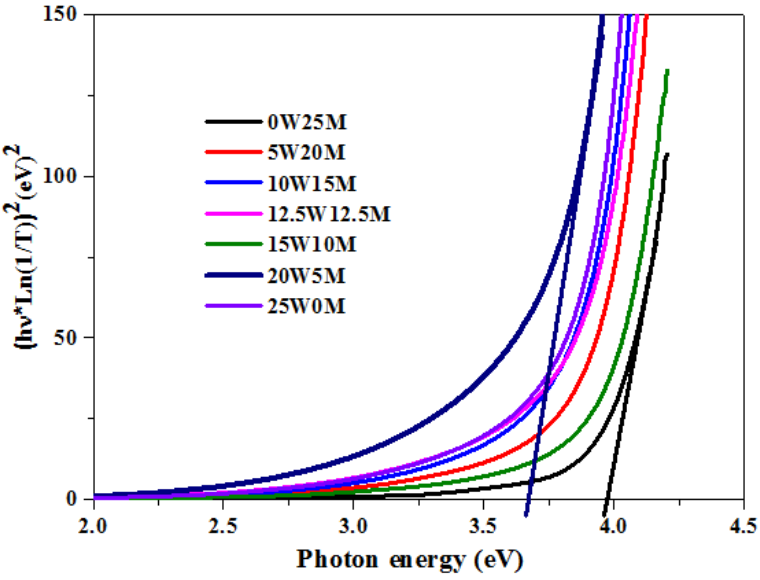

Fig.IV.6. Band-gap (Eg) estimation from Tauc's relation of undoped SnO_2 thin films with various solvent (water/methanol) ratios in the starting solution.

At lower values of the absorption coefficient a (*i.e.* near the band edge), the extent of the exponential tail of the absorption edge is characterized by the Urbach energy (E_u) indicating the width of band tails of the localized states within the optical band gap and is given by [23]:

$$\alpha = \alpha_0 exp\left(\frac{h\nu}{E_u}\right) \qquad \text{(IV.4)}$$

where α_0 and E_u are respectively a constant and width of the band tail of localized states at the optical band gap. E_u is also known as band tail width and is due to the disorder in the thin film material. The variation of bond length and bond angle from their standard value in the crystalline material is called disorder [24]. The Urbach energy of prepared SnO_2 thin films depends on the structural defects, dislocations density and some defects of the vacancy and interstitial states in the films [25]. It can be determined from the reciprocal gradient of the linear portion of $ln(\alpha)$ versus $(h\nu)$ plots. From the Urbach energy values of SnO_2 thin films with different solvent ratio (water/methanol) in the starting solution illustrated in Table IV.1

Table IV.1: Optical properties of SnO_2 thin films

Water to methanol (ratio)	Urbach energy E_u(meV)	Optical gap E_g(eV)
0W25M	651.82	3.971
5W20M	656.21	3.903
10W15M	660.82	3.834
12.5W12.5M	659.20	3.858
15W10M	653.22	3.949
20W5M	672.85	3.665
25W0M	662.88	3.804

One can see that E_u fluctuates between 651.82 and 672.85 meV indicating a considerable influence on E_g.

IV.3.3Electrical properties

The carrier concentration, mobility and electrical resistivity of undoped SnO_2 thin films were measured using van der Pauw method (Hall measurements).The carrier concentration (n_e) is derived from the relation [26]:

$$n_e = \frac{1}{eR_H} \qquad \text{(IV.5)}$$

where R_H is the Hall coefficient and e is the absolute value of the electron charge. The Hall mobility of charge carriers is determined using the relation [26]:

$$\mu = \frac{1}{\rho e n_e} \qquad \text{(IV.6)}$$

where ρ is resistivity. The negative sign of Hall coefficient confirmed that the deposited films are n- type semiconductor.

The carrier concentration, mobility and electrical resistivity of undoped SnO_2 thin films were also summarized in Table IV.2.

Table IV.2: Electrical properties of SnO_2 thin films

Water to methanol	ρ (Ωcm)	μ (cm^2/vs)	n_e (cm^{-3})
0W25M	---	---	---
5W20M	3.36×10^{-2}	45.8	4.00×10^{18}
10W15M	2.24×10^{-2}	25.3	1.00×10^{19}
12.5W12.5M	2.96×10^{-2}	6.25	3.35×10^{19}
15W10M	1.81×10^{-2}	156	2.20×10^{18}
20W5M	28.4×10^{-2}	1.35×10^{-2}	1.60×10^{21}
25W0M	67.6×10^{-2}	1.77×10^{3}	6.48×10^{15}

It is seen that resistivity decreases with the increase in ratio water content (*5W20M*), it starts in decrease until the water content of 15*W10M* and then increases Fig.IV.7.

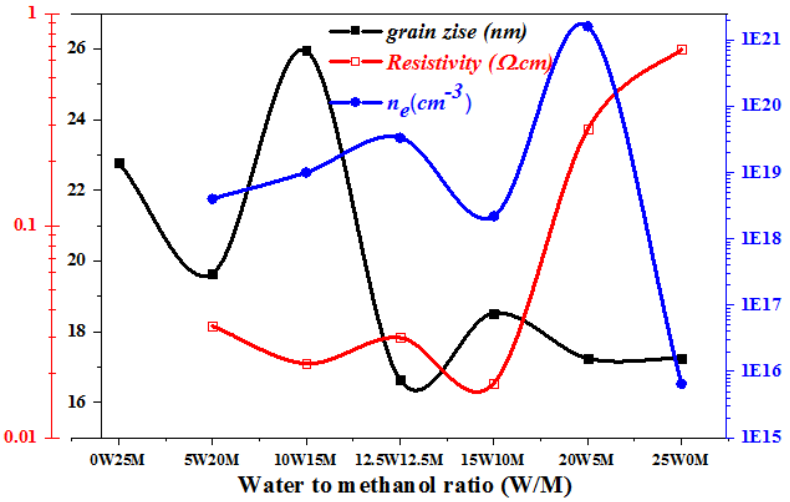

Fig. IV.7. The carrier concentration, crystallinity and electrical resistivity of undoped SnO_2 thin films with various solvent (water/methanol) ratios in the starting solution.

The increase in resistivity with an increase in ratio water content is due to decrease in crystallinity of the samples. From the Hall effect measurements, it was observed that the undoped SnO_2 films exhibited n-type conductivity. The nature of the carrier concentration ($\boldsymbol{n_e}$) and carrier mobility ($\boldsymbol{\mu}$) of the as-deposited undoped SnO_2 thin film as a function of the ratio of water is as shown in Fig.IV.9.

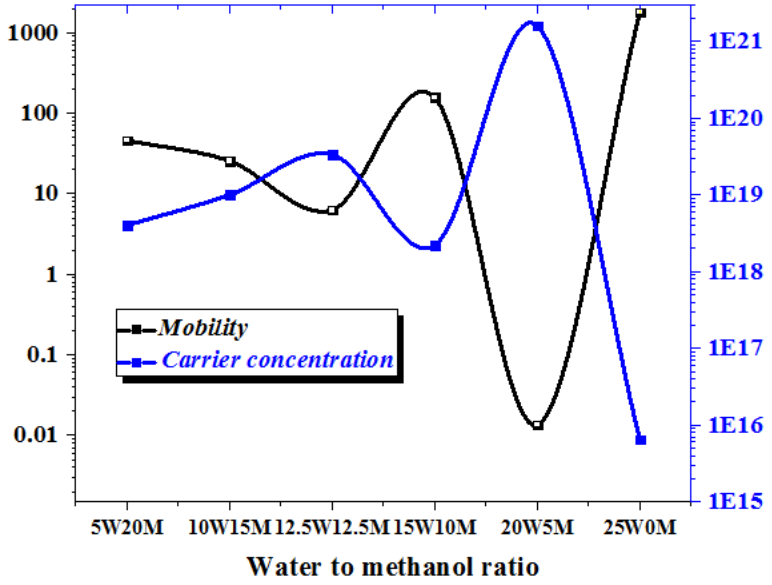

Fig.IV.9. The carrier concentration and carrier mobility of undoped SnO_2 thin films with various solvent (water/methanol) ratios in the starting solution.

The decrease in mobility with an increase in the ratio of water is due to increase in conductivity and carrier concentration. The mobility values for the films prepared with a ratio of solvent (water/methanol) are of the order between $1.35x10^{-2}$ and $1.77x\ 10^{3}$ $cm^2/V.s$. A carrier density as high as $1.60x10^{21}$ cm^{-3} is observed for the S_6=20W5M sample. The carrier density goes on decreasing with a decrease in conductivity as described above. The film degeneracy was confirmed by evaluating Fermi energy values and carrier concentration using the relation from the literature. It is found that the $\boldsymbol{E_F}$ values are proportional to $n^{2/3}$ that is the characteristic for the degeneracy of materials. Hence, it is established that the deposited films degenerate semiconductors [27]. As results, interesting in high free carrier concentration of undoped SnO_2, preparing with 15W10M as ratio of water

to methanol will be the preferred concentration in the precursor for this technique.

IV.4. Conclusions

In this Chapter, we have reported the effect of varying ratio of water and methanol in starting solution on physical properties of SnO_2 thin films deposited on 480°C heated glass substrates using spray ultrasonic technique Since the optimized temperature for ultrasonically deposited SnO_2 thin films in this work was 480°C and as preferred concentration of $SnCl_2$ in the precursor was 0.125M for this technique; Transparent conducting SnO_2 thin films have been deposited on 480°C heated glass substrates by a spray pyrolysis technique using ($SnCl_2 \cdot 2H_2O$) as precursors and mixture of water and methanol as solvent. At varying ratio of water and methanol (W/M) solvent in the spraying solution in the following range as (0W25M, 5W20M, 10W15M, 12.5W12.5M, 15W10M, 20W5M, and 25W0M) physical properties of SnO_2 thin films were studied. For this purpose, X-ray diffraction (XRD), UV-visible spectrophotometer, conventional four-point probe techniques and Hall Effect are used. The as-deposited films are polycrystalline SnO_2 with a tetragonal crystal structure and are preferentially orientated along the (*110*) direction with high texture coefficient as 2.14. The crystallite size varies between 16.63 and 25.94 nm for the as-deposited sample within the ratio of water to methanol. The direct band gap energy was found to vary between 3.665 and 3.971eV whereas the transmittance at 550 nm varies from 51.64 to 80.12% within the water content in the starting solution (i e ratio of water to methanol).

The electrical resistivity of deposited thin films decreases with the water

content, reaching a minimum value closely to $1.81x10^{-2}$ Ωcm, with the starting solution having a ratio of 15W10M (*i. e* 15 ml per 25 ml) of the solution; further increase in water content augments the corresponding resistivity of the deposited thin films. For high free carrier concentration of undoped SnO_2, elaborating with 15W10M will be the preferred ratios in the precursor for this technique.

References

[1] Z. Jarzebski, J. Marton, Physical properties of SnO2 materials I. Preparation and defect structure, Journal of the electrochemical Society, 123 (1976) 199C-205C.
[2] K. Chopra, S. Major, D. Pandya, Transparent conductors—A status review, Thin solid films, 102 (1983) 1-46.
[3] G.J. McCarthy, J.M. Welton, X-ray diffraction data for SnO 2. An illustration of the new powder data evaluation methods, Powder Diffraction, 4 (1989) 156-159.
[4] A. Banerjee, K. Chattopadhyay, Recent developments in the emerging field of crystalline p-type transparent conducting oxide thin films, Progress in Crystal Growth and Characterization of Materials, 50 (2005) 52-105.
[5] J. Berry, D. Ginley, P.E. Burrows, Organic light emitting diodes using a Ga: ZnO anode, Applied Physics Letters, 92 (2008) 170.
[6] E. Fortunato, D. Ginley, H. Hosono, D.C. Paine, Transparent conducting oxides for photovoltaics, MRS bulletin, 32 (2007) 242-247.
[7] W. Hamd, Y. Wu, A. Boulle, E. Thune, R. Guinebretière, Microstructural study of SnO 2 thin layers deposited on sapphire by sol–gel dip-coating, Thin Solid Films, 518 (2009) 1-5.
[8] A. Moholkar, S. Pawar, K. Rajpure, C. Bhosale, J. Kim, Effect of fluorine doping on highly transparent conductive spray deposited nanocrystalline tin oxide thin films, Applied Surface Science, 255 (2009) 9358-9364.
[9] K. Omura, P. Veluchamy, M. Tsuji, T. Nishio, M. Murozono, A Pyrosol Technique to Deposit Highly Transparent, Low-Resistance SnO2: F Thin Films from Dimethyltin Dichloride, Journal of The Electrochemical Society, 146 (1999) 2113-2116.
[10] A. Rahal, A. Benhaoua, C. Bouzidi, B. Benhaoua, B. Gasmi, Effect of antimony doping on the structural, optical and electrical properties of SnO 2 thin films prepared by spray ultrasonic, Superlattices and Microstructures, 76 (2014) 105-114.
[11] N. Shaalan, T. Yamazaki, T. Kikuta, Influence of morphology and structure geometry on NO 2 gas-sensing characteristics of SnO 2 nanostructures synthesized via a thermal evaporation method, Sensors and Actuators B: Chemical, 153 (2011) 11-16.
[12] T. Tsuchiya, K. Daoudi, I. Yamaguchi, T. Manabe, T. Kumagai, S. Mizuta, Preparation of tin oxide films on various substrates by excimer laser metal organic deposition, Applied surface science, 247 (2005) 145-150.

[13] A. Benhaoua, A. Rahal, B. Benhaoua, M. Jlassi, Effect of fluorine doping on the structural, optical and electrical properties of SnO 2 thin films prepared by spray ultrasonic, Superlattices and Microstructures, 70 (2014) 61-69.
[14] E. Elangovan, K. Ramamurthi, A study on low cost-high conducting fluorine and antimony-doped tin oxide thin films, Applied Surface Science, 249 (2005) 183-196.
[15] A. Rahal, A. Benhaoua, M. Jlassi, B. Benhaoua, Structural, optical and electrical properties studies of ultrasonically deposited tin oxide (SnO 2) thin films with different substrate temperatures, Superlattices and Microstructures, 86 (2015) 403-411.
[16] R.M. Organ, J. Mandarino, Romarchite and hydroromarchite. Two new stannous minerals, The Canadian Mineralogist, 10 (1971) 916.
[17] P. Paufler, CS Barrett, TB Massalski. Structure of Metals. Pergamon Press Oxford, New York, Toronto, Sydney, Paris Frankfurt/M 1980 654 Seiten, 113 Abbildungen, 19 Tabellen und über 1400 Literaturhinweise. Preis US $20.–, Crystal Research and Technology, 16 (1981) 982-982.
[18] C. Marcel, N. Naghavi, G. Couturier, J. Salardenne, J. Tarascon, Scattering mechanisms and electronic behavior in transparent conducting Zn x In 2 O x+ 3 indium–zinc oxide thin films, Journal of applied physics, 91 (2002) 4291-4297.
[19] P. Scherrer, Bestimmung der inneren Struktur und der Größe von Kolloidteilchen mittels Röntgenstrahlen, in: Kolloidchemie Ein Lehrbuch, Springer, 1912, pp. 387-409.
[20] B.D. Cullity, Answers to Problems: Elements of X-ray Diffraction, Addison-Wesley Publishing Company, 1978.
[21] J. Tauc, R. Grigorovici, A. Vancu, Optical properties and electronic structure of amorphous germanium, physica status solidi (b), 15 (1966) 627-637.
[22] W. Spence, The UV absorption edge of tin oxide thin films, Journal of Applied Physics, 38 (1967) 3767-3770.
[23] F. Urbach, The long-wavelength edge of photographic sensitivity and of the electronic absorption of solids, Physical Review, 92 (1953) 1324.
[24] C. Lokhande, K. Gadave, Chemical deposition of MnS thin films from thiosulphate bath, Turk. J. Phys, 18 (1994) 83-87.
[25] F. Al-Shaikley, Electrical and optical properties dependence on annealing temperature for CdS thin films, Indian J. Appl. Res, 3 (2013) 544-548.
[26] R. Chwang, B. Smith, C. Crowell, Contact size effects on the van der Pauw method for resistivity and Hall coefficient measurement, Solid-State

Electronics, 17 (1974) 1217-1227.
[27] A. Moholkar, S. Pawar, K. Rajpure, C. Bhosale, Effect of solvent ratio on the properties of highly oriented sprayed fluorine-doped tin oxide thin films, Materials Letters, 61 (2007) 3030-3036.

Effect of doping elements

V.1. Introduction

The main objective of this chapter was to obtain transparent conducting oxides using both Antimony (Sb) and fluorine (F) doped SnO_2 thin films ultrasonically sprayed and to investigate their optical and electrical properties with different doping levels of Sb ([Sb]/[Sn] = 0-1 wt.%) and F ([F]/[Sn] = 0-12 wt.%); those concentration levels are arbitrary chosen in this work in order to obtain high figure of merit which means better optoelectrical properties. For those two dopants (Sb) and (F) we will exhibit only the results under the above-cited objective.

V.2. Antimony doping (Sb)

V.2.1.Results and discussion

V.2.1.a Optical properties

Fig.V.1 shows the optical transmission *T(λ)* curves as a function of the wavelength of undoped and Sb-doped SnO_2 thin films.

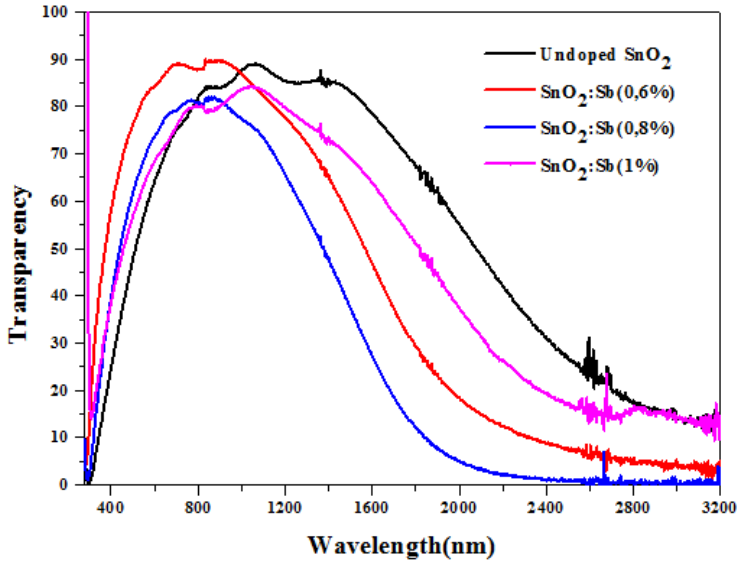

Fig. V.1. Spectral transmittance plot of Sb (0-1 wt. %) doped SnO_2 thin films ultrasonically sprayed [1].

It was observed that the average transparency in the visible range is around 80%. All films exhibit significant oscillations in the visible range; those oscillations, which are related to the interference phenomenon, are generated by the smooth of film and are affected by the thickness. Also one can see that the envelope of transmission $T(\lambda)$ curves becomes contracted and exhibits a shift toward lower wavelength for the Sb doping level lower than 0.8 wt.% with minimum value of transmittance at this given doping level and then become large for 1 wt.% Sb doping level restoring its initials transmittance values.

In heavily doped semiconductors, (having carrier concentration between 10^{+19} and $10^{+21}cm^{-3}$), which is the case of 0.8 wt.% doped film), the Drude's model is generally used for the attribution of the decrease in the transmittance [2]. This model illustrates the drop in transmittance in the near infrared region which is associated with the plasma frequency of free electrons. This case is well meted in 0.8 wt.% Sb-doped film where the high carrier concentration is achieved and drop in transmittance in the near infrared region is well remarked. This suggests that the decrease in the transmittance of SnO_2: Sb films, with an increase in doping concentration, may be due to the increased absorption by free electrons. The latter is generated by oxygen vacancies caused through the distortion of SnO_2: Sb films, as reported in Table V.1.

Table.V.1: Structural and electrical properties of SnO_2: Sb thin films.

Sb (wt.%)	Crystallite size (nm)	$\langle\varepsilon^2\rangle.10^{-6}$	$n \times 10^{19}$ (cm^{-3})
0	33.253	1.424	1.8
0.6	27.206	2.132	4.65
0.8	24.933	2.541	11.8
1	33.249	1.425	3,07

Hence the transmission spectra recorded for different Sb doping levels show a consistent decrease with increasing Sb doping concentration until 0.8 wt.%. Further, the more decreasing absorption by free electrons is observed due to its concentration decrease. This behavior correlates well with electrical properties as it will be seen in the electrical results (see below).

The optical gap (E_g) of the films can be obtained by plotting $((\alpha h\upsilon)^2$ vs. $h\upsilon$) (α is the absorption coefficient and $h\upsilon$ is the photon energy) and extrapolating the straight-line portion of this plot to the energy axis. The obtained E_g values for the undoped and Sb-doped SnO_2 films are recapitulated in Table V.2.

Table V.2: Optical and electrical properties of SnO_2: Sb thin films.

Sb (wt.%)	R_{sh} ($\Omega\,cm^{-2}$)	$\rho \times 10^{-3}$ (Ω cm)	$n \times 10^{19}$ (cm^{-3})	E_g (eV)
0	138	11.1	1.8	3.651
0.6	47.43	4.43	4.65	3.829
0.8	31.07	2.17	11.8	3.929
1	56.09	3.92	3,07	3.869

With increasing Sb concentration, from 0 to 0.8 wt.%, the absorption edge of the films shifts to a shorter wavelength, which is due to Moss–Burstein

effect [3]. The direct optical band gap (E_g) has increased from 3.651 to 3.929 eV. As Sb concentration increases further, the absorption edge shifts slightly to the longer wavelength and E_g has decreased from 3.929 eV to 3.869 eV.

V.2.1.b Electrical properties

Fig.V.2 shows the resistance sheet ($\boldsymbol{R}_{sh}$) and carrier concentration $\boldsymbol{n}$ as a function of Sb concentration.

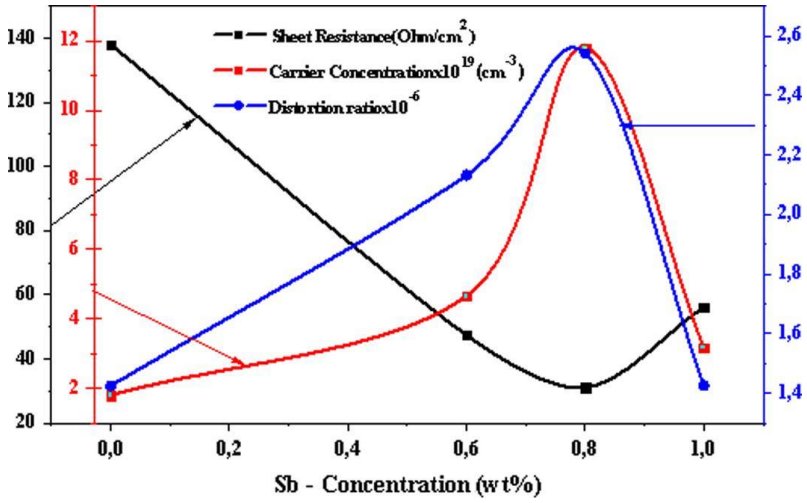

Fig. V.2. Variation of distortion, carrier concentration ($\boldsymbol{n}$), and sheet resistance R_{sh} of ultrasonic sprayed SnO_2: Sb thin films with different Sb concentration [1].

All Sb-doped SnO_2 thin films were conducting at 300 K with resistivity values much less than of undoped SnO_2 one (see Table V.2) and $\boldsymbol{R}_{sh}$ of the undoped SnO_2 is relatively high compared to the doped ones. For the 0-1% doped films, the sheet resistance decreases at first from 138 to 31.07 Ω/□ until 0.8 wt. % Sb doping level and then increases to reach 56.09 Ω/□ for the 1 wt.% Sb doping level. It is worth noting that from the Hall effect

measurement, carrier concentration (***n***) increases at first from 1.8 10^{+19} to 11.8 10^{+19} cm^{-3}, then decreases to 3.92 $10^{+19}cm^{-3}$.

Those behaviors can be explained as fellow: Antimony can play two roles due to its two oxidation states namely Sb^{3+} (0.93 Å) and Sb^{5+} (0.62 Å). At doping level lower than or equal to 0.8 wt.%; since the Sn^{4+} ionic radius is lower than Sb^{3+} one but higher than of Sb^{5+}one; substitutions of Sn^{4+} by Sb^{3+}resulting in increasing in the lattice parameters of SnO_2 which may considered as the predominante phenomenon. The amount of Sb^3 substitutional (Sb_{sub}) can play other role, as accepter, in electrical properties of SnO_2 thin films but its existence, in SnO_2 matrices, can generate more oxygen vacancies, as donors, due to the distortions in the structure. As mentioned, in spray deposited polycrystalline oxides, oxygen vacancies are known to be the most common defects and play donors role [4], which compensate at first the existents Sb^3, as acceptors, and then participate in films resistance decrease ($\boldsymbol{R}_{sh}$). More than 0.8 wt.% Sb doping, the predominate phenomenon may be that many Sb_{sub} enter the interstitial sites, and participating in oxygen vacancies decrease (*i.e*. feeble donors concentration) which leads to $\boldsymbol{R}_{sh}$ enhancement; but $\boldsymbol{R}_{sh}$ is still lower than of the undoped one. This predominate phenomenon do not expelled of course the hypothesis of the co-existence of Sb^{5+}donors together with Sb^{3+} acceptors, even there is no change in the experimental temperature, in the range doping over than 0.8 wt.%; only the amount of oxygen vacancies becomes feeble but it still dominant, as donors, compared to Sn^{4+} and Sb^{3+} acceptors.

V.3. fluorine doping (F)

V.3.1.Results and discussion

V.3.1.a Optical properties

The optical transmission $T(\lambda)$ measurements as a function of the wavelength are depicted in (Fig. V.3). In this figure, we have gathered the undoped SnO_2 and doped F (0-12 wt. %) SnO_2 spectra.

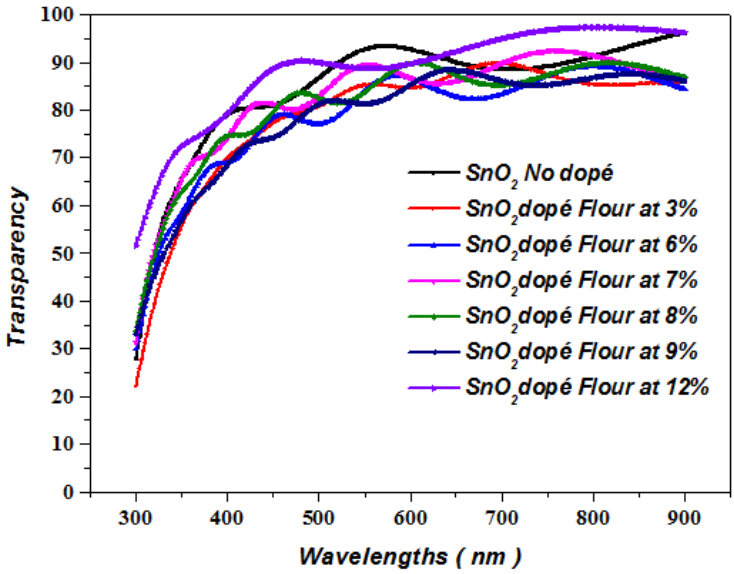

Fig. V.3. Spectral transmittance plot of F (0-12 wt.%) doped SnO_2 thin films [5].

As it can be seen, a height transparent spectra $T(\lambda)$ of undoped SnO_2 in visible region, the average transmission is more than 92% and the film exhibit significant oscillations in long wavelength; this oscillation may be due to the roughness of the top surface of undoped SnO_2 film which can generate interference phenomenon; even at nuked eye one can see that the undoped SnO_2 lattice is very smooth. Then the transmission decreased because of the onset fundamental absorption in the region round 340nm.

For the doped SnO_2 films the value of transmission $T(\lambda)$, in the visible region, is located in the average 81.3-92.88% revealing slight decrease upon the increasing F doping amount as it shown in (Fig. V.3). The region of the absorption edge in all layers due to the transition between the valence band and the conduction band is located between 317-340 nm until 7 wt. % of (F/Sn); in this region the transmission decreased because of the onset fundamental absorption. One can note that the doping effect is clearly observed in the layer quality such as in the average between 317-340 nm; blue shift of the absorption edge was observed as function of doping level until 7 wt.% reveling Burstein-Moss effect [3, 6] then sleight return to the initial values of the absorption edge revealing the Roth effect [7] which indicates that the increasing of doping amount can change the lattice structure.

V.3.1.b Electrical properties

All F-doped SnO_2 (FTO) thin films were conducting at 300 K with resistivity values much less than of undoped SnO_2 one. The resistance sheet ($\boldsymbol{R}_{sh}$) of the undoped SnO_2 is relatively high compared to the doped ones.

The Hall Effect measurements, which were recapitulated in Table V.3, have been carried out to evaluate different electrical parameters such as resistivity, mobility and free carrier concentration of the 0-12wt% F-doped SnO_2.

Table V.3: Optical and electrical properties of SnO_2: Sb thin films.

F (wt.%)	R_{sh} (Ω)	$\rho \times 10^{-3}$ (Ω ∗ cm)	$N \times 10^{19}$ (cm^{-3})	E_g (eV)
0%	138	11.1	–	3.651
3%	75	7.01	0.75	3.764
6%	21	1.47	2.04	3.842
7%	22	1.54	3.07	3.902
8%	23	1.77	2.45	3.867
9%	24	2.10	0.98	3.786
12%	50	4.88	0.04	3.666

Firstly Hall measurements indicate that the ultrasonic sprayed FTO films have n-type semiconductors character; Secondly, as it was seen in (Fig. V.4) that the variations of sheet resistance and free carrier concentration, as a function of fluorine concentration of SnO_2: F films, were inverted. This may be explained as follow: when fluorine is incorporated in tin oxide films, each F^- anion substitutes an O^{2-} anion in the lattice and the substituted O^{2-} anion introduces more free electrons. This results in an increase in free electrons and decreases the value of R_{sh} (or resistivity). This can be attributed as the reason for decreasing R_{sh} with increasing fluorine doping.

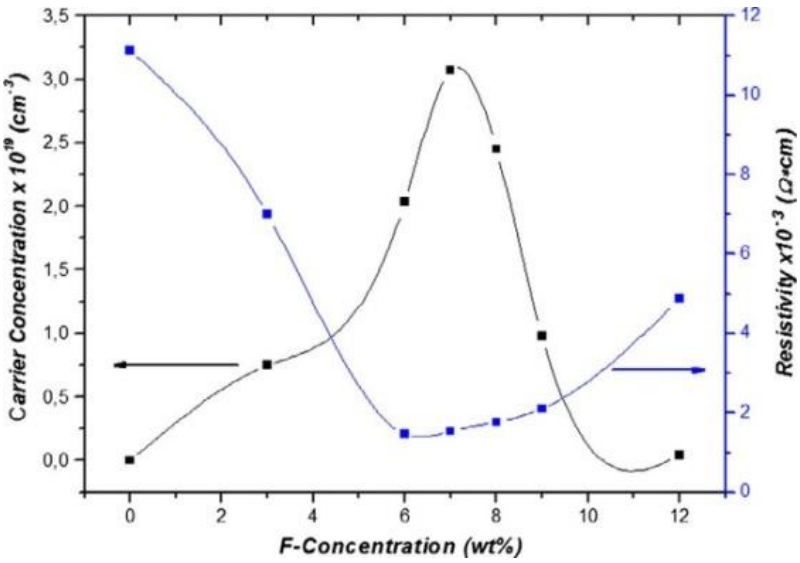

Fig. V.4. Variation of carrier concentration and resistivity of ultrasonic sprayed SnO_2: F thin films with different fluorine doping concentration [5].

The decrease in the free electrons with an increase in the value of $\boldsymbol{R}_{sh}$ beyond a certain doping concentration of fluorine (7 wt.% in our work) probably represents a solubility limit of fluorine in the tin oxide lattice [8]. The excess F atoms do not occupy the proper lattice positions to contribute to the free carrier concentration while, at the same time, it enhance the disorder of the structure leading to an increase in sheet resistance.

V.4.Opto-electrical studies

V.4.1. Figure of merit

In many applications requiring transparent conducting films, the optical transmission and electrical conductivity should be as high as possible. This is particularly important for solar cell applications because high optical transmission in the visible region enhances the photogenerated current and low sheet resistance (*i.e*. high electrical conductivity) reduces the series resistance of the cell. The performance of transparent conductors is often

assessed through figures of merit (Ω^{-1}) which incorporate both electrical and optical parameters [9-11]. The figure of merit is calculated by using Haacke formula as follow [12]:

$$\varphi = \frac{T^{10}}{R_{sh}}$$

Both transmittance and resistivity were significantly affected by the film thickness. The figure of merit was used to determine the thickness at which the films present the best condition for their use in solar cells as widow and collector. Whereas plots of the figure of merit for undoped SnO_2 and F/Sb-doped SnO_2 were shown in Fig.V.5.

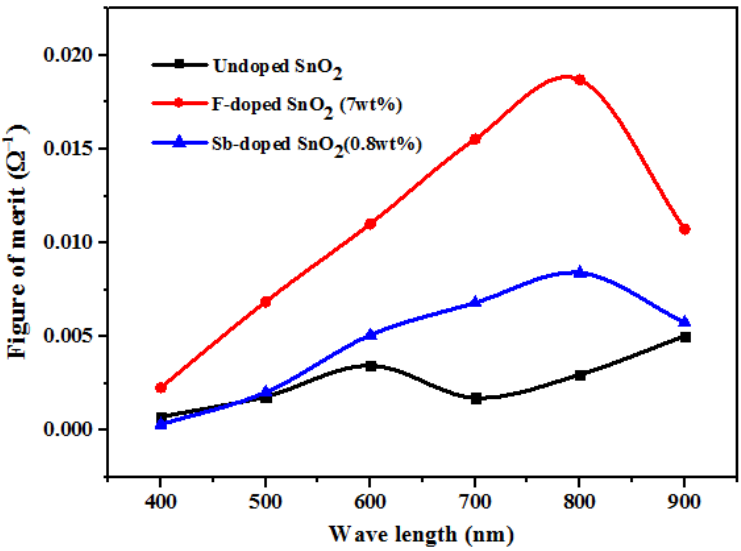

Fig. V.5. Figure of merit of undoped SnO_2, 7 wt.% F-doped $SnO_2$and 0.8 wt.% Sb-doped SnO_2 as a function of wavelengths

It was noted that an enhancement of the values of the figure of merit in the visible region was well remarked. The values of the figure of merit increase as a function of wavelength after fluorine and antimony doping. At 800nm figures of merit reach maximum values of $1.78x10^{-2}\Omega^{-1}$ and

$8.4x10^{-3}\Omega^{-1}$ for FTO (7%) and ATO (0.8%) respectively and they are higher than ones in the literature [13-16].

V.5 Conclusions

- Undoped and F or Sb-doped SnO_2 thin films are successfully prepared using inexpensive spray ultrasonic technique.
- For both elements F or Sb the films have n-type electrical conductivity and depend upon the dopants concentration.
- The average optical transparency (T(λ) % of the films in visible spectra decreases from 93% for the undoped to more than 80%.it depended on the
- The deduced E_g, of the films, increase from 3.651 eV to 3.902 eV with increasing For Sb doping level.
- Sb doping until 0.8 wt.% level, the substitution of some Sn^{4+} by Sb^{3+}states into the SnO_2 network is the favored one to cause more distortion and more oxygen vacancies generation. Beyond this level namely when Sb doping reaches 1%, Sb^{3+}occupying the Sn^{4+} sites miss its role in substituting Sn^{4+} and enter in the interstitial sites leading to feeble oxygen vacancies.
- The minimum resistance sheet ($\boldsymbol{R}_{sh}$) and maximum carrier concentration n, achieved for SnO_2: Sb thin films, have been found to be 31Ω/□and 11.8 $x10^{+19}$ cm^{-3} at 0.8 wt.% Sb doping level.
- Also, The minimum resistance sheet ($\boldsymbol{R}_{sh}$) and maximum carrier concentration n, achieved for SnO_2: F thin films, have been found to be 21Ω/□ and 2.04 $x10^{+19}$ cm^{-3} at 6.0 wt.% F doping level.
- A maximum value of figure of merit, $1.78x10^{-2}\Omega^{-1}$, $8.4x10^{-3}\Omega^{-1}$ at 800 nm for FTO (7%) and ATO (0.8%) respectively. The obtained

high conducting and transparent FTO and ATO thin films are promising to be useful in various optoelectronic applications, in particular, as a window layer in solar cells.

References

[1] A. Rahal, A. Benhaoua, C. Bouzidi, B. Benhaoua, B. Gasmi, Effect of antimony doping on the structural, optical and electrical properties of SnO 2 thin films prepared by spray ultrasonic, Superlattices and Microstructures, 76 (2014) 105-114.
[2] S.-Y. Lee, B.-O. Park, Structural, electrical and optical characteristics of SnO 2: Sb thin films by ultrasonic spray pyrolysis, Thin solid films, 510 (2006) 154-158.
[3] E. Burstein, Anomalous optical absorption limit in InSb, Physical Review, 93 (1954) 632.
[4] A. Babar, S. Shinde, A. Moholkar, C. Bhosale, J. Kim, K. Rajpure, Sensing properties of sprayed antimony doped tin oxide thin films: solution molarity, Journal of Alloys and Compounds, 509 (2011) 3108-3115.
[5] A. Benhaoua, A. Rahal, B. Benhaoua, M. Jlassi, Effect of fluorine doping on the structural, optical and electrical properties of SnO 2 thin films prepared by spray ultrasonic, Superlattices and Microstructures, 70 (2014) 61-69.
[6] T. Moss, The interpretation of the properties of indium antimonide, Proceedings of the Physical Society. Section B, 67 (1954) 775.
[7] A.P. Roth, J.B. Webb, D.F. Williams, Band-gap narrowing in heavily defect-doped ZnO, Physical Review B, 25 (1982) 7836.
[8] E. Elangovan, K. Ramamurthi, Optoelectronic properties of spray deposited SnO 2: F thin films for window materials in solar cells, Journal of Optoelectronics and Advanced Materials, 5 (2003) 45-54.
[9] M. Gracia, F. Rojas, G. Gordillo, Morphological and optical characterization of SnO2: F thin films deposited by spray pyrolysis, in: 20th European Photovoltaic Solar Energy Conference, 2005, pp. 6-10.
[10] T. Hauger, A. Zeberoff, B. Worfolk, A. Elias, K. Harris, Real-time resistance, transmission and figure-of-merit analysis for transparent conductors under stretching-mode strain, Solar Energy Materials and Solar Cells, 124 (2014) 247-255.
[11] N. Manjula, K. Usharani, A. Balu, V. Nagarethinam, Studies on the Physical Properties of three Potentially important TCO Thin Films fabricated by a Simplified Spray Technique under same Deposition conditions, Int. J. ChemTech Res, 6 (2014) 705-718.
[12] G. Haacke, New figure of merit for transparent conductors, Journal of Applied Physics, 47 (1976) 4086-4089.
[13] A. Moholkar, S. Pawar, K. Rajpure, C. Bhosale, J. Kim, Effect of fluorine doping on highly transparent conductive spray deposited

nanocrystalline tin oxide thin films, Applied Surface Science, 255 (2009) 9358-9364.
[14] A. Babar, S. Shinde, A. Moholkar, C. Bhosale, J. Kim, K. Rajpure, Structural and optoelectronic properties of antimony incorporated tin oxide thin films, Journal of Alloys and Compounds, 505 (2010) 416-422.
[15] P. Bhuvaneswari, P. Velusamy, R.R. Babu, S.M. Babu, K. Ramamurthi, M. Arivanandhan, Effect of fluorine doping on the structural, optical and electrical properties of spray deposited cadmium stannate thin films, Materials Science in Semiconductor Processing, 16 (2013) 1964-1970.
[16] X. Ding, F. Fang, J. Jiang, Electrical and optical properties of N-doped SnO 2 thin films prepared by magnetron sputtering, Surface and Coatings Technology, 231 (2013) 67-70.

SUMMARY AND CONCLUSION

This thesis reports the essential experimental results and characterizations on the ultrasonically deposition of transparent oxide materials based on undoped SnO_2 and both doped Fluor and Antimony SnO_2 at room pressure. The effects of different ultrasonically deposition parameters are considered to explain and discuss the physical, structural, electrical and optical properties of these oxide thin films. The importance of the three different parameter conditions (effect of substrate temperatures, the effect of tin precursor concentration and effect of a solvent such as ration of water to methanol are undergone to be optimized for elaborating SnO_2 films with good quality and competitive to ITO. Furthermore, the potential use of these oxides is attempted and demonstrated for future considerations in solar cell fabrications as collector electrodes. The significant results achieved and presented in the previous chapters are summarized in this chapter and suggestions for future work are discussed too.

The aim ideas, we would like to clarify in this purpose, are the effect of parameters, undertaken in this work, optimizing SnO_2 thin films for future application in solar cells. Those parameters are the substrate temperatures, the tin precursor concentrations, the different ratios of water to methanol and the different doping elements such as fluorine and antimony.

VI.1. SnO_2 thin films with different substrate temperatures

The undoped SnO_2 thin films of were deposited onto microscopic glass substrates using an ultrasonic spray pyrolysis technique. The films were deposited at various substrate temperatures ranging from 400 to 500°C in steps of 20°C. The effect of substrate temperature on structural, electrical

and optical properties was studied. The X-ray diffraction study showed that all the films were polycrystalline with major reflex along (*110*) plane, which its surface needs the lowest energy to form, and manifested with amelioration of grain size with elevating substrate temperature. Among all the samples, the films deposited at 480°C exhibited lowest resistivity ($9.19x10^{-3}$ Ω.cm) which means the highest n-type conductivity. The direct band gap energy was found to vary from 4.03 to 4.133 eV and transmittance at 550 nm varies from 43.8 to 66% with a rise in substrate temperature.

VI.2. SnO_2 thin films: effect of tin precursor concentration

Since the optimized temperature for ultrasonically deposited SnO_2 thin films in this work was 480°C, effect of 0.05-0.2 M as the concentration of tin in precursor solution on physical properties, of SnO_2 thin films deposited on heated glass substrates at 480°C, was investigated. Different molarities were prepared by dissolving pure stannous chloride ($SnCl_2 \cdot 2H_2O$) in a mixture of double distilled water and methanol at fixed ration ½:½ (not optimized at the departure). X-ray diffraction (XRD), UV-visible spectrophotometer, conventional four-point probe techniques and Hall Effect are used for this purpose to evaluate structural, optical and electrical properties of the obtained thin films.

Most of the appeared diffraction peaks matched well with the tetragonal rutile SnO_2, and the rest others peaks are associated to SnO and cubic crystal system of SnO_2. Crystallite size (***D***), in general, decreases gradually as the concentration of tin in solution increases. This behavior may be explained the excess of tin generating the nucleation and the poor arrival

of oxygen to form SnO_2 on the substrates.

The average transmission at a wavelength of 550 has been found to be ranged in 67-91.3% and decreases gradually with the concentration of tin in solution. The band gap energy values of all SnO_2 thin films samples are ranged in 3.65-3.97eV revealing a decrease with increasing the concentration of tin in the solution. The free carrier concentration ($\boldsymbol{n_e}$) has a minimum value (n_e = 4.17. $10^{14}cm^{-3}$) at (C_1=0.05M) and increases with concentration until (C_4=0.125M) where it reaches $2.56.10^{19}cm^{-3}$ as maximum value and drastically decrease to reach the value (n_e= 1.37. $10^{14}cm^{-3}$) for (C_3=0.2M) in the solution. An attempt to explain this behavior is given: For all concentrations, the mobility is directly inverted to the free carrier but the values of mobility are more than ones in literature. As results elaborating SnO_2 thin films with (C_4=0.15M) of $SnCl_2$ will be the preferred concentration in the precursor for this technique.

VI.3. SnO_2 thin films with different ratios of water to methanol

Since the optimized temperature for ultrasonically deposited SnO_2 thin films in this work was 480°C and as preferred concentration of $SnCl_2$ in the precursor was 0.15M for this technique; Transparent conducting SnO_2 thin films have been deposited on 480°C heated glass substrates by a spray pyrolysis technique using ($SnCl_2 \cdot 2H_2O$) as precursors and mixture of water and methanol as solvent. The concentration of ($SnCl_2 \cdot 2H_2O$) is kept fixed and the ratio of water and methanol (W/M) solvent in the spraying solution is varied in the range as follow (0W25M, 5W20M, 10W15M, 12.5W12.5M, 15W10M, 20W5M and 25W0M). X-ray diffraction (XRD), UV-visible spectrophotometer, conventional four-point probe techniques and Hall Effect are used for this purpose to evaluate the physical properties

of the obtained thin films. The as-deposited films are polycrystalline SnO_2 with a tetragonal crystal structure and are preferentially orientated along the (110) direction with high texture coefficient as 2.14. The crystallite size varies between 16.63 and 25.94 nm for the as-deposited sample within the ratio of water to methanol.

The direct band gap energy was found to vary between 3.665 and 3.971eV whereas the transmittance at 550 nm varies from 51.64 to 80.12% with the water content in the starting solution it means the ratio of water to methanol.

The electrical resistivity of deposited thin films at 480˚C decreases with the water content, reaching a minimum value closely to $1.81x10^{-2}\Omega cm$, with the starting solution having ration of 15W10M (*i. e* 15 ml per 25 ml) of solution; further increase in water content increases the corresponding resistivity of the deposited thin films.

VI.4. SnO_2 thin films with different doping elements

VI.4.1. F: SnO_2 (FTO)

For commodities reasons, the films are sprayed on heated glass substrates at 480°C and given a ration of 1:1 water-methanol, the 0-12wt. % fluorine doped tin oxide (SnO_2) thin films are synthesized by using the cost-effective spray. The dependence of structural, optical and electrical properties of SnO_2 films on the concentration of fluorine is investigated using X-ray diffraction, UV-visible, four-point probe and Hall Effect studies have been performed on undoped and fluorine-doped SnO_2 (FTO) films. X-ray diffraction pattern reveals the presence of cassiterite structure with (200) as preferential orientation for FTO films. The crystallite size

varies from 10.3 to 27.12 nm and was affected by F concentration having maximum value beyond 6 wt. % fluorine doping and remains constant in respect to the rest of average doping.

All films exhibit optical transmission T(λ) more than 83.9% in the visible region; based on the existence of interferences optically estimated film thickness varies from 700 to 975 nm for the same given time (3min deposition) and band gap (E_g) varies from 3.65 to 3.90eV. The electrical study reveals that the films have n-type electrical conductivity and depend upon fluorine concentration too. The sprayed FTO film doped at 6 wt. % fluorine has the minimum resistivity of 1.47x 10^{-3}Ωcm and minimum resistance sheet (R_{sh}) of 21 Ω whereas the carrier concentration and mobility were about 2.04x10^{19} cm^{-3} and 208.4 $cm^2V^{-1}s^{-1}$ respectively as reported in the literature.

VI.4.2. Sb: SnO_2 (ATO)

As it was elaborated with FTO, antimony-doped tin oxide (ATO) or (Sb: SnO_2) thin films have been prepared by spray ultrasonic on heated glass substrates at 480 °C for 3 min as time deposition. The dependence of structural, optical and electrical properties of Sb: SnO_2 films on the Sb concentration (0-1 wt.%), is investigated. X-ray diffraction pattern reveals the presence of cassiterite structure with (211) as preferred orientation for ATO thin films with the presence of other orientations. Focused analysis, on (211) peaks, indicated that the interplanar spacing of SnO_2 (211) increases, after Sb doping until 0.8 wt.% level, this increase is due to the substitution of some Sn^{+4} by some Sb in Sb^{+3} state, (Sb_{sub}), into the SnO_2 lattice, causing distortion and generated oxygen vacancies. Good agreement has been found between AFM topographical images of the Sb:

SnO_2 samples and XRD grain size measurements. The crystallite size varies from 24.93 to 33.25 nm and was affected by Sb concentration whereas the lattice parameters such as *a* and *c* are found to increase with Sb doping concentration until 0.8 wt. % level and then decreased. Sb: SnO_2 thin films transparency in the visible range was around 80% at Sb doping level lower than 0.8 wt.%; all the envelopes of transmission T(λ) curves, in the whole wavelength range 200-3100nm, were become contracted and shift toward lower wavelength revealing the behavior effect of plasma carrier concentration in absorbing light. The optical band gap (E_g) increases from 3.65 to 3.92 eV and then decreases. Minimum resistance sheet and maximum carrier concentration have been achieved for SnO_2: Sb thin films and found to be 31.07 Ω and $11.8x10^{19}$ cm^{-3} at 0.8wt% Sb doping level.

VI.5 General conclusions

VI.5.1. Effect of T on SnO_2 properties

- The XRD analyses revealed that the deposited SnO_2 have tetragonal structure.
- Transparency in the visible region of deposited SnO_2 thin films is in range 43.8-75%.
- The resistivity is limited by the grain size at low substrate temperature.
- As results elaborating SnO_2 thin films with (T_{sub} =480 °C) of temperature will be the preferred substrate temperature for this technique.

VI.5.2. Effect of C on SnO_2 properties

- Most of the appeared diffraction peaks matched well with the tetragonal rutile SnO_2, and the rest others peaks are associated to SnO and cubic crystal system of SnO_2.
- The average transmission at a wavelength of 550 has been found to be ranged in 67-91.3%.
- As results elaborating SnO_2 thin films with (C_4=0.15M) of $SnCl_2$ will be the preferred concentration in the precursor for this technique.

VI.5.3. Effect of Ratio W/M on SnO_2 properties

- The as-deposited films are polycrystalline SnO_2 with a tetragonal crystal structure and are preferentially orientated along the (110.
- The crystallite size varies between 16.63 and 25.94 nm for the as-deposited sample within the ratio of water to methanol.
- The transmittance at 550 nm varies from 51.64 to 80.12% with the water content in the starting solution it means the ratio of water to methanol.
- Reaching a minimum value closely to $1.8x10^{-2}$ Ωcm, with the starting solution having a ratio of 15W10M (*i. e* 15 ml per 25 ml) of the solution.

VI.5.4. Effect of doping on Figure of merit

- A maximum value of figure of merit, $1.78x10^{-2}\Omega^{-1}$, $8.4x10^{-3}\Omega^{-1}$ at 800 nm for FTO (7%) and ATO (0.8%) respectively. The obtained high conducting and transparent FTO and ATO thin films are promising to be useful in various optoelectronic applications, in particular, as a window layer in solar cells.

Publications

Superlattices and Microstructures 86 (2015) 403–411

Contents lists available at ScienceDirect

Superlattices and Microstructures

journal homepage: www.elsevier.com/locate/superlattices

Structural, optical and electrical properties studies of ultrasonically deposited tin oxide (SnO_2) thin films with different substrate temperatures

Achour Rahal [a,c], Atmane Benhaoua [a,b], Mohamed Jlassi [d], Boubaker Benhaoua [a,*]

[a] Lab. VTRS, Faculty of Science & Technology, University of El-Oued, El oued 39000, Algeria
[b] Faculty of Mathematics and Material Sciences, Univ. Ouargla, Ouargla 30000, Algeria
[c] Faculty of Science, University of Biskra, Biskra 07000, Algeria
[d] Laboratoire de Photovoltaïque, Centre de Recherche et des Technologies de l'Energie, Technopole de Borj-Cédria, BP95, 2050 Hammam-Lif, Tunisia

ARTICLE INFO

Article history:
Received 8 July 2015
Accepted 10 August 2015
Available online 11 August 2015

Keywords:
Tin oxide
Thin films
Spray ultrasonic
Four-point probe technique
X-ray diffraction

ABSTRACT

Undoped thin films of tin oxide (SnO_2) were deposited onto microscopic glass substrates using an ultrasonic spray pyrolysis technique. The thin films were deposited on glass at large scale of temperature ranged in 400–500 °C and stepped by 20 °C. The effect of substrate temperature on structural, electrical and optical properties was studied using X-ray diffraction (XRD), UV–visible spectrophotometer and a conventional four point probe technique. XRD showed that all the films were polycrystalline with major reflex along (1 1 0) plane, manifested with amelioration of grain size from 6.51 to 29.80 nm upon increasing substrate temperature. Lattice constant '*a*', '*c*', microstrains and dislocation densities were affected by the substrate temperature. Transmittance of about 75% at more than 800 nm for films prepared at 480 °C has been observed. With increasing the substrate temperature the direct band gap energy was averaged in 4.03–4.133 eV. Plasma frequency (ω_p) was estimated to be $4 \cdot 10^{14}$ Hz and optically estimated free electrons number N leading to predict that, in SnO_2 material, the effective density of conduction band states is about $5 \cdot 10^{19}$ cm^{-3}. Among all the samples the film that deposited at 480 °C exhibited lowest resistivity of about 9.19×10^{-3} Ω cm.

1. Introduction

Tin oxide (SnO_2) is a non-stoichiometric semi conductor with a wide band gap ($E_g \geqslant 3.6$ eV) at room temperature with tetragonal structure [1,2]. SnO_2 films have unique characteristics such as high transmittance in visible wavelength region, low resistivity, high chemical and thermal stabilities compared to other transparent conductive oxides (TCOs) [3]. It has low cost. SnO_2 films are widely used in optoelectronic applications, heat mirror coatings, photocatalysis, organic light emitting diodes, gas sensors, solar energy collectors [4–9]. There are several methods for preparing SnO_2 thin films: The screen printing technique, chemical vapor deposition, reactive evaporation, dc and rf sputtering, pulsed laser ablation, thermal evaporation, electron beam evaporation, metal–organic deposition, sol–gel deposition, spray pyrolysis and thermal evaporation [10–19]. Among these methods, spray ultrasonic has the advantages of producing high purity crystalline products

* Corresponding author.
E-mail address: benhaouab@yahoo.fr (B. Benhaoua).

http://dx.doi.org/10.1016/j.spmi.2015.08.003
0749-6036/

and durable films in a single step [20]. Various parameters such as substrate temperature annealing, deposition rate, oxygen partial pressure and have significant influence on characteristics of SnO_2 films. Among these parameters, substrate temperature has a major role in decreasing the intrinsic stress, increasing mobility of charge carriers, and improving homogeneity and crystallinity of films to get better. To the best of our knowledge, no much attention has been paid to the study of the substrate temperature effect on characteristics of undoped SnO_2 specifically when it was deposited by spray ultrasonic.

In this work, the structural, optical and electrical properties of SnO_2 thin films sprayed ultrasonically on various heated temperatures glass substrates were investigated using X-ray diffraction (XRD), UV–visible spectrophotometer and a conventional four point probe technique.

2. Experimental details

SnO_2 films were ultra sonically deposited on glass substrate heated between 400–500 °C. As a precursor for tin, used in this work, was a 99.99% pure stannous chloride ($SnCl_2$ $2H_2O$) dissolved in double distilled water and methanol (volume ratio1:1) with adding few drops of (HCl). The precursor concentration was (0.1 M). The later was stirred at room temperature (*rt*) for half an hour to yield a clear and transparency solution. The blend so obtained was used as a stock solution for spray ultrasonic. An R217102 microscopic glass slide in a size of ($75 \times 25 \times 1.1$ mm^3) was used as substrates. Those substrates were cleaned with alcohol in an ultrasonic bath and distilled water then blow-dried with dry nitrogen gas. The substrate temperature was varied between 400–500 °C and steeped by 20 °C [21]. To read and control the substrate temperature a Chromel–Alumel and K type thermocouple were used. The time deposition was maintained 3 min for each experiment. After deposition, the films were allowed to cool down naturally to room temperature.

The structural properties of the film were investigated using X-ray Diffractometer (XPERT-PRO X-ray Diffractometer system under 30 kV, 30 mA conditions) equipped with X'Pert High Score under Cu Kα (λ = 1.5406 Å) radiation in the scanning range of (2θ) between 20–90°. The grain size of the films was estimated using X'Pert High Score. The optical transmission spectra were obtained using an UV–visible spectrophotometer (Shimadzu, Model 1800) and measured in the range of 300–900 nm; whereas the different optical parameters such as the band gap, Urbach energy, electron plasma frequency and film thickness were determined using data and fitting of transmission spectrum. The resistivity of thin films was characterized using four point probe method on 1×1 cm^2 sample sheet. All measurements were carried out at room temperature (*rt*).

3. Results and discussion

3.1. X-ray diffraction studies

The XRD patterns of SnO_2 thin films deposited at various substrate temperatures are shown in (Fig. 1). As it can be seen the diffraction peaks were observed at 2θ = 26.65°, 33.939°, 38.035°, 51.771°, 54.7124°, 61.886°, 65.898° and 78.597° which are related to the following plans (1 1 0), (1 0 1), (2 0 0), (2 1 1), (2 2 0), (3 1 0), (3 0 1) and (3 2 1) respectively. The obtained XRD spectra matched well with the space group P42mnm according to JCPDS (No. 41-1445) of the tetragonal, rutile SnO_2 structure [1] and indicated the polycrystalline nature of the thin films; the tin dioxides thin films deposited at temperature down to 420 °C were partially crystalline in nature [22] and they contain (1 0 1) SnO peak according to JCPDS (No. 06-395) this peak is signalized by a start (*) in Fig. 1. It is worth noting that the crystallinity was increased as the substrate temperature increases (peak intensities) from 420 °C to 500 °C, indicating the formation of more crystallites with well-defined orientation along (1 1 0) plane and some other less prominent peaks such as (2 0 0) and (2 1 1) planes which were also present in the XRD

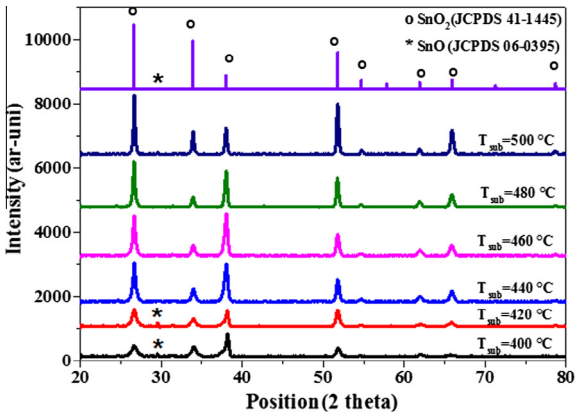

Fig. 1. XDR patterns of undoped SnO_2 thin films with different substrate temperatures.

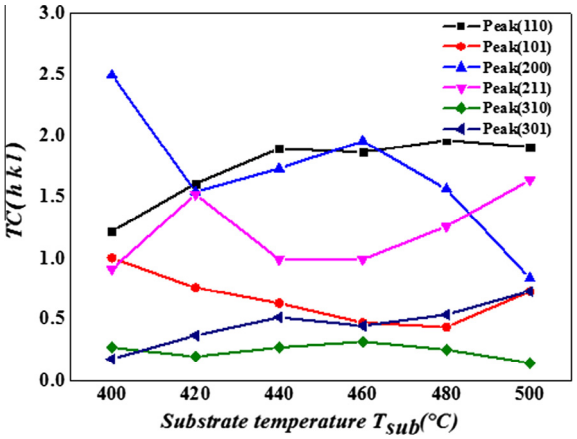

Fig. 2. Variation of *TC* (*hkl*) with different substrate temperatures in SnO_2 thin films.

patterns (Fig. 1). Increase in crystallinity with substrate temperature is may be due to the optimum rate of supply of thermal energy for recrystallization with substrate temperature as reported by Nikale et al. [23].

The texture coefficient *TC*(*hkl*) represents the texture of the particular plane, deviation of which from unity implies the preferred growth. The different texture coefficient *TC*(*hkl*) have been calculated from the X-ray data using the well-known formula [24]:

$$TC(hkl) = \frac{I(hkl)/I_0(hkl)}{N^{-1}\sum_n^N I(hkl)/I_0(hkl)}$$

where $I(hkl)$ is the measured relative intensity of a plane (*hkl*), $I_o(hkl)$ is the standard intensity of the plane (*hkl*) taken from the JCPDS data, N is the reflection number and n is the number of diffraction peaks. $TC(hkl)$ values of all the films for (1 1 0), (1 0 1), (2 0 0), (2 1 1), (3 1 0) and (3 0 1) with increasing substrate temperature are shown in (Fig. 2). The peaks were less than unity confirming the polycrystalline nature of the films. However, the films deposited up to 480 °C presented a possible oriented growth along the (1 1 0) plane direction and with other less oriented growth along the (2 1 1) plane as seen in Fig. 2. It is worth noting that preparation of the (1 1 0) surface in vacuum alone always results in an oxygen deficient surface [25], the (1 1 0) surface exhibits the lowest energy surface followed by the (2 1 1), and (2 0 0) surfaces.

The lattice constant '*a*' and '*c*', for the tetragonal phase structure is determined by the relation [26]:

$$2d_{hkl}\sin(\theta) = n\lambda \quad \text{and} \quad \frac{1}{d_{hkl}^2} = \frac{h^2+k^2}{a^2} + \frac{l^2}{c^2}$$

where '*d*' is the interplaner distance and (*hkl*) are miller indices, respectively. The lattice constants *a* and *c* are calculated and given in Table 1. The lattice constant *a* and *c* first increase to reach a maximum value at around 480 °C and then decrease. It was observed that lattice constants *a* and *c* calculated for 480 °C match well with the standard JCPDS data card [1]. The variation in lattice constant (Δa and Δc) for the spray-deposited thin film over the bulk clearly suggests that the film grains are strained, which may be due to the nature and concentration of the native imperfections changing (oxygen vacancies, vacancy clusters and local lattice disorders) [27].

The average nanoparticles crystallite size of SnO_2, with a varying substrate temperature was determined from XRD broadening using the Debye–Scherer formula [28]:

$$D = \frac{0.9\lambda}{\beta\cos(\theta)}$$

Table 1
Crystallite size *D*, dislocation density δ, strain ε, and lattice parameters *a* and *c* of undoped SnO_2 thin films with different substrate temperatures.

Substrate temp (°C)	Crystallite size (nm)	$\delta \times 10^{15}$ (lines/m^2)	$\varepsilon \times 10^{-3}$	*a*	Lattice constants (Å)		$\Delta c = c - c_0$
					$\Delta a = a - a_0$	*c*	
400	6.52	23.51	−27.00	4.72263	−0.01557	3.17327	−0.01383
420	8.23	14.75	−18.00	4.72576	−0.01244	3.17956	−0.00754
440	13.27	5.67	−7.00	4.72475	−0.01345	3.17963	−0.00747
460	15.52	4.15	−4.00	4.72759	−0.01061	3.18024	−0.00686
480	20.27	2.43	−2.00	4.73126	−0.00694	3.18473	−0.00237
500	29.80	1.12	−1.00	4.72480	−0.01340	3.18394	−0.00316

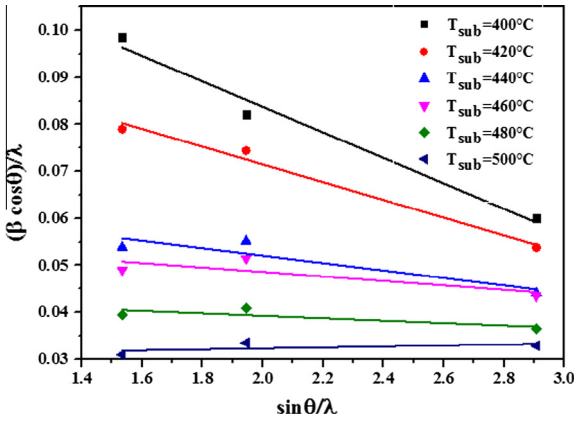

Fig. 3. Williamson–Hall plots of undoped SnO_2 thin films with different substrate temperatures.

where λ is the wavelength of X-ray radiation, β is the full width at half maximum of the peak at diffraction angle θ [29] and the average crystallite sizes were found to be in the range of 6.52–29.80 nm and increases with increasing substrates temperature. The increase may due to non uniform stress or strain during the grain growth or to the existence of local structural disorder in the material. In fact, the growth mechanism involving dislocation is a matter of importance. Dislocations are imperfect in a crystal associated with the mis-registry of the lattice in one part of the crystal with respect to another part. Unlike, vacancies and interstitials atoms, dislocations are not equilibrium imperfections i.e., thermodynamic considerations are insufficient to account for their existence in the observed dislocation densities [19]. In our case, dislocation density (δ) was determined using the relation [30] as given below:

$$\delta = \frac{1}{D^2}$$

The calculated dislocation density (δ) was given in Table 1. It was observed that δ decreases with increasing substrate temperatures from 400 °C to 500 °C and having accordance with the lattice constant *a*, *c* and microstrain tendency, as seen in Table 1.

The effective lattice strain, of the present synthesized SnO_2 nanoparticles, was calculated by using Williamson–Hall equation [31]:

$$\frac{\beta \cos\theta}{\lambda} = \frac{0.9}{D} + \varepsilon \frac{\sin\theta}{\lambda}$$

where β is the full-width at the half maximum (FWHM) of the diffraction peak, θ is the Bragg angle, λ is the wavelength of X-ray used, D is the average crystallite size and ε is the effective lattice strain.

The effective lattice strain calculated by using the above equation was plotted in (Fig. 3). The slope of straight line of (β cos θ/λ) vs. (sin θ/λ) represents the effective strain. The average crystallite size, lattice parameters and strain values obtained from the XRD pattern and Williamson–Hall plots are given in Table 1. The negative value of strain implies a compressive strain in lattice [31,32].

3.2. Optical transmission and optical band gap

Fig. 4 shows the variation of transmittance with respect to wavelength of SnO_2 thin films deposited at various substrate temperatures. The average transmission in the visible region has been found to be ranging from 43.8% to 66% depending upon the substrate temperature. An increase in transmission is observed with increase in temperature. At lower temperatures, i.e. at 400 °C, relatively lower transmission is well remarked which is due to the formation of milky films and that is because of incomplete decomposition of the sprayed droplets. Relatively higher transmittance of about 75% at more than 800 nm for films prepared at 480 °C has been observed. A drastic decrease in transparency is located between 300–360 nm reveling the region of the absorption edge in the layers due to the transition between the valence band and the conduction band (optical band gap: E_g); in this region the transmission decreases because of the onset fundamental absorption. The band gap (E_g) values of pure SnO_2 were deduced from the transmittance data according to Tauc's relation [33] giving $(\alpha h\nu)^2$ versus incident photon energy, ($h\nu$), plots. The graphs are represented in (Fig. 5). The band gap energy values, as shown in Table 2, were found to be ranged in 4.03–4.133 eV for SnO_2 thin films with increasing the substrate temperature from 400 to 500 °C. These results are in good agreement with that obtained ones from bulk SnO_2 [34,35]. More investigations will be taken below using Urbach energy.

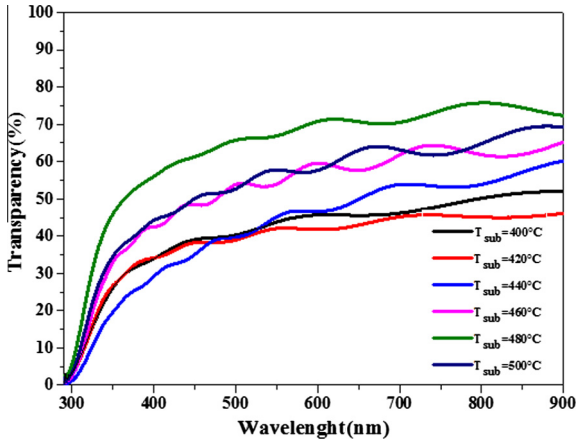

Fig. 4. Spectral transmittance plots of undoped SnO_2 thin films with different substrate temperatures.

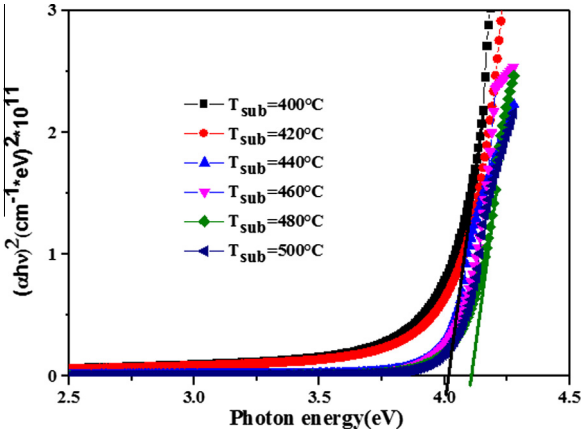

Fig. 5. Band-gap (E_g) estimation from Tauc's relation of undoped SnO_2 thin films with different substrate temperatures.

Table 2
Optical gap (E_g), Urbach energy (E_u), refractive index(n), Permitivity (ε_L), number of free electrons N, and Plasma frequency ω_p with different substrate temperatures.

Substrate temp (°C)	Thickness (nm)	Optical gap E_g (eV)	Urbach energy E_u (meV)	Refractive index (n)	Permitivity ε_L	N (10^{19}cm^{-3})	ω_p (10^{14} Hz)
400	446	4.0303	328.45	1.937	3.643	5.259	4.09
420	600	4.1328	290.61	1.823	3.228	4.489	3.78
440	716	4.0120	189.37	1.963	3.745	5.460	4.17
460	788	4.1327	192.66	1.903	3.521	5.011	3.99
480	696	4.1328	206.68	1.755	2.994	4.221	3.66
500	707	4.0716	182.01	1.905	3.526	5.025	4.00

At lower values of the absorption coefficient α (i.e. near the band edge), the extent of exponential tail of the absorption edge is characterized by the Urbach energy (E_u) indicating the width of band tails of the localized states within the optical band gap and is given by [36]:

$$\alpha = \alpha_0 \exp\left(\frac{h\nu}{E_u}\right)$$

where α_0 and E_u are respectively a constant and width of the band tail of localized states at the optical band gap. E_u is also known as band tail width and is due to the disorder in the thin film material. The variation of bond length and bond angle from their standard value in the crystalline material is called disorder [37]. The Urbach energy of prepared SnO_2 thin films

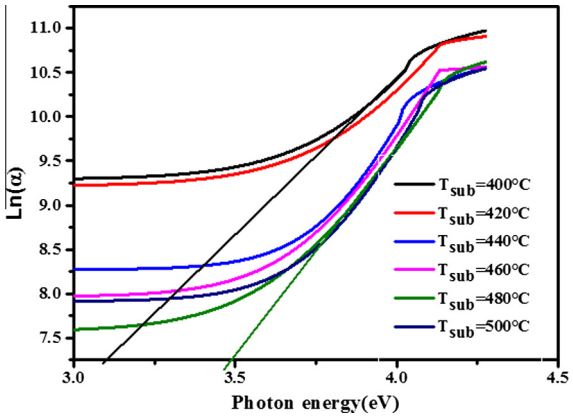

Fig. 6. Urbach energy (E_u) estimation of undoped SnO_2 thin films with different substrate temperatures.

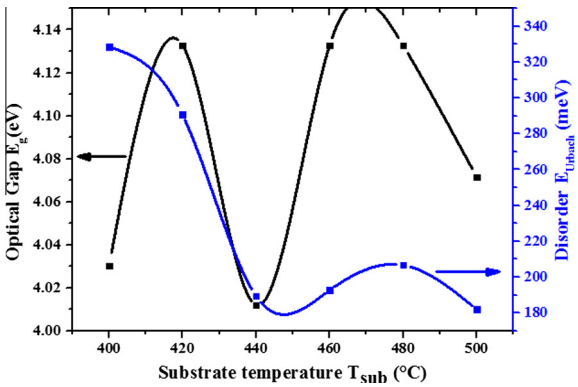

Fig. 7. Variation of Band-gap (E_g) and Urbach energy (E_u) for undoped SnO_2 thin films as functions substrate temperatures.

depends on the structural defects, dislocations density and some defects of the vacancy and interstitial states in the films [38]. It can be determined from the reciprocal gradient of the linear portion of ln(α) versus ($h\nu$) plots. Fig. 6 shows the Urbach energy plot of SnO_2 thin films with substrate temperature. From Table 2 one can that E_u decreases from 328 to 182 meV. This decrease in Urbach energy with increasing substrate temperature is due to the disappearance of localized states [39] and highlighting the correlation of E_u with decrement in energy band gap (see Fig. 7). It also correlates with the improvement in crystallinity of films observed from XRD results.

Lattice dielectric constant ($\varepsilon_L = n^2$) can be evaluated from the mathematical equation which is associated with refractive index (n) and wavelength (λ) and it is given by the following equation [40]:

$$\varepsilon = n^2 = \varepsilon_L - \left(\frac{e^2 N}{4\pi^2 c^2 \varepsilon_0 m^*}\right)\lambda^2$$

where ε_L is the lattice dielectric constant, e is the electronic charge, c is the velocity of light, N the free carrier concentration, m^* the effective mass of the charge carriers and ε_0 is free space dielectric constant (8.854×10^{-12} F/m) [41]. The nature of the dispersion of $\varepsilon_L = n^2$ as a function of wavelength (λ^2) for different substrate temperatures is shown in (Fig. 8). The values extracted from the intercept and slope gives the amount of ε_L and N respectively and they are shown in Table 2. With increasing substrate temperature it was found that both ε_L and N exhibit a little fluctuation, as shown in the insert of Fig. 8. N fluctuated around $5 \cdot 10^{+19}$ cm^{-3}, which may be due to the interaction between free carrier and low lattice phonon. It is worth noting that N estimated from the above law leads to predict that, in SnO_2 material, the effective density of conduction band states is about $5 \cdot 10^{19}$ cm^{-3}as minimum limit.

Plasma frequency (ω_p) is the characteristic frequency at which the material response changes from metallic to dielectric behavior. It is given by the relation:

$$\omega_p^2 = \frac{e^2 N}{\varepsilon_0 m^*}$$

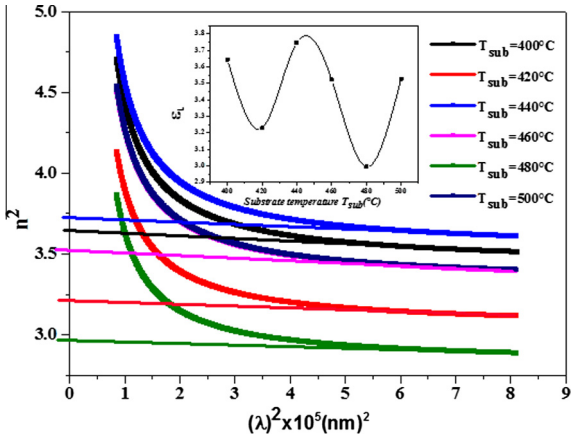

Fig. 8. Plots of n^2 versus (λ^2) of undoped SnO_2 thin films for different substrate temperatures. Insert represent the variation of the lattice dielectric constant ε_L as functions substrate temperatures.

The plasma resonance frequency (ω_p) of all electrons involved in the optical transitions was calculated using the above relation and the values are reported in Table 2. Plasma frequency (ω_p), which was estimated from the above law was about $4 \cdot 10^{14}$ Hz of the elaborated SnO_2 thin films.

3.3. Electrical conductivity

Fig. 9 shows the plot of films resistivity (ρ) and crystallite size D as a function of substrate temperature. As can be seen until 420 °C slight increase in resistivity then decreases to reach 9.19×10^{-3} Ω cm, for the sample deposited at 480 °C, which is comparable to the reported one [42] and increases again (see Table 3). Initially, with increase in temperature up to 480 °C, the thickness increases (see Table 2) leading to decreases in resistivity. Furthermore 480 °C the resistivity increases again even thought the thickness remains constant which means that the resistivity and the thin films thickness are not inverted whereas the crystallite size D increases from 6 to 29.8 nm with increasing temperature in the considered average.

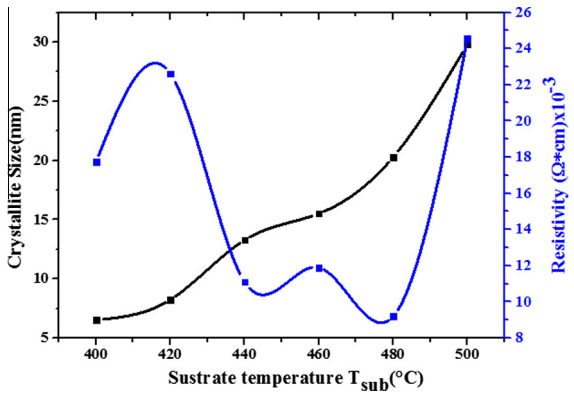

Fig. 9. Plots of resistivity and crystallite size of undoped SnO_2 thin films with different substrate temperatures.

Table 3
Sheet resistance (R_{sh}) and Resistivity (ρ) with different substrate temperatures.

Substrate temp (°C)	Sheet resistance R_{sh} (Ω)	Resistivity ρ (Ω cm)10^{-3}
400	397.76	17.75
420	376.72	22.62
440	154.96	11.10
460	150.96	11.89
480	132.05	9.19
500	347.31	24.55

Under the optics of crystallite size D of the films at the average temperature lower than 420 °C; hence D (6–8 nm) is not higher than the mean-free path l of the electron in SnO_2 materials (l = 4 nm) as given by Prins et al. [43] one can considered that the porters diffusion is limited by grain size leading to high resistivity of the films. Whereas the films prepared at 440–480 °C had low R_{sh} leading to low resistivity owing to their considerable crystallite size (D = 13.27–20.27 nm) which is higher than the mean-free path l of the electron in SnO_2 materials, the porters diffusion is not limited by grain size yielding to low resistivity. Beyond 480° it was mentioned that the growth of the films have (1 1 0) surface as preferred one leading to out diffused oxygen. This out diffusion of oxygen (oxygen vacancies) leads to an increase in surface defect concentration [44] (*i.e.* a decrease in surface conductivity); as consequence an increase in resistivity (sheet resistance) was expected which was observed in the case of the sample elaborated at 500 °C even thought the increase in grain size (D = 29.8 nm) .

4. Conclusions

In this work, we have reported the preparation and characterization of the SnO_2 thin films ultrasonically sprayed onto heated microscopic glass substrates. The thin films were deposited on glass at large scale of temperature ranged in 400–500 °C and stepped by 20 °C. The effect of substrate temperature on structural, electrical and optical properties was studied using X-ray diffraction (XRD), UV–visible spectrophotometer and a conventional four point probe technique. XRD showed that all the films were polycrystalline with major reflex along (1 1 0) plane and minimum surface energy, manifested with amelioration of grain size from 6.51 to 29.80 nm upon increasing substrate temperature. Lattice constant '*a*', '*c*', microstrains and dislocation densities were affected by the substrate temperature. Transmittance of about 75% at more than 800 nm for films prepared at 480 °C has been observed. With increasing the substrate temperature the direct band gap energy was averaged in 4.03–4.133 eV. Plasma frequency (ω_p) of the elaborated thin films reveling the change from metallic to dielectric response was estimated to be $4 \cdot 10^{14}$ Hz whereas the optically deduced number of free electrons N leads to predict that, in SnO_2 material, the effective density of conduction band states was round $5 \cdot 10^{19}$ cm^{-3}. Among all the samples the film that deposited at 480 °C exhibited lowest resistivity of about 9.19×10^{-3} Ω cm.

Acknowledgments

This work was supported in part by VTRS laboratory of El-Oued University. X-ray diffraction data in this work were acquired with an instrument supported by Pole Technique de Borj Cedria, Tunisia. We thank Mohamed Jlassi for the assistance in XRD data acquisition.

References

[1] The Joint Committee on Powder Diffraction Standards (JCPDS), Card No. 41–1445, International Centre for Diffraction Data, 1997.
[2] A. Benhaoua, A. Rahal, B. Benhaoua, M. Jlassi, J. Superlattices Microstruct. 70 (2014) 61–69.
[3] B. Thangaraju, Thin Solid Films 402 (2002) 71–78.
[4] I.H. Kim, J.H. Ko, D. Kim, K.S. Lee, T.S. Lee, J.-H. Jeong, et al, Thin Solid Films 515 (2006) 2475–2480.
[5] Y.M. Lu, C.P. Hu, J. Alloys Compd. 449 (2008) 389–392.
[6] S.S. Srinivasan, J. Wade, E.K. Stefanakos, Y. Goswami, J. Alloys Compd. 424 (2006) 322–326.
[7] D. Vaufrey, M. Ben Khalifa, M.P. Besland, C. Sandu, M.G. Blanchin, V. Teodorescu, Synth. Met. 127 (2002) 207–211.
[8] M.R. Yang, S.Y. Chu, R.C. Chang, Sens. Actuators B 122 (2007) 269–273.
[9] S. Peng, F. Cheng, J. Liang, Z. Tao, J. Chen, J. Alloys Compd. 481 (2009) 786–791.
[10] E. Fortunato, D. Ginely, H. Hosono, D.C. Paine, MRS Bull. 32 (2007) 242.
[11] J.J. Berry, D.S. Ginley, P.E. Burrows, Appl. Phys. Lett. 92 (2008) 193304.
[12] K. Omura, P. Veluchamy, M. Tsuji, T. Nishio, M. Murozono, J. Electrochem. Soc. 146 (1999) 2113.
[13] B.D. Ann, S.H. Oh, D.U. Hong, D.H. Shin, A. Moujoud, H.J. Kim, Cryst. Growth 310 (2008) 3303.
[14] A.N. Banerjee, R. Maity, P.K. Ghosh, K.K. Chattopadyay, Thin Solid Films 474 (2005) 261.
[15] N.M. Shaalan, T. Yamazaki, T. Kikuta, Sens. Actuators B: Chem. 153 (2011) 11–16.
[16] A.F. Khan, M. Mehmood, M. Aslam, M. Ashraf, Appl. Surf. Sci. 256 (2010) 2252–2258.
[17] T. Tsuchiya, K. Daoudi, I. Yamaguchi, T. Manabe, T. Kumagai, S. Mizuta, Appl. Surf. Sci. 247 (2005) 145–150.
[18] W. Hamd, Y.C. Wu, A. Boulle, E. Thune, R. Guinebretiere, Thin Solid Films 518 (2009) 1–5.
[19] D. Paul Joseph, P. Renugambal, M. Saravanan, S. Philip Raja, C. Venkateswaran, Thin Solid Films 517 (2009) 6129–6136.
[20] A. Rahal, A. Benhaoua, C. Bouzidi, B. Benhaoua, B. Gasmi, J. Superlattices Microstruct. 76 (2014) 105–114.
[21] R.R. Kasar, N.G. Deshpande, Y.G. Gudage, J.C. Vyas, Ramphal Sharma, Physica B 403 (2008) 3724–3729.
[22] J. Melsheimer, D. Ziegler, Thin Solid Films 129 (1985) 35–47.
[23] V.M. Nikale, N.S. Gaikwad, K.Y. Rajpure, C.H. Bhosale, J. Mater. Chem. Phys. 78 (2003) 363.
[24] C.S. Barret, T.B. Massalski, Structure of Metals, Pergamon Press, Oxford, 1980.
[25] M. Batzill, U. Diebold, Prog. Surf. Sci. 79 (2005) 47–154.
[26] C. Marcel, N. Naghavi, G. Couturier, J. Salardenne, J.M. Tarascon, J. Appl. Phys. 91 (2002) 4291.
[27] C. Agashe, M.G. Takwale, B.R. Marathe, V.G. Bhide, J. Mater. Sci. 24 (1989) 2628–2636.
[28] P. Scherrer, Gottinger Nachr. 2 (1918) 98.
[29] B.D. Cullity, Elements of X-Ray Diffraction, second ed., vol. 99, Addison-Wesley publishing company Inc., Philippines, 1978 (printed in U.S.A.).
[30] G.B. Williamson, R.C. Smallman, Dislocation densities in some annealed and cold-worked metals from measurements on the X-ray debye-Scherrer spectrum, Philos. Mag. 1 (1956) 34.
[31] G.K. Williamson, W.H. Hall, X-ray line broadening from filed Al and W, Acta Metall. 1 (1953) 22–31.
[32] L. John Kennedy, P. Magesan, J. Judith Vijaya, M.J. Umapathy, Udaya Aruldoss, Mater. Sci. Eng., B 190 (2014) 13–20.
[33] J. Tauc, Amorphous and Liquid Semiconductors, Plenum Press, New York, 1974.
[34] K.L. Chopra, S. Major, D.K. Pandya, Thin Solid Films 102 (1983) 1.
[35] W. Spence, J. Appl. Phys. 38 (1967) 3767.

[36] F. Urbach, Phys. Rev. 92 (1953) 1324.
[37] C.D. Lokhande, K.M. Gadave, J. Phys. 18 (1994) 83–87.
[38] F.Y. Al-Shaikley, Indian J. Appl. Res. 3 (2013) 544–548.
[39] J.I. Shadia, N.A. Riyad, Phys. Scr. 84 (2011) 055801–055807.
[40] M.B. El-Den, M.M. El-Nahass, Opt. Laser Technol. 35 (2003) 335–340.
[41] T.S. Moss, G.J. Burrell, E. Ellis, Semiconductor Opto-Electronics, Butterworths, London, 1973.
[42] M. Bender, J. Trube, J. Stollenwerk, Thin Solid Films 354 (1999) 100.
[43] M.W.J. Prins, K.-O. Grosse-Holz, J.F.M. Cillessen, L.F. Feiner, J. Appl. Phys. 83 (2) (1998) 15.
[44] J.W. Erickson, S. Semancik, Surf. Sci. 187 (1987) L658.

Abstract

Transparent conducting oxides (TCO) continue to attract considerable attention in terms fundamental and application, mainly because of their highly exploited properties. Special consideration was given to SnO_2 which is an n-type semiconductor with excellent optoelectronic properties either with or without doping; that give it the potential to be exploited in large-area applications as an alternative to ITO.

In this perspective, we studied in the first part of this work, the importance of the parameter condition (effect of substrate temperatures, effect of tin precursor concentration and effect of solvent) in order to optimize these parameters for elaborate a SnO_2 films on the crystal phase and optoelectronic properties of film elaborated by ultrasonic spray method.

In the second part, we studied effects of (F or Sb) doping on SnO_2 for optimize figure of merit.

Résumé :

Les oxydes transparents conducteurs (TCO) continuent à susciter une attention considérable du point de vue fondamental et application, principalement en raison de leurs propriétés très exploitées. Une considération particulière a été portée sur SnO_2 qui est un semi-conducteur de type n possédant d'excellentes propriétés optoélectroniques soit avec ou sans dopage ; qui lui confèrent la possibilité d'être exploité dans de nombreux domaines comme alternative aux l'ITO .

Dans cette perspective, nous avons étudié, dans la première partie de ce travail, l'influence de conditions d'élaboration (conditions opératoires : choix du précurseurs, l'effet de la température du substrat, le concentration d'étain dans le précurseur et le solvant) dans le système SnO_2 sur la phase cristalline et les propriétés optoélectroniques des films élaborés par la méthode spray ultrasonique.

Dans la deuxième partie, nous avons étudié l'optimisation de facteur de mérite par les effets de dopage (F ou Sb) sur les structures de SnO_2

ملخص:

تستمر الاكاسيد الشفافة و الناقلة للكهرباء (TCO) في جذب الكثير من الباحثين، وذلك بسبب خصائصها الواسعة الاستغلال. اهتمامنا خص اوكسيد القصدير (SnO_2) الذي هو بمثابة شبه ناقل من نوع n يتمتع بخصائص كهروضوئية ممتازة؛ التي تعطيه ميزة لاستغلاله في العديد من المجالات و يمكنه ان يكون بديل عن اوكسيد الأنديوم المطعم بالقصدير (ITO) .

في هذا المنظور، خلال الجزء الاول من العمل قمنا بدراسة تأثير مختلف الوسائط (كدرجة حرارة الركيزة او تركيز المحلول السائل الابتدائي او نوع المحلول) المؤثرة على تحضير وترسيب الشرائح الرقيقة من اوكسيد القصدير (SnO_2) المحضرة بواسطة تقنية الرش فوق الصوتي و ذلك لضبط الشروط التي تؤدي الى نتائج و خصائص بلورية و كهروضوئية جيدة للشرائح الرقيقة .

في الجزء الثاني من هذا العمل درسنا مدى تأثير تطعيم عينات اوكسيد القصدير بذرات (الفليور او الانتيموان) في تحسين الخصائص الكهروضوئية (عامل الجودة).